UNIVERSITÀ DEGLI STUDI DI TRENTO

QUEEN MARY
UNIVERSITY OF LONDON

Erasmus Mundus Joint Doctorate School in Science for MAnagement of Rivers and their Tidal System

---

Simone Zen

Bio-morphodynamics of evolving river meander bends from remote sensing, field observations and mathematical modelling

Erasmus Mundus

October 2014

Doctoral thesis in Science for MAnagement of Rivers and their Tidal System,
Cycle: 1
Primary Institution:
Department of Civil, Environmental and Mechanical Engineering, University of Trento
Secondary Institution:
Department of Physical Geography, Queen Mary University of London
Supervisors:
prof. Guido Zolezzi, University of Trento
prof. Angela M. Gurnell, Queen Mary University of London

Academic year 2014/2015

Front Cover: Raften, Bill, South Fork of Koyukuk River, Kanuti National Wildlife Refuge, Alaska.

This page is intentionally left blank

The SMART Joint Doctorate Programme

Research for this thesis was conducted with the support of the Erasmus Mundus Programme [1] , within the framework of the Erasmus Mundus Joint Doctorate (EMJD) SMART (Science for MAnagement of Rivers and their Tidal systems). EMJDs aim to foster cooperation between higher education institutions and academic staff in Europe and third countries with a view to creating centres of excellence and providing a highly skilled 21st century workforce enabled to lead social, cultural and economic developments. All EMJDs involve mandatory mobility between the universities in the consortia and lead to the award of recognised joint, double or multiple degrees. The SMART programme represents a collaboration among the University of Trento, Queen Mary University of London, and Freie Universität Berlin. Each doctoral candidate within the SMART programme has conformed to the following during their 3 years of study:

(i) Supervision by a minimum of two supervisors in two institutions (their primary and secondary institutions).

(ii) Study for a minimum period of 6 months at their secondary institution.

(iii) Successful completion of a minimum of 30 ECTS of taught courses.

(iv) Collaboration with an associate partner to develop a particular component / application of their research that is of mutual interest.

(v) Submission of a thesis within 3 years of commencing the programme.

[1] This project has been funded with support from the European Commission. This publication reflects the views only of the author, and the Commission cannot be held responsible for any use which may be made of the information contained therein.

this thesis is dedicated
to Karina

Acknowledgements

Undertaking this PhD has been a great life-changing experience for me and it would not have been possible without the both scientific and non-scientific support of many people. I wish therefore to express my sincere appreciation to those whose contribute positively influence my career and highly improved the present research.

Foremost, I would like to express my deepest gratitude to my advisors, Angela Gurnell and Guido Zolezzi for supporting me during these three years, for their patience and their thoughts, and especially for their contagious enthusiasm for research that has always been source of inspiration.

In particular, I'm grateful to Guido Zolezzi, who has constantly encouraged and guided me through the research work and has always been available to advise me, being not only my supervisor but a good Mentor and friend.

I would like to include in this list of acknowledgements also Marco Tubino, for the inspiring talks and discussions and for the patience to explain 'that' complex theories.

A special acknowledgement goes to Walter Bertoldi whose expertise and precious suggestions have contributed in highly improved this research work; and Bob Grabowski for the assistance on remote sensing techniques provided me during the period spent at the Queen Mary University. I would like to thank also Marco Toffolon for the fundamental contribution given in the development of the model proposed and Alfonso Vitti for his technical support and guidance for the field measurement activities. Finally, a special thanks goes to Martino Salvaro and Stefano Tettamanti for their help during the field campaign.

I'm grate also to Nicola Surian and Luca Ziliani for providing all the historical aerial photographs have been used in the research work.

Many thanks to the SMART secretaries Marina Rogato and Laura Martuscelli, as well as Jennyfer Murray for their help in managing tedious bureaucratic stuff.

I would like to extend my gratitude to the SMART students, particularly those of the first cohort with who I have shared difficulties and

satisfactions within the PhD programme. Particularly, I want to thank Marco for his precious advices and the stimulating discussions, Prima for her support during my staying in London and Lydia (adopted SMART student) for the good time shared in Trento. A big thanks for the nice time spent in London goes also to Jean-Philippe, Cagri, Hossein, Ulfa and Francesca. Thanks guys, we met as colleagues and we end up to be friends!

A warm acknowledge is deserved to Karina, the sweetest surprise of this three years, for kindly sustaining me and for her special support during these last months of writing. There are no words that can express my gratitude and appreciation for you.

I am also grateful to all my friends that have supported me during these three years. I'm indebt to Enrico, Daniele, Barbara and Anna for the amazing shared moments. I want also to thank los paraguayos for the parties in Trento and for introducing me to the paraguayan culture.

Finally I would love to give a heartfelt thank you to my Mum, Dad, Gianluca, Alexia and her family, my uncle and my grandparents for always believing and encouraging me.

Thanks all, especially to those of you that at the very beginning managed to overcome my skepticism on the PhD programme.

Abstract

Interactions between fluvial processes and vegetation along the natural channel margins have been shown to be fundamental in determining meandering rivers development. By colonizing exposed sediments, riparian trees increase erosion resistance and stabilize fluvial sediment transport through their root systems, while during a flood event the above-ground biomass interacts with the water flow inducing sediment deposition and altering scour patterns. In turn river dynamics and hydrology influence vegetative biomass growth, affecting the spatial distribution of vegetation. These bio-morphological dynamics have been observed to direct control accretion and degradation rates of the meander bend. In particular, vegetation encroachments within the point bar (i.e. colonizing species and strand wood), initiate pioneeristic landforms that, when evolving, determine the lateral shifting of the margin that separates active channel from river floodplain and thus inner bank aggradation (*bar push*). This diminishes the portion of the morphologically active channel cross-section, influencing the erosion of the cutting bank and promoting channel widening (*bank pull*). As a result of the cyclical occurrence of these erosional and depositional processes, meandering rivers floodplain show a typical ridge and swale pattern characterized by the presence of complex morphological structures, namely, benches, scrolls and chutes within the new-created floodplain. Moreover, difference in migration rate between the two banks have been observed to induce local temporal variations in channel width that affect river channel morphodynamics and its overall planform through their influence on the local flow field and channel bed morphology.

Despite enormous advances in field and laboratory techniques and modelling development of the last decades, little is known about the relation between floodplain patterns and their controlling bio-morphological interactions that determine the bank accretion process. This knowledge gap has so far limited the development of physically-based models for the evolution of meandering rivers able to describe the lateral migration of banklines separately. Most existing meander migration models are indeed based on the hypothesis of constant channel width.

Starting from this knowledge gap, the present doctoral research has aimed to provide more insight in the mutual interactions among flow, sediment transport and riparian vegetation dynamics in advancing banks of meandering rivers. In order to achieve its aims, the research has been designed as an integration of remote sensing and in-situ field observations with a mathematical modelling approach to i) provide a quantitative description of vegetation and floodplain channel topography patterns in advancing meanders bend and to ii) explore the key control factors and their role in generating the observed patterns.

The structure of the present PhD work is based on four main elements.

First, two types of airborne historical data (air photographs and Lidar survey) have been investigated, in order to quantify the effects of spatial-temporal evolution of vegetation pattern on meander morphology and to provide evidence for the influence of vegetation within the topography of the present floodplain. Such remote sensing analysis has highlighted a strong correspondence between riparian canopy structure and geomorphological patterns within the floodplain area: this has clearly shown the need to interpret the final river morphology as the result of a two-way interaction between riparian vegetation dynamics and river processes.

Second, field measurments have been conducted on a dynamic meander bend of the lower reach of the Tagliamento River, Italy, with the initial aim of checking the outcomes of the remote sensing analysis through ground data. The outcomes of the field measurements have further supported the results, providing ground evidence on the relations between vegetation and topographic patterns within the transition zone that is intermediate between the active channel bed and the vegetated portion of the accreting floodplain. The influence of vegetation on inner bank morphology has also been interpreted in the light of the expected time scales of inundation and geomorphic dynamics that characterize the advancing process of the inner bank. The combined analysis of both remotely sensed data and field measurements associated with the historical hydrological dataset have allowed to quantitatively characterize the biophysical characteristics of the buffer zone, close to the river edge, where the accretion processes take place.

The third research element has foreseen the development of a biophysically-based, simplified bio-morphodynamic model for the lateral migration of a meander bend that took advantage of the empirical knowledge gained in the analysis of field data. The model links a minimalist approach that includes biophysically-based relationships to describe the interaction between riparian vegetation and river hydro-morphodynamic processes, and employs a non linear mathematical model to describe the morphodynamics of meander channel bed. Model application has allowed to reproduce

the spatial oscillations of vegetation biomass density and ground morphology observed in the previous analyses. Overall, the model allows to understand the role of the main controlling factors for the ground and vegetation patterns that characterize the advancing river bank and to investigate the temporal dynamics of the morphologically active channel width, providing insights into the bank pull and bar push phenomena.

The fourth and concluding element of the present PhD research is a analytical investigation of the fundamental role of unsteadiness on the morphodynamic response of the river channel. Results obtained in the previous elements have clearly showed the tendency of a meander bend to develop temporal oscillations of the active channel width during its evolution, but no predictive analytical tool was previously available to investigate the channel bed response to such non-stationary planform dynamics. A non linear model has therefore been proposed to investigate the effect of active channel width unsteadiness on channel bed morphology. The basic case of free bar instability in a straight channel has been used in this first investigation, which has shown the tendency of channel widening to increase river bed instability compared to the steady case, in qualitative agreement with experimental observations.

Overall, the research conducted within the present Doctoral Thesis represents a step forward in understanding the bio-morphodynamics of meandering rivers that can help the development of a complete bio-morphodynamic model for meandering rivers evolution, able to provide support for sustainable river management.

Contents

List of Figures

List of Tables

Chapter 1

Introduction

River meanders are complex natural features that have fascinated writers, artists and stimulated the interest of researchers for many years. The term *meanders* refers to the bends and loops that these sinuous rivers generate in their flowing down the valley. It took its name from the Meander River (Büyük Menderes Irmağı), a winding stream that flows in south-western Turkey, known in the ancient Greece as river-god Maiandros (from greek $Μαιανδρος$ or Maeander in the latin version).

From aerial photographs or satellite images (see the examples reported in Figure 1.1), the successive curves of meandering rivers appear to be organized in a continuous twisted path, typical of many natural channels, where bends are characteristically skewed according to the direction of migration, the inner bank is characterized by sediment depositing on the point bar and presents a convex profile, and the outer bank shows a concave shape. Their morphological development depends on the interactions between water flow, sediments and riparian vegetation that affect sediment deposition and erosion processes, thus ultimately playing a role in the processes of inner bank advancing and outer bank retreating. As a result of their lateral migration, meandering rivers floodplain is typically characterized by a corrugated surface due to the presence of complex morphological structures (e.g. scrolls formation, see Figure 1.1b).

Bend growth processes increase river channel sinuosity until the occurrence of neck cut offs, where river flow abandons the meander loop, thus originating an oxbow lake. Moreover, presence of vegetation within the inner bank interacts with the over-bank flow altering scour/depositional patterns and leading to the formation of chute that may be scoured and enlarged during a subsequent flood inducing channel bifurcation i.e. chute cut off phenomena (see Figure 1.1b). This process can be further supported by an unbalance between bank erosion and accretion able to induce local variation in channel width modifying river flow patterns and

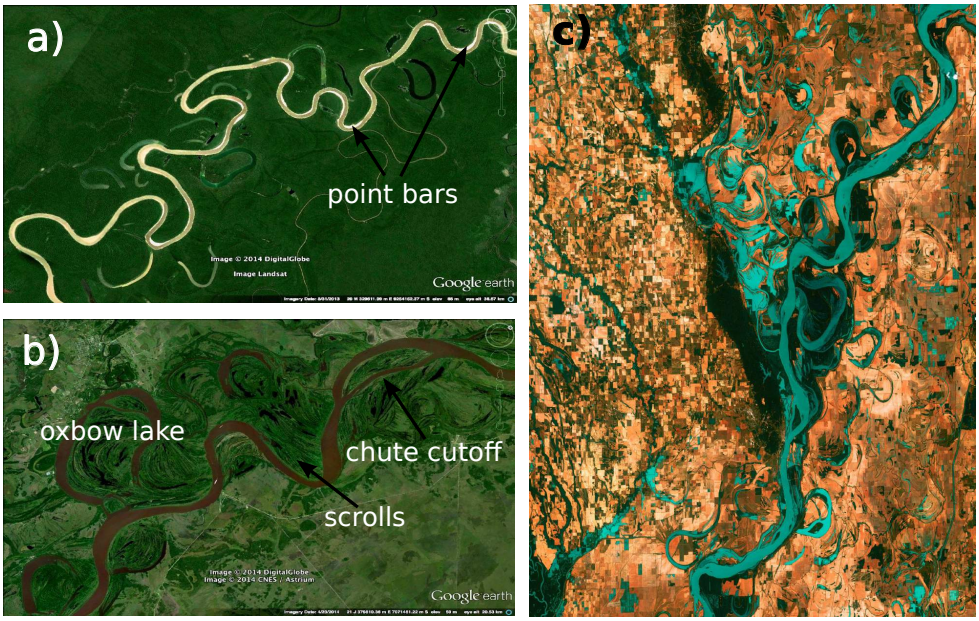

Figure 1.1: Aerial imageries of a)Purus River (Brazil), b)Paraguay River, south of Villa Franca, Paraguay extracted from Google Earth and c) satellite image of the Mississippi River, south of Memphis, Tennessee - Landsat7, NASA's Goddard Space Flight Center/USGS.

the overall river planform.

It has been shown since almost two decades (Howard, 1992; Gurnell et al., 1994) that tracking meanders historical evolution and predicting their future dynamics is achievable from the interpretation of aerial imageries and by means of mathematical morphodynamics models of increasing complexity. While uncertainties are still widespread in both approaches, they somehow allow to broadly delineate the extensions of the actively meandering river corridor, and to suggest their future evolutionary trajectories. However integration between the two approaches and between them and in-situ field measurements has seldom been tested for the same purpose, despite having strong potential for increasing our understanding of processes and for reducing present uncertainties.

From a management point of view, because river meandering often occur within populated floodplains, it is relevant to understand such dynamics, for both fundamental scientific reasons and in order to increase our ability of simulating river planform evolution and of defining the areas at risk for future channel erosion. This will provide a valid support for river-associated risk management and guidance in reducing risks for human communities and hydraulic structures (e.g. bridges, levees).

This problem is particularly relevant in those floodplain areas of the world where active channel meandering still takes place, and might be viewed as less relevant in European countries where more than 80% of the river reaches have been modified to serve the needs of the human population and presents constrains (e.g. artificial levees, bank protection and groynes) that prevent any morphological evolution. However, in the last year river management has been increasingly focusing on river restoration with the aim to partially restore the natural functioning of river systems, also as a tool to directly sustain the aims of the Water Framework Directive.

Several types of interventions make up the ensemble of possible approaches to river restoration. By re-connecting rivers to their floodplain and providing more space for their morphological evolution, for instance, some river restoration projects allow the initiation and planform development of meander bends. This may also serve to increase the diversity of the river ecosystem and to enhance recreational opportunities associated with the use of the river and with its visual amenity, therefore able to generate economic benefits i.e. tourism and recreational activities. Furthermore, restoring rivers may in some case also increase their natural flood storage capacity, thus damping flood peaks and possibly reducing the related risk for human population and activities. In the event of high flow, excess water can be absorbed by the natural features, such as meanders, reducing the amount of damage with respect to the analogous case in which engineered structures are overwhelmed.

This latter aspect results to be particularly relevant in our country where changes in rainfall regime associated with climate change have exponentially increased the risk of flooding. In particular, the extreme events that have occurred in the last years have highlighted the limits of the classic flood risk management approach; which is based, essentially, on providing constrains to the watercourse.

However, many river restoration projects are not yet adequately supported by state-of-art morphodynamics studies, both in the design and assessment stages. Many river restoration projects fail in their aims or induce undesirable effects, implying a waste of resources. On the other hand, the complex nature of the dynamic river processes relevant for channel restoration and, more in general, for river management, determine a knowledge gap whereby our understanding of fundamental biophysical interactions is still in its infancy in many cases. A clear examples are the interactions between river processes and riparian vegetation dynamics that play a key role in the evolution of river meanders and in the related process of new floodplain creation. Such existing knowledge gap has prevented the development of a comprehensive predictive ability for meanders evolution

that can support, properly, river management and restoration of meandering channels. The present Doctoral Thesis focuses on this knowledge area, at the intersection of river mopho-dynamics and eco-hydraulics, with the general goal to provide novel insights in these mutual feedback processes and to allow the development of complete bio-morphodynamic predictive tools able to provide enhanced scientific support to sustainable river management.

In order to reach this aim, the river is viewed in this work as the result of a dynamic equilibrium between biotic dynamics and fluvial processes. This fundamental approach of the research is reflected in the setup of a multidisciplinary approach able to involve river ecology, geomorphology and fluid-mechanics.

By investigating river channel bio-morphodynamics from the combination of different techniques (e.g. remote sensing, field observations and modelling) this thesis work aims to represent a step forward in this direction. This has been possible throughout the cooperation between the two departments where the work of thesis has been carried out within the SMART Joint Doctorate Programme: Department of Civil, Environmental and Mechanical Engineering at the University of Trento, Italy, and Department of Physical Geography at the Queen Mary University of London, UK.

Chapter 2

Interactions between riparian vegetation, sediments and water flow within fluvial system

This chapter provides a review of the state of art on the present understanding about the interactions between river processes and riparian vegetation, with a special focus on meandering rivers. The review has been thought with the aim of introducing the reader to the terms and the concepts on which the present PhD thesis is based, and it leads to highlight the research gaps that motivated the research presented in this thesis.

2.1 Introduction

The fundamental role played by riparian vegetation in the evolution of river channel patterns has only recently been widely recognized and set as a key element in the scientific literature focused on modelling and analysing the evolution of river patterns, including meandering rivers (Camporeale et al., 2013; Gurnell, 2014). Although modelling the river active corridor as a complex system generating by the dynamic equilibrium between biological and fluvial processes may appear a forgone conclusion, this represents an important step in a scientific dialogue between fluid mechanicists, geomorphologists and ecologists that have stimulated the research on river morpodynamics within the last decades, but only very recently is being reflected in interdisciplinary scientific outcomes.

The debate on the role played by riparian vegetation in the morphodynamics of meandering rivers has indeed started only recently, while previous approaches were mainly grounded in the disciplines of fluid mechanics and of physical geography.

The fluid mechanicistic approach finds among its initial contributors Einstein (1926), who was the first to understand the importance of helical

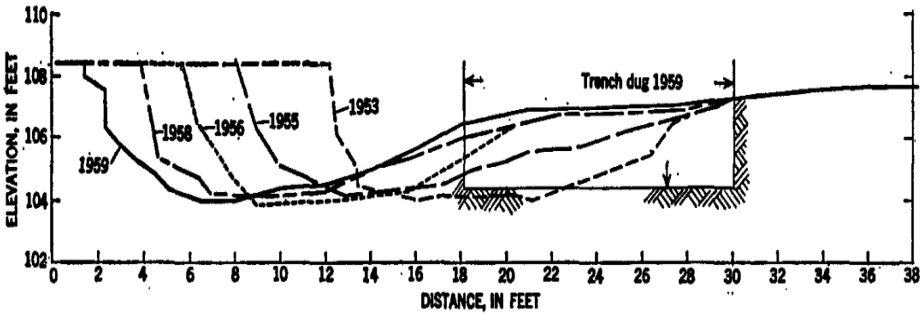

Figure 2.1: Successive cross-sectional surface profiles of meander channel and point bar, 1953-59 (Leopold and Wolman, 1960).

flow in meanders formation and development. Using an analogy with a cup of tea, he inferred that secondary current induced by channel curvature or Corioli's forces lead to scour at the outer bank and sediment deposition at the center of the channel, such as the tea leaves in a cup of tea collect at the center of the cup when the tea is forced to rotate by a spoon. This is due to the secondary currents associated with the shear stress between the tea and the lateral wall of the cup. About 30 years later Friedkin (1945); Rozovskij (1957) quantify Einstin's early observations and Leopold and Wolman (1960) investigated the effects induced by meandering flow patterns on the processes of lateral deposition and erosion and their influence on river channel evolution (see figure 2.1). Moreover, in their review paper, Leopold and Wolman (1960) pointed out the inadequateness of the available frameworks at the time in describing the complex dynamics that characterize meander bends evolution. Along the same time frame, empirical research based on geomorphological approaches concentrated on describing the physical parameters that influence river form, and also some of them began recognizing riparian vegetation as an important control on fluvial dynamics, associating changes in channel planforms with the presence of different vegetation coverage within the river margins (Mackin, 1956).

At the end of the twentieth century, theoretical analyses and laboratory observations have revealed that formation of meandering patterns is related to instability mechanisms generated by the presence of a movable interface between the fluid and the erodible boundary which appears to be intrinsically unstable (Seminara, 2006). On the base of these considerations, integrated field, laboratory and theoretical research, which have been carried out within the first years of the twenty-first century, have contributed in deeper understanding the effect of riparian plants on fluvial processes, giving evidence of both a passive and an active role play

by vegetation in influencing river morphology.

The present chapter reviews the progressive evolution of the scientific debate leading to a shift from the idea of the river as static element, in which vegetation merely represents an increase in wall roughness, towards a more comprehensive and realistic view interpreting the river corridor as a dynamic system sustained by the mutual interactions between biological and fluvial processes.

This review chapter builds the state of art by separately addressing field and laboratory observations (section 2.2) from modelling approaches (section 2.3)for the sake of clarity. Moreover the second part of this chapter highlights the research gaps that emerge from the review of the state of art, introducing the main objectives of the present doctoral project and providing the outline of the research elements that have been designed to overcome the main detected research gaps.

2.2 Field and Laboratory investigations

River corridor morphology

Meander bends migrate laterally as a result of the curvature - forced flow pattern that causes erosion of the outer bank and deposit sediments at the inner, convex bank (Leopold and Wolman, 1957, 1960). The progressive deposition of point bar at the convex bank is known to be associated to the development of a currugated floodplain surface, characterized by a succession of ridges and swales (see Figure 2.2), which have been referred in literature with the term of *meander scrolls* or *scroll bars* (Hickin, 1974; Hickin and Nanson, 1975; Nanson, 1980; Nanson and Croke, 1992). Analysis conduced by Hickin (1974) on the point bars of the Beatton River (British Columbia, Canada), has revealed that meanders developed following an erosion-path orthogonal to the apexes of the scroll bends, where direction and migration rate are controlled by the value of the ratio of the radius of curvature to channel width. On the basis of such observation, scrolls formation within the floodplain area have been investigated to estimate meandering river historical evolution, through dendrochronology analysis on the vegetation that they support Hickin and Nanson (1975) or with direct measurements that can provide three dimensional information on the scroll bar structure, such as optical (Rodnight et al., 2005) and ground penetrating (Bridge et al., 1995; Leclerc and Hickin, 1997) remote sensing techniques.

Furthermore, it has been observed that the natural variability in river discharge contributes to channel planform evolution by contributing to both bank erosion and bank accretion processes. In particular, high flows

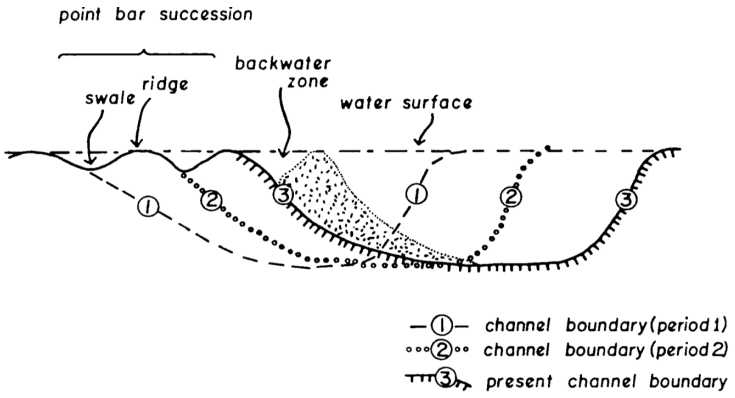

Figure 2.2: Point bar succession in a laterally migrating meandering channel (Hickin, 1974).

determine channel widening through net bank erosion mechanism, while, conversely, absence of high magnitude floods causes width contraction through aggradation associated with deposition of benches (scrolls) at the convex bank. Moreover, over-bank deposition contributes in rising river channel margins (Nanson, 1986; Pizzuto, 1994; Visconti et al., 2010). On the short-term (say 20-30 years) it has been observed that the unbalance between rate of cutbank erosion and point-bar accretion leads to a *'concertina-like'* movement of the channel with the cutbank retreating and then pausing, and afterwards the convex bank 'catching up'(Nanson, 1981; Nanson and Hickin, 1983). This discontinuous process has been observed to be linked with fluvial processes at the scale of the overall river planform (Hooke, 2007, 2008), namely with longitudinal variations in river channel width associated with mid channel bars formation (Bertoldi and Tubino, 2005) (Ashmore, 1982, 1991). Furthermore, from geometry considerations Lauer and Parker (2008) demonstrated that, at the local scale, differences in length and vertical accretion rate between the two banks determine a net removal of sediments, incrementing the sediment flow within the river channel.

Mutual interaction between vegetation and river meanders morphology

Early analysis conduced to understand the role of vegetation on fluvial processes have revealed two principal mechanisms through which riparian vegetation exerts a control on the river morphology patterns (Hickin, 1984): by trapping and strenghtening alluvial sediments (active role) and by influencing flow field patterns (passive role). The above-ground biomass interacts with the river (over-bank) flow by increasing the local roughness

and modifying its turbulent structure (i.e. Armanini et al., 2005; Righetti, 2008; White and Nepf, 2008), thus inducing changes in sedimentation patterns (Vargas-Luna et al., 2014), or by directly trapping the transported material (sediment or wood). More specifically, over-bank deposition induced by the presence of vegetation has been observed to be particularly relevant in the aggradation processes of meander inner banks (Hickin, 1974). However, McKenney et al. (1995) have observed that this induced effect tends to decrease far from the river edge, since mature vegetation drag resistance is lower than that showed in its earlier phases (i.e. brush form).

The active role played by vegetation on river morphology is mainly related with its influence on bank processes, sediment retention and initiation of pioneer landforms. Several researchers have observed a reduction in bank erosion rates due to the action of trees' root structures that increase soil cohesion (Micheli and Kirchner, 2002b; Allmendinger et al., 2005; Pollen-Bankhead et al., 2009; Pizzuto et al., 2010) and have tried to quantify the effect of riparian vegetation on stream bank lateral migration (Micheli and Kirchner, 2002a; **?**; O'Neal and Pizzuto, 2011) Moreover, research conduced on gravel bed river systems has shown that live or dead (uprooted trees that can sproot asexually) vegetation, by trapping and reinforcing fluvial sediments, initiates pioneer landforms, such as vegetated islands in braided streams (Gurnell et al., 2001, 2005).

Because the development of riparian trees is controlled by flow disturbance and moisture availability, the structure of these riparian communities is largely influenced by the hydrological regime. Variation in water discharge influences recruitment phase (recruitment model box proposed by Mahoney and Rood, 1998) and determines plant success and growth by modifying the water table level and altering sediment moisture retention (Perona et al., 2012). During floods flow may reduce vegetation coverage by eroding vegetated areas or by uprooting trees (Crouzy and Perona, 2012) and, at the same time, it deposits new sediments (i.e. point bar at the inner bank) that can be colonized during the low stage phase. As a result, vegetation structure and distribution within the riparian corridor reflects the proximity to the river edge, the river topography and hydrological conditions (McKenney et al., 1995; Robertson and Augspurger, 1999; Robertson, 2006), localizing a hotspot of 'plant engineering' (Gurnell and Petts, 2006) between areas mainly dominated by fluvial disturbance and by plants (Gurnell et al., 2012); see Figure 2.3.

Recent advances in flume experiments have further supported the field observations on the active role of riparian vegetation on channel morphodynamics, showing that these mutual feedbacks are often critical controls on the overall river planform (Gran and Paola, 2001; Braudrick et al.,

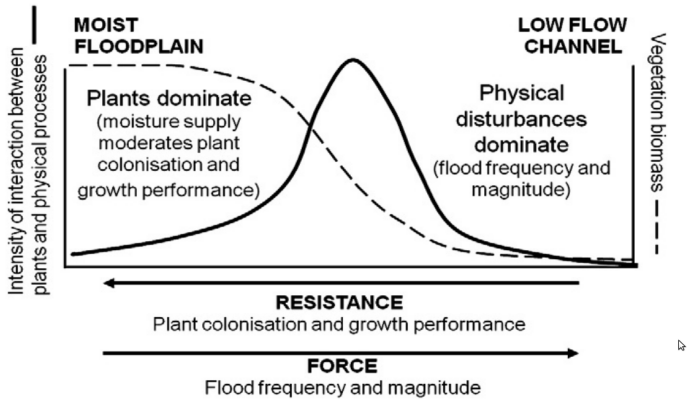

Figure 2.3: Zone of interaction between riparian vegetation and fluvial processes at the connection between plant dominated and flood disturbance dominated zones (Gurnell et al., 2012).

2009; Tal and Paola, 2010; van Dijk et al., 2013). Another important factor related to the influence of vegetation on river morphology, presence of uprooted trees stranded on the point bar has been recognized as responsible for initiation of scroll bars within the point bar itself and therefore an important aspect of the planform evolution of river meanders (Nanson, 1981; Gurnell and Petts, 2006). Moreover during over-bank flow vegetation acts as an obstacle altering scour and depositional patterns, thus inducing deposit in corrispondence of the deposited tree and scouring on its sides (McKenney et al., 1995; Nakayama et al., 2002). In particular, for the purpose of the present analysis, the conceptual model proposed by (McKenney et al., 1995) (Figure 2.5) results to be much appropriate in summarizing the physical processes described above. Figure 2.5 show the evolution sequance of the inner bank of an ideal evolving meander. After the creation of the point bar during the flood event, vegetation grows during the low flow stage (time 0), assuming adequate moisture is available. During the subsequent floods, over-bank deposition occurs in the newly vegetated band because flow resistance is higher than in the surrounded area where flow induce scour channels, which may be viewed as possible initiator of chutes (time 1). The cross-section becomes narrower and the subsequent high flow causes scour of the main channel and erosion of the outer bank (time 2). This induces a reduction in water stage, thus creating a surface which can support colonization by a new band of vegetation. Furthermore, field investigations as well as flume experiments have individuated in ridges and swales pattern within the floodplain area a fundamental element for the occurrence of chute cut-off (Grenfell et al.,

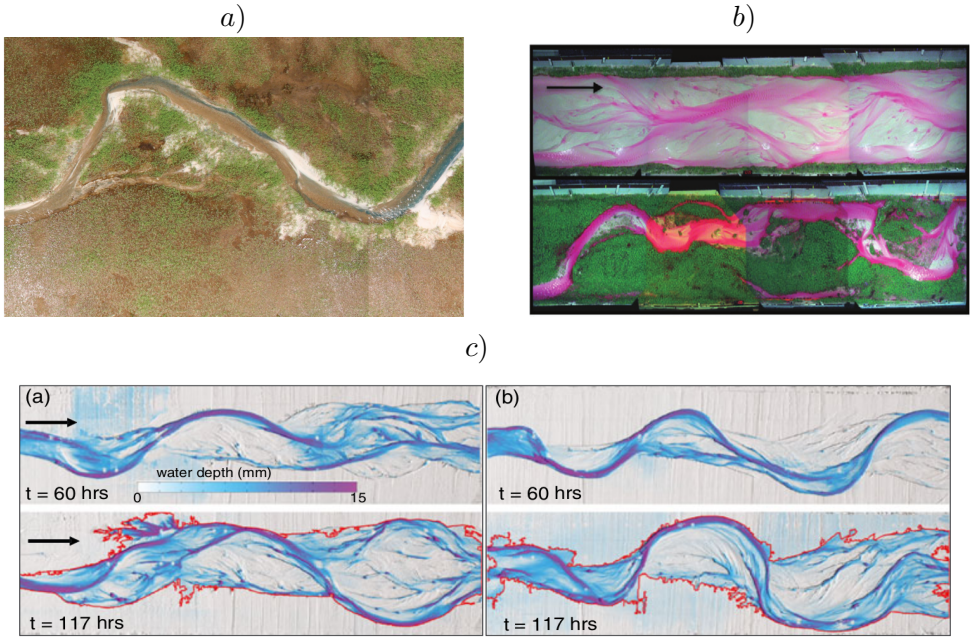

Figure 2.4: Example of flume experiments conducted to investigate the role of a) and b) vegetation and c) cohesive sediments on river channel morphodynamics; a) Braudrick et al. (2009), b) Tal and Paola (2010), c) van Dijk et al. (2013).

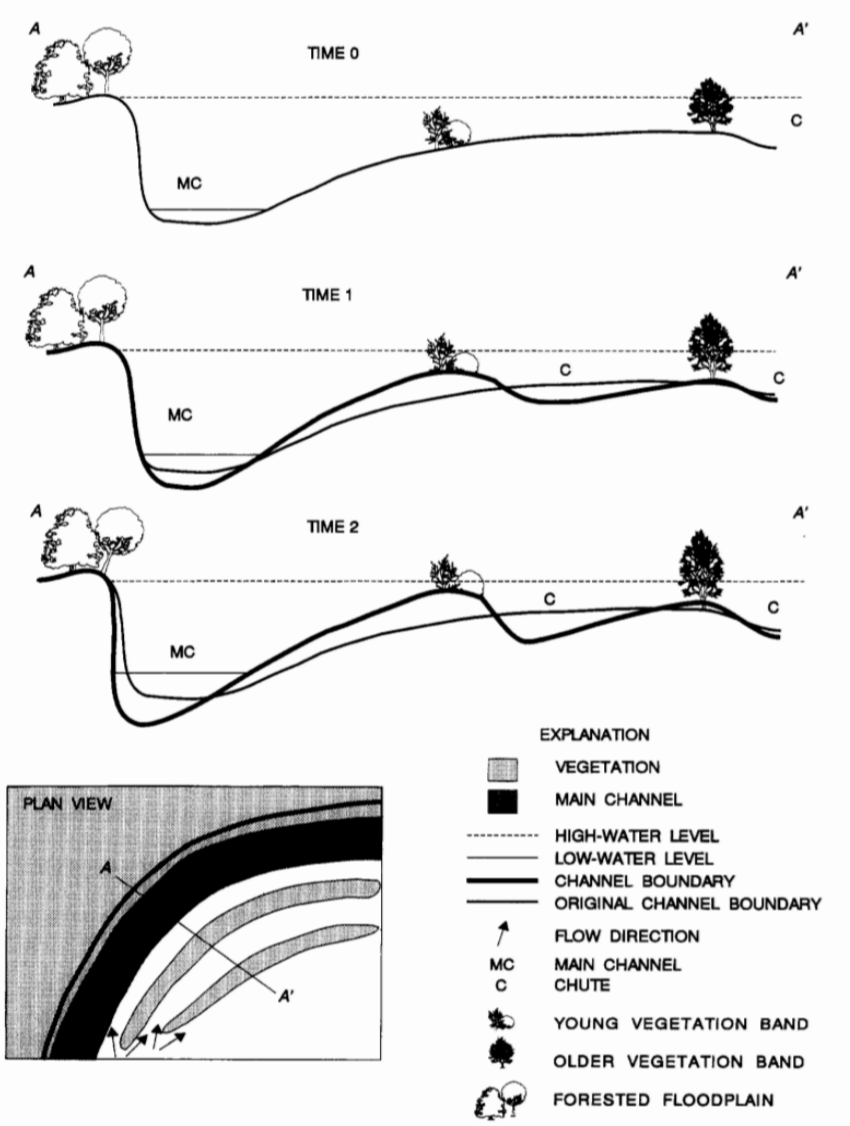

Figure 2.5: Conceptual model of channel morphogenesis for meandering rivers with vegetated floodplain from McKenney et al. (1995).Time 0) vegetation growth on the point bar; time 1) over-bank flow during flood induce deposition on the vegetation bands and scour on the chute; time 2) deposition at the inner bank induce erosion in the main channel, diminishing the water stage and creating new bare sediments for colonization.

2011; van Dijk et al., 2012; Rozo et al., 2012).

2.3 Modelling

This section focuses on the analytical model that have been proposed so far to quantitatively investigate the planform evolution of meandering rivers, with special attention to the role of riparian vegetation dynamics. Thanks to their simplified hypothesis, these models often represent powerful tools to quantitatively predict and to gain insight into the biophysical mechanics governing the evolution process and on their controls.

2.3.1 Morphodynamic models for meandering rivers

Most models proposed in literature to quantitatively predict meandering planform evolution are based on the well known *bend theory*, originally proposed by Hasegawa (1977) and Ikeda et al. (1981); this initial approach to the bend theory will be named "HIPS model" following Parker et al. (2011). In the HIPS model, and in the subsequent models based on it, the lateral channel migration rate is linearly proportional to the near-bank excess velocity compared to that occurring at the channel centerline. The proportionality is expressed through a dimensionless coefficient E essentially accounting for bank properties but also for numerical issues:

$$\zeta = E\Delta U \tag{2.1}$$

where ΔU represents the difference in streamwise velocity between the inner and outer bank. In equation (2.1) ζ and U represent the lateral migration rate of the channel and the longitudinal velocity, respectively, made dimensionless using a reference uniform flow velocity U_0^*. Under the fundamental assumption that the channel width does not change throughout the evolution process, the equation (2.1) is applied to the channel axis. Therefore, the river spatial-temporal evolution is represented through the evolution of its centreline, which is governed by a non linear partial integrodifferential equation that can be derived geometrically considering that each point along the line migrates along a normal direction according to the law (2.1) (Seminara et al., 2001; Seminara, 2006).

Among the major achievements, the original bend theory based on the HIPS model and its subsequent refinements have allowed predicting the characteristic spatial scales of developing meanders (Edwards and Smith, 2002; Frascati and Lanzoni, 2009), understanding conditions under which a meander can grow towards mature loops (Parker et al., 1983; Blondeaux and Seminara, 1985); reproducing typical meander loop migration rates (Crosato and Mosselman, 2009) and shapes (Seminara et al., 2001; Zolezzi

et al., 2009); investigating the nature of meander instability (Lanzoni and Seminara, 2006); distinguishing stable and unstable bends in field cases (Luchi et al., 2007); and the dominant direction of upstream/downstream 2D morphodynamic influence (Zolezzi and Seminara, 2001; Zolezzi et al., 2005). When coupled with planform evolution models at larger time scales, long-term simulation of meander floodplain development (Howard, 1992; Sun et al., 1996) and assessment of possible existence of chaotic behaviors (Frascati and Lanzoni, 2010) also have been achieved.

However, the HIPS-based approach presents two major limitations: the paucity of the physical basis for the erosion law, particularly on the estimate of the lateral migration coefficient E, and the assumption of constant channel width that underpin a perfect balance between the erosion and depositional processes that occur at the outer and inner bank, respectively.

In recent years, the need to separately address the dynamics of the two opposite meander banks has increasignly been recognized, based on the acknowledging that opposite banks in meander bends are actually characterized by markedly different processes. However, a strong bias towards bank erosion in comparison with accretion is evident in the number of studies. Most studies have indeed been focusing on understanding more quantitatively the mechanisms of bank erosion, and very little advancement in bank accretion is observed.

The processes of bank stability and failure mechanisms are typically incorporated into a bank retreat model where an excess shear stress law uses two erodibility parameters (erodibility coefficient and crtical shear stress value) that account for bank properties (Darby et al., 2007). This has later been coupled with an hydrodynamic model by Rinaldi et al. (2008) describing bank retreat as a complex process due to the combined action of bank failure and fluvial erosion. According to them most critical condition for bank erosion are not reached during the flow peak but during the rising phase between subsequent peaks. Recently Motta et al. (2012a,b) implemented the approach proposed by Darby et al. (2007) into a HIPS-based modelling framework (RVR Meander model proposed by Abad and Garcia, 2006), proposing a phisically-based erosion model to investigate the effect of floodplain soil heterogeneity on the evolution of meandering rivers. Other authors have showed, through a stochastic analysis, the influence of heterogeneity in floodplain erosional resistance on meander evolution (Güneralp and Rhoads, 2011; Posner and Duan, 2012).

In the attempt to overcome the hypothesis of constant channel width that characterizes the HIPS-based model for meanders evolution, Luchi et al. (2011); Zolezzi et al. (2012b) have showed that in sine-generated meandering channels, channel width spatial variation interacts non lin-

early with the curvature spatial variations thus affecting bend instability and, because of changes in flow pattern, increasing lateral erosion, with potential consequences for incipient channel bifurcation. Following a similar approach Frascati and Lanzoni (2013) extended the model to the case of channel with arbitrarily variable curvature.

Only recently Eke et al. (2014) proposed a coupled model between in-channel morphodynamics and bank processes based on the general framework for meander evolution presented by Parker et al. (2011). In this approach, the lateral migration of the retreating and of the advancing banks is modelled using different closure relationships based on different erosion and deposition rates and acknowledging that two different physical processes occur. Under the assumption of quasi-steady condition the in-channel morphodynamic submodel is used to compute the near-bank shear stress that determines bank erosion or deposition depending on the relative difference between the computed shear stress value and a threshold value. By relaxing the hypothesis of constant channel width, this model allows insight into the physical mechanisms of '*bank pull*' and '*bar push*' that govern channel widening/narrowing.

2.3.2 Modelling the interaction between river processes ad riparian vegetation dynamics

Although the crucial effect of vegetation on meandering river dynamics is well known in general terms (see paragraph 2.2), the complexity of the factors that control the mutual interaction between river processes and biological dynamics has so far limited the development of a comprehensive model for meanders development.

Several numerical models have been proposed to investigate the influence of riparian vegetation on the overall river planform evolution. Li and Millar (2011), accounting for the stabilizing effect induced in vegetation on bank stability Millar (2000), have observed reduced lateral migration of the channel due to an increase in bank stability associated with a diminishing in near-bank velocity. Quite realistic and complex morphological patterns have been obtained by Nicholas (2013) who divided the computational grid in active channel and vegetated cells, according to two simple rules for vegetation colonization and removal: if the maximum depth experienced within a cell, over a fixed time period, does not overcome a threshold, the cell becomes vegetated and its roughness increases; on the contrary if a threshold velocity is exceeded vegetation is removed (see the example reported in Figure 2.6).

Recently, few bio-morphodynamic model that fully couple vegetation dynamics with river morphodynamics have been proposed by Perucca

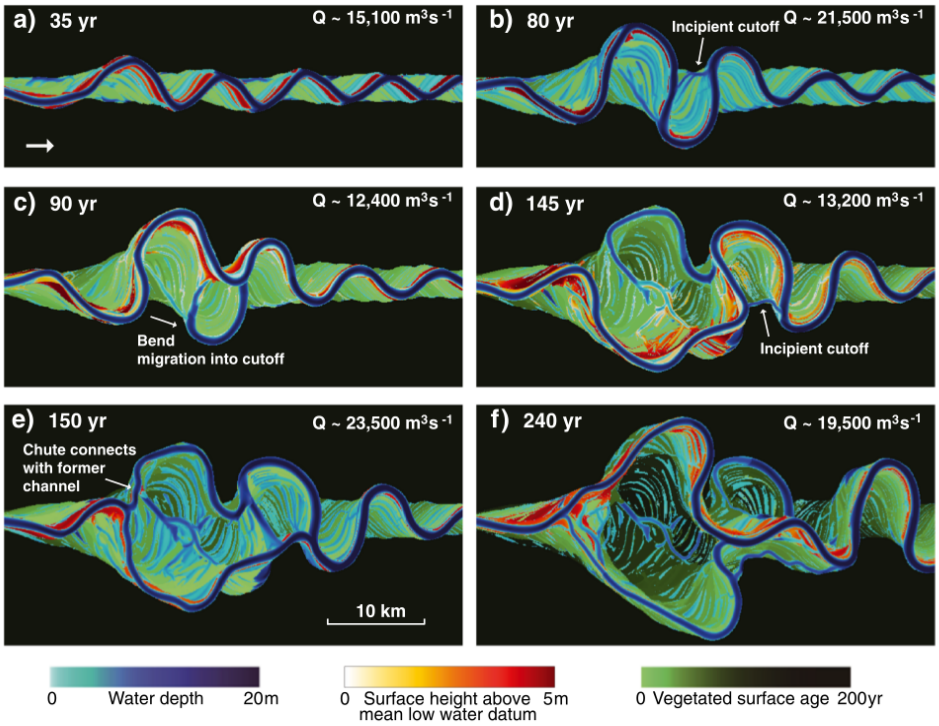

Figure 2.6: Temporal evolution of a meandering rivers from the application of teh model proposed by Nicholas (2013).

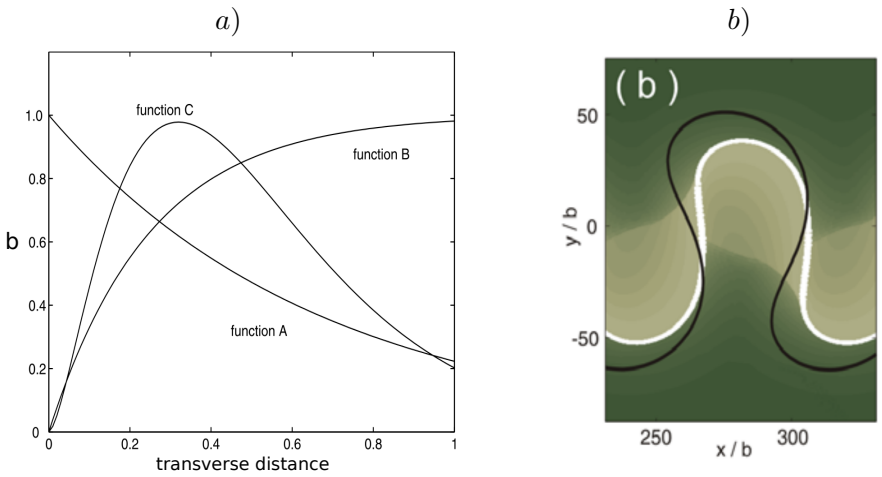

Figure 2.7: Example of a) the three curves that describe biomass density distribution along a river transect (Perucca et al., 2006) and b) result obtained from the application of the model proposed by Perucca et al. (2007) where the black line correspond to the case of constant erodibility.

et al. (2006, 2007); Crosato and Saleh (2011). In the first models river-induced processes are summarized by three different lateral distribution curves of biomass densities along the river transect and the morphodynamic processes are modelled through the physically-based model for meandering rivers proposed by Zolezzi and Seminara (2001). In the first contribution Perucca et al. (2006) have investigated the influence of river migration on vegetation spatial-temporal patterns for different ratios between the time scales of vegetation dynamics and of river planform evolution. A complementary analysis has been performed by Perucca et al. (2007), who modelled the vegetation active role on river meandering planform by relating the lateral migration coefficient E with vegetation biomass density b, such that $E_b = E + q\,b$, whith E referring to the bare bank and q a coefficient to be suitably calibrated.

Minimalist models have provided insight into the physical controls that govern the reciprocal influence between riparian vegetation, river flow and sediments. By using a minimalist approach Camporeale and Ridolfi (2006) investigate the hydrological, river-induced effects on the lateral distribution of vegetation biomass, referring to a quasi-trapezoidal cross-section that simulates the river morphology. In this model vegetation temporal dynamics is accounted for through a dycothomic relation, on the basis of the curves for the maximum vegetation biomass development suggested by Perucca et al. (2006). On the basis of their approach it has been investigated how riparian vegetation dynamics is affected by changes in river

morphology due to the planform dynamics of meandeiring channels (Camporeale and Ridolfi, 2010) and by hydrological processes (Gurnell et al., 2012).

Furthermore, the double-exponential equation propsed by Marani et al. (2013) for describing vegetation biomass distribution along a section transect, even tough derived for tidal marsh, has been adopted to investigate the effect of vegetation on free river bars dynamics (Bertoldi et al., 2014).

2.4 Discussion and Research gaps

In the last 20 years, advances in laboratory techniques and modelling have contributed in deeper understanding of the dynamics at the base of the bio-morphological interactions within the fluvial systems. The scheme presented in Figure 2.8 summarizes the main mechanisms involved in these interactions. Morphological patterns similar to those observed in nature have been reproduced from numerical model simulations, as well as from physical model experiments, allowing to increase understanding of the relations between biotic and abiotic processes inferred from field observations. Moreover, theoretical investigations have explored the scales-dependence of the physical phenomena and quantified the effects of the different controls on these processes (Camporeale et al., 2013; Gurnell, 2014).

Colonization and growth of riparian plants are highly influenced by the hydrology and by the morphology of the river (river-induced processes) throughout moisture and nutrients supply and plants removal. On the other hand, riparian species, playing an active role on fluvial morphology, affect river channel morphodynamic altering erosion/deposition patterns and generating new landforms (vegetation-induced processes). According to the '*fluvial biogeomorphic succession concept*' introduced by Corenblit et al. (2007), the influence that hydrogeomorhic processes exert on vegetation dynamics depends on the stage of succession of the plants, thus riparian trees are disposed from early stage to mature vegetation along the river transect moving far from the channel edge. Analogously, the impact of vegetation on river processes varies because below- and above-ground biomass also change through time.

These mechanisms are crucial at the interface between areas of the river corridor dominated by fluvial processes and areas covered by mature vegetation, where particular riparian species (after Gurnell and Petts (2006) 'riparian enginneers') may initiate pioneeristic landforms, determining the lateral shifting of the margin that separates active channel from river floodplain (Gurnell, 2014).

Since the dynamics described above have been recognized at the base of the accretion processes that occur at the convex bank of meander bends, accurate field observations are required to provide insight in the phenomena that can inform biophysically-based modelling developments. However, data informations obtainable from field measurements presents several limitation in space and time scale. Nevertheless, the combination of these with remote sensing techniques can provide information on the ground and vegetation structure, through LiDAR survey (Bertoldi et al., 2011b), analysis of satellite images (Bertoldi et al., 2011a; Henshaw et al., 2013) and on vegetation spatial coverage distribution throughout time (Zanoni et al., 2008; Garófano-Gómez et al., 2013), providing temporal and spatial extension of field observations.

Overall, the complexity of the dynamics involved in bio-morphological interactions within the river corridor suggests that these processes can be investigated successfully only through a multidisciplinary approach, where field and modelling activities cooperate together. Field data are required to provide insight into modelling approach, while, on the other hand, models elucidates mechanisms that otherwise would be hidden behind the complexity of the real cases (Gurnell et al., 2012; Camporeale et al., 2013).

To date meandering rivers modelling has been mainly focusing on in-channel processes and have only partially investigated the influence of riparian vegetation in fluvial morphology processes within the active corridor. Despite vegetation encroachment at the point bar and plants influence on over-bank erosion/deposition have been recognized as crucial processes in the evolution of the meander bend, they have not yet been included in physically-based models because of a lack of understanding their mechanisms. Therefore, specific field investigations focused on the temporal and spatial evolution of morphological patterns and structure are required to understand how riparian species, river hydrology and morphology are related in the evolution of river meanders. Further research is also required to quantify the effect of tree's rooting in stabilizing river banks and to individuate an efficient method for the calibration of bank migration rate; such results could provide useful information for the validation of models with real data.

A quite accurate description of meander development can be obtained by linking the most accurate solution available for in-channel morphodynamics with erosion or accretion models for the river banks. Under the assumption that river banks migrate with a much slower time scale compared to that of the channel bed, the two processes can be decoupled and described through a hybrid model: analitical for the active channel and numerical for the banks (Seminara and Bolla Pittaluga, 2012). This approach would allow the two banks to migrate according with the flow

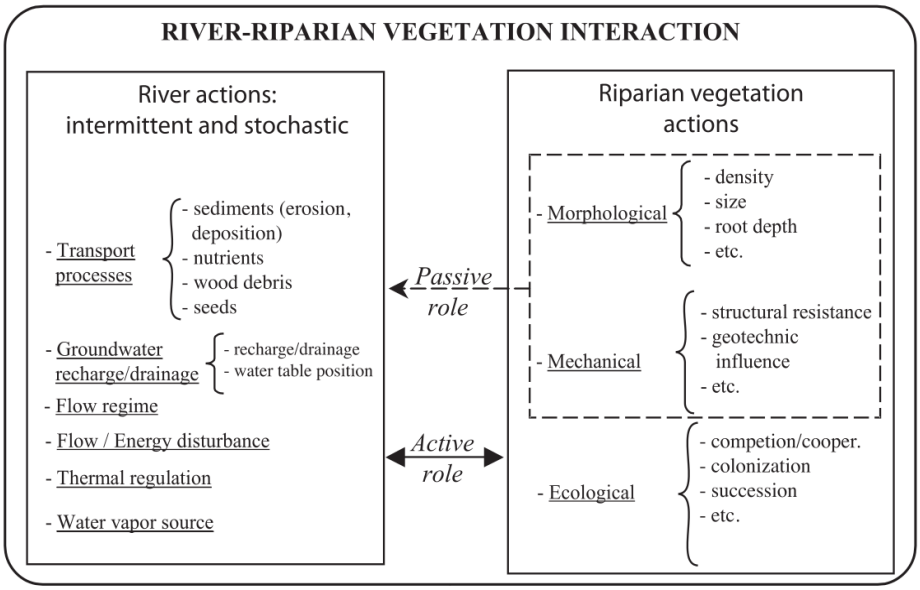

Figure 2.8: Principal interactions between riparian vegetation and fluvial processes (Camporeale et al., 2013).

pattern computed in the channel and therefore under certain condition the inner/outer bank deposits/erodes or, in other cases, both will erode. As a result, on the short term, such type of model could allow to investigate the scale-dependence of channel widening-narrowing process and investigate the key controls of the phenomena. Moreover, deep understanding in river bank dynamics can allow development of physically-based bank migration models that can replace the present simplified closure relationships proposed for both bank advance and retreat.

Research is needed to investigate meandering dynamics under non stationary conditions, when the hypothesis of different evolutionary timescales between banks and channel bed does not hold and channel bed adjusts instantaneously with river margins lateral migration and vice versa. This configuration would be quite interesting because will allow the improvement of accurate bend theory-based morphodynamic models to quantitatively understand the effect of channel width temporal variation on the river flow pattern, thus on river morphodynamics and planform evolution.

2.5 Principal objectives and structure of the present work

In the light of the state of art review, this doctoral research aims to:

i) provide a quantitative description of vegetation and floodplain channel topography patterns in advancing meanders bends;

ii) analyse the relation between these patterns and the interaction between flow, sediment transport and riparian vegetation responsible for their development during bank accretion processes;

iii) explore the key control factors and their role in generating the observed patterns.

The research integrates remote sensing and in situ field observations with mathematical modelling. Because little is known about the bio-morphological interactions that drive bank advance, a preliminary field activity is required to collect information that can provide insight in the physical controls of both river- and vegetation-induced processes. Therefore, the present research combined remote sensed technique with field measurement to investigate vegetation and morphological spatial-temporal evolution. Moreover, a first attempt of understanding the influence of width oscillation induced by self evolving bank on river channel morphodynamics is presented. A simplified bio-morphodynamic model for meandering rivers evolution is then proposed, in which river banks dynamics are treated separately. In particular, inner bank lateral migration is associated with the interactions between riparian vegetation and river processes that initiate pioneeristic landforms within the point bar.

In order to achieve the above goals, the present thesis is organized in four research elements, which outline as follow:

remote sensing analysis (Chapter 3): two types of airborne historical data (air photographs,and Lidar) are investigated to extract information on i) temporal evolution of river channel and woodland extent over a multi-decadal time scale (1966 - 2001) on freely migrating meander bends of the lower Tagliamento River in NE Italy; ii) present channel and riparian morphology and vegetation structure in the same bends; (iii) relations between vegetation and morphology revealed by (i) and (ii);

field observations (Chapter 4): field measurements are conducted on an evolving natural meander bend of the lower reach of the Tagliamento River (Italy), with the aim of i) investigating morphological structure and its association with vegetation patterns to quantify the linkages between the spatial distribution of vegetation, river flows and the detailed local floodplain morphology; ii) supporting the remote sensing analysis (presented in Chapter 3) and giving evidence of their potential for providing information for bio-morphodynamics models;

bio-morphodynamic model for meandering river (Chapter 5): a bio-morphodynamic model is developed to quantitatively describe patterns observed in the previous analysis (Chapter 3,4) in relation to vegetation dynamics. The model links a minimalist approach for the interaction between riparian vegetation and river processes with a non linear analytical model for the morphodynamics of a meander bend, with the aims to: i) investigate the bio-physical controls of inner bank accretion, ii) quantitatively asses the role of river- and vegetation-induced processes on the developing riparian patterns and iii) quantify channel width temporal variation in a freely migrating meander;

instability of river bars under unsteady conditions (Chapter 6): a theoretical model is proposed to investigate the effect on river bar stability of the temporal oscillations of the active channel width as observed in a meander during its evolution; this represents a first step towards a more complete modelling approach compared to that proposed as a first step in Chapter 5.

Chapter 3

Quantifying riparian vegetation dynamics and their interaction with river morphology on two meander bends of the Tagliamento River

This chapter investigates the evolution of the vegetation and morphology on two meander bends in the lower reaches of the Tagliamento River, Italy. The aim of the research is to reconstruct how meander morphodynamics and vegetation relate to one another using historical records to provide a real example that can inform model development.

3.1 Introduction

Historical reconstruction of river morphodynamics depends upon assembling as many historical sources of information as are available for a site, so that information on different properties can be extracted from different source types and integrated. Grabowski et al. (2014) summarise the wide range of historical sources that can provide information on river dynamics including documentary evidence (e.g. land surveys, tax records, agricultural censuses, records from private estates or ecclesiastical sources); cartographic records (map sources covering different themes and at a wide range of scales); other topographic surveys (e.g. channel cross section and long profile surveys); and remotely sensed data (ground, airborne and satellite derived data). However, to achieve the required spatial resolution for the present analyses, the current analysis is based entirely on remotely-sensed data.

The advent of remote sensing techniques has provided an enormous range of data sets of varying spectral and spatial resolution, which have revolutionised the way in which river dynamics can be investigated. Aerial photography provides the longest remotely sensed records, with coverage

over the last 70+ years for many areas. The analysis of historical series of air photographs has supported many analyses of river and riparian environment changes, which have benefited from the high spatial resolution of photographic sources across large areas, although often with restricted temporal resolution (e.g. Johnson, 1994; Shafroth et al., 2002; O'Connor et al., 2003; Beechie et al., 2006; Zanoni et al., 2008; Garófano-Gómez et al., 2013). Since the launch of NASA's Landsat 4 satellite in 1982, satellite data of reasonable spatial (minimum 30 m) and spectral (7 bands) resolution at a potential temporal resolution of 16 days has been available globally. Multi-spectral satellite data has been used to investigate the dynamics of reasonably large rivers (e.g. Bertoldi et al., 2011a; Henshaw et al., 2013) but higher spatial resolution is required for smaller rivers and depends on the collection of relevant multi- and hyper-spectral data sets from aircraft (e.g. Marcus et al., 2003; Whited et al., 2007; Marcus and Fonstad, 2008). Recently, airborne Lidar data sets have become available, providing an ability to investigate detailed three-dimensional properties of rivers and their margins (e.g. Geerling et al., 2009; Bertoldi et al., 2011b, 2013).

In this chapter, two types of airborne historical data are investigated: air photographs (panchromatic and colour), and Lidar. Information extracted from these sources is used to investigate (i) changes in channel position and riparian woodland extent (1966-2001); (ii) channel and riparian morphology and vegetation structure (2001); (iii) relationships between vegetation and morphology revealed by (i) and (ii) for the investigated meanders of the Tagliamento River.

3.2 Study area

The study area (Figure 3.1) is located on the lower reaches of the Tagliamento River, Italy. The Tagliamento is a large gravel bed river in the Friuli-Venezia Giulia region, northeastern Italy. From source to mouth, the river traverses part of the Julian and Carnian Alps and then crosses a wide coastal plain to reach the Adriatic sea, draining an area of 2580 km^2. The upper catchment has an Alpine climate characterized by high precipitation and low temperatures, whereas in the lower reaches the climate is more Mediterranean in character. As a result the flow regime is governed by both snowmelt and rain and tends to show the highest peak flows in spring and autumn, with high discharge variability throughout the year. Moreover, the low human pressures along the river have allowed a relatively natural riparian zone to be retained, reflecting the functional characteristics of the system and its dynamism. The river corridor is char-

acterized by different geomorphological styles of river planform, ranging from multiple thread to single thread patterns (Tockner et al., 2003).

In the river's lower reaches, which are the focus of the present research, the riparian vegetation is dominated by *Populus nigra* (black poplar) (Karrenberg et al., 2003), which regenerates very freely from uprooted trees and pieces of large wood. This is a key process in the regeneration of the riparian woodland along the Tagliamento River and, in the river's meandering lower reaches, has been observed to be associated with scroll bar development as the river migrates laterally (Gurnell et al., 2001; Gurnell and Petts, 2006).

The study reach extends from 45°48'11"N, 12°58'39"E downstream to 45° 47'36"N, 12°58'42"E, through the villages of Ronchis and Latisanotta. It is approximately 3km long and includes two meander bends. The river channel is bordered by riparian forest, dominated by black poplar (*Populus nigra*), and until the early twenty-first century the river in this reach was able to migrate freely. Human activities within the active river corridor, principally agriculture, have changed progressively the land use of the floodplain. In particular, the natural riparian woodland has been cut and new plantations have been introduced. Because of this, the study was restricted to the areas near the main channel that are still covered by natural vegetation (see the inset close up of Figure 3.1). Despite human influence, the meanders in this study reach have been developing until 2002, since when protective engineering structures (i.e. groynes and riprap) have been built to prevent river bank erosion, preserve the cultivated areas and stop the river reaching the levees. Moreover the process of meander migration in the study reach might not be considered completely 'free', because of documented channel adjustment occurring at the same time within the whole single-thread reach of the Tagliamento (Ziliani and Surian, 2012).

3.3 Methods

The methodology applied to quantitatively investigate the mutual feedbacks between vegetation dynamics and river processes (Gurnell et al., 2012) that take place in the inner bank of evolving meanders bend are here reported. Because the research work is comprised of a combination of two remote sensing techniques, we separate the two analysis involved and provide a detailed step by step description of the method applied to the two types of data.

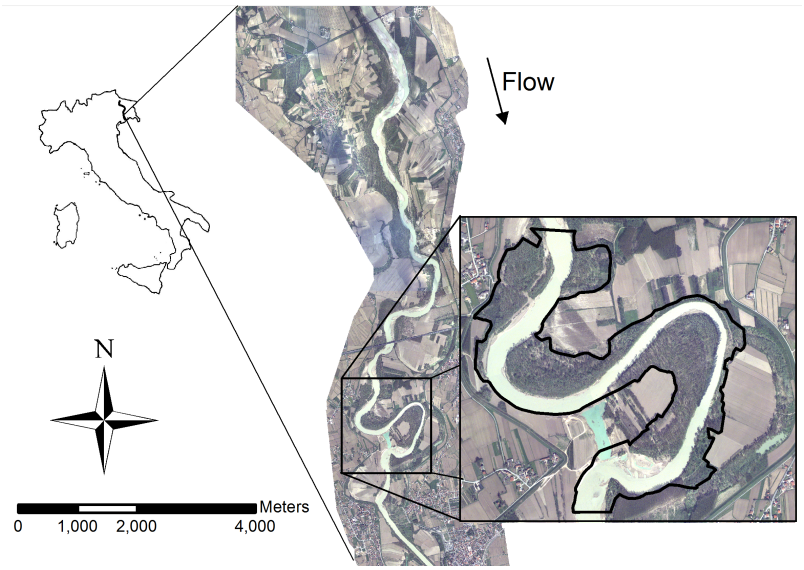

Figure 3.1: The study reach of the Taglaimento River in 2001 with (right) a close up of the study area (thick line).

3.3.1 Historical Sources

To quantify riparian vegetation dynamics and their interactions with evolution of the meandering river morphology, six sets of air photographs were assembled for the period 1966-2001 (Figure 3.2 and Table 3.1). Although more recent images were available, this period was selected because the meanders in the study reach have been able to evolve and migrate during this time and also a Lidar survey was conducted in early April 2001 (from 9 to 13 of April for the study area), providing topographic information following the planform dynamics summarised in the aerial photographs. This choice allowed us to compare spatial-temporal changes of riparian vegetation patterns with the final canopy structure and river morphology at the end of the 1966-2001 study period. The 2001 Lidar survey was conducted by the Autorità di Bacino dell'Alto Adriatico and has an average spacing between data points of approximately 1.6 m.

3.3.2 Data preparation

In order to compare results obtained from the analysis of the Lidar data and the aerial photographs, it was necessary to register them to a common geographical base. The aerial photographs were already geocorrected and registered to the Gauss-Boaga Est datum Roma 1940 projection while the Lidar data coordinates referred to the reference system UTM 33 datum ED 1950. In order to directly compare the Lidar and air photograph data,

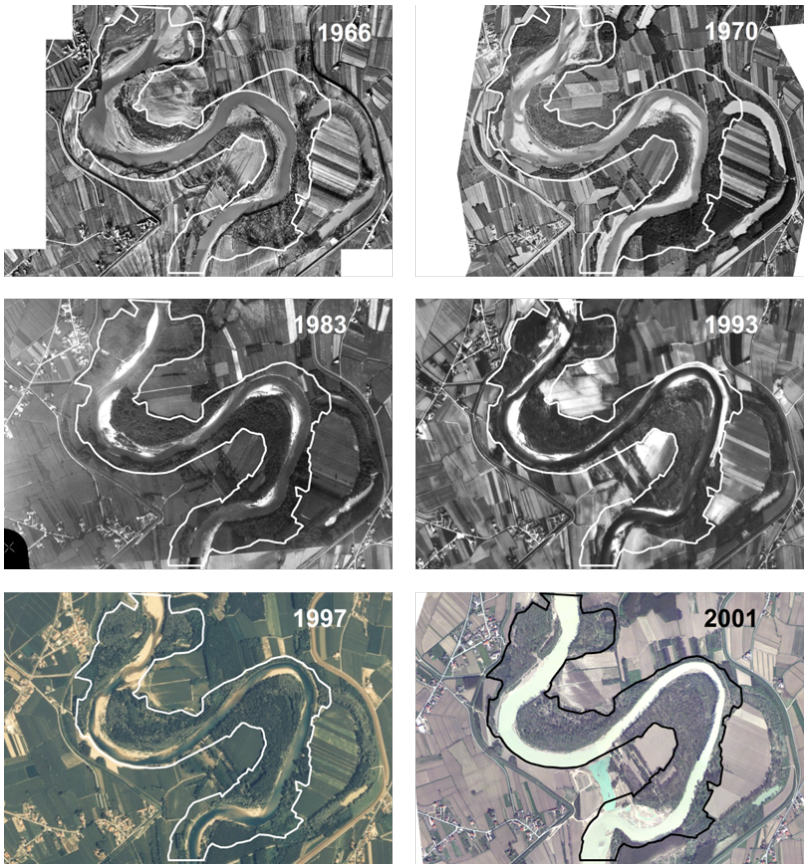

Figure 3.2: Historical data set used in the analysis. Solid line delimitates the investigated area, covered by naturally-colonize vegetation.

Year	Type	Scale	Resolution (dpi)	Pixel size (m)	Date
1966	A,B/W	12,492	800	0.40	30thNov-15thDec
1970	A,B/W	13,312	800	0.41	-
1983	A,B/W	18,045	800	0.55	-
1993	A,B/W	31,807	1200	0.80	May-June
1993	A,B/W	31,807	1200	0.80	May-June
2001	O,C	-	-	0.50	April

Table 3.1: Details of the aerial photograph surveys analysed in this study; A = aerial photo, O = Ortho-photo, B/W = panchromatic, C = colour.

the coordinates of the Lidar data were transformed using the software Traspunto developed by the Italian Ministry for the Environment to match those of the air photographs.

3.3.3 Analysis of Air Photograph Data

High-resolution aerial photographs for different dates (Table 3.1) were used to estimate temporal changes in the spatial distribution of areas that were under water, unvegetated and vegetated within the study area.

A first step was to define the area of naturally-colonised vegetation along the river margin in each of the images. The margins of this area were digitised for each image and then the polygons for each image date were overlain to define the polygon which enclosed naturally-colonised vegetation in all of the studied images (see Figure 3.2). The second step was to classify the land cover within the defined polygon for each of the images. Figure 3.3 summarises the steps involved in this process. The aerial photographs were classified using a supervised pixel-based approach into three classes: vegetation, bare ground and water, using a Maximum Likelihood Classification (MLC) method (Mather and Koch, 2011), where the pixel size conformed to that indicated in Table 3.1 for each image. Most of the images were panchromatic, providing limited information on which such a classification could be based and thus there was the potential for significant misclassification of pixels to occur, although there was also some misclassification associated with the colour (RGB) images.

Training data was carefully selected for each land cover class (water, bare sediment, vegetation) using prior knowledge of the study area depicted in the photographs (Figure 3.2). The selection of training areas for obtaining training data sets can affect the accuracy of the classification (Hubert-Moy et al., 2001; Landgrebe, 2003), although the accuracy of any classification is more influenced by the spatial resolution of the data (Chen and Stow, 2002). Irregular polygons were used to select a large number of pixels in order to give a good representation of each class from which summary statistics could be extracted. Similarity in vegetation and water colour intensity in the panchromatic images prevented good discrimination between these classes, although this was less of a problem with the colour images. However, there was consistently good discrimination of the bare sediment class (Table 3.2). Figure X.3 illustrates a typical frequency distribution of colour intensity for the three cover classes and Table 3.2 provides summary statistics for the colour intensity of the three cover classes in one of the analysed panchromatic images. A maximum likelihood approach was used to separate the cover classes based upon the training data.

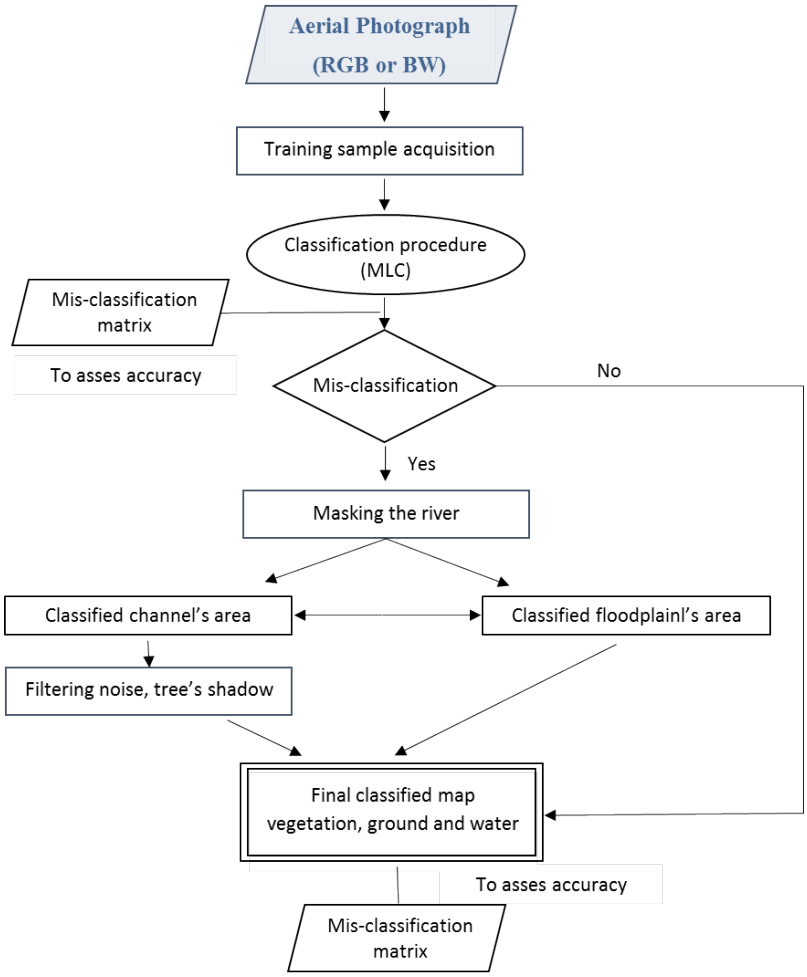

Figure 3.3: Sketch showing the steps involved in the image classification process.

	Min	Max	Mean	Std. dev	Covar
Vegetation	17.00	162.00	59.31	22.99	529.39
Ground	144.00	227.00	214.91	7.56	57.18
Water	96.00	177.00	140.94	10.76	115.70

Table 3.2: Example of the principal statistics computed for the frequency distribution of the vegetation, bare ground and sediments training area extracted from the 1970 panchromatic image (Figure 3.4).

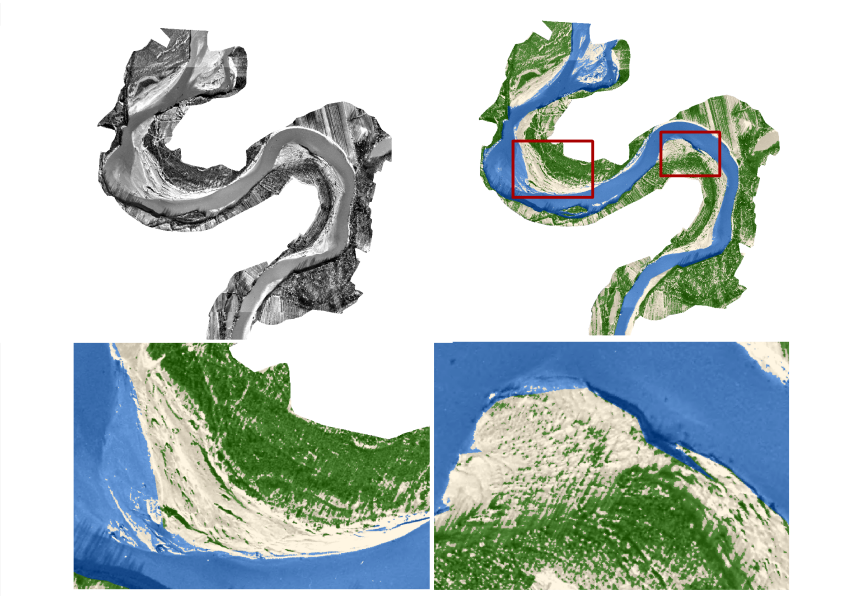

Figure 3.4: Panchromatic photograph (top left), classified photograph (bottom left) and close-ups (top right and bottom right) of the two areas indicated in red on the classified photograph.

Following the initial classification of the photographs, the problem of misclassification was carefully investigated. Two main problems were apparent: the strong similarity in colour intensity between pixels belonging to the classes water and vegetation and also some changes in colour intensity across the area covered by the aerial photographs, particularly in relation to the water areas. The misclassifications were almost entirely confined to the water-covered areas and so the following procedures were used to deal with this problem. The margins of the water-covered area in each photograph were digitised to construct a mask to represent the water area. In addition, a filter was applied to the classified image to sharpen the class boundaries. As vegetated pixels had previously been assigned a value of 1, and water a value of 2, a moveable square, 3x3 pixel, window was passed across the classification and the maximum pixel value within this window was extracted. Figure 3.4 shows a classified panchromatic image following this operation. The close ups of two small areas in Figure 3.4 clearly show the effect of this procedure in identifying the vegetated scroll bars that appear as linear features in the vegetation parallel to the channel margins. For sake of brevity all the results of the classification analysis conducted are reported in appendix A together with the related historical image.

The thematic maps created by the above classification process were

then combined to depict the temporal evolution of vegetation coverage across the study area. The vegetated area varied greatly between images (Figure 3.5) because of the different months in which the photographs were taken (Table 3.1) and thus the different density of foliage that was present. During winter or spring when the foliage is absent or less developed, the area classified as vegetation is less than would be obtained for the same pattern of vegetation in a summer image, because sparse and young vegetation is not easily identified when foliage is absent or under-developed. Therefore, to gain an overall assessment of changes in vegetation pattern through the period covered by the images, the number of times each pixel was classified as vegetation was counted across the six images that were analysed. In this way, pixels that were covered consistently by mature vegetation were distinguished from those where vegetation varied from young or sparse to mature, those where it varied from young or sparse to unvegetated and those which remained unvegetated throughout the six image dates. To achieve this, each classified map was reclassified to give vegetated pixels a value of 1 and other (water or bare sediment) pixels a value of zero. The six map layers were then overlain and summed pixel by pixel to assign a number from 0 (never vegetated) to 6 (always vegetated) in an aggregated map layer which indicated the relative persistence of vegetation through the 35 year period (1966 to 2001) covered by the six images. Lastly, because the channel had migrated laterally for more than the channel width over this period, the water-covered area in the 2001 image was used to mask those pixels whose vegetation cover reflected a change in the position of the pixel from one bank to the other (i.e. they were initially vegetated on one bank, then eroded).

3.3.4 Accuracy Analysis

Evaluation of classification results represents a fundamental step in the classification procedure that can involve different criteria, ranging from qualitative to quantitative approaches (Congalton, 1994). In this analysis we assessed accuracy through two different techniques. In a first attempt, the quality of the classification procedure applied was estimated based on a visual appraisal of the derived map. Essentially, the classified map was compared with the original image to see if the classification appeared to represent the land cover patterns that were apparent on the original image (i.e. comparison between the original and classified image in Figure 3.4). The second stage involved a more objective method, which relates the category assigned to a selected number of points (Figure 3.6) with ground information extracted for the same points – 30 points were investigated for each category giving a total number of 90. The main result of this process

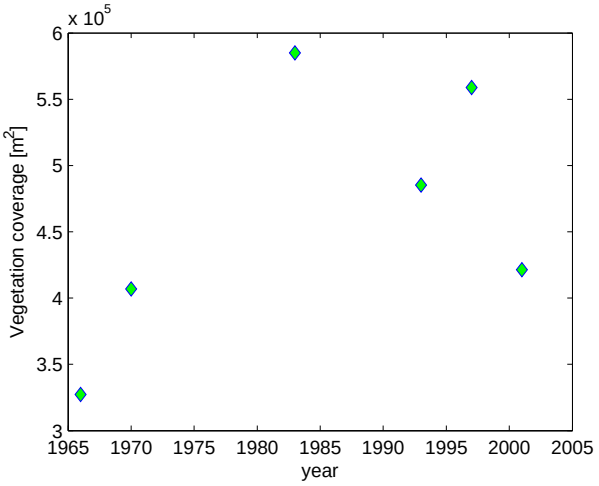

Figure 3.5: The total vegetated area within the classified images at different dates. Oscillations are due to the different periods of the year in which the aerial photographs were taken (see Table 3.1).

is a confusion matrix (or error matrix) that indicates the percentage of cases (pixels) classified correctly (or incorrectly). This allows the accuracy of the classification to be estimated quantitatively. Moreover, from this matrix several parameters such as overall accuracy, user's accuracy, producer's accuracy, omission error, commission error, and kappa coefficient, can be derived in order to assess the goodness of fit between the derived classes and the ground knowledge (Congalton, 1991; Foody, 2002). This technique has been found reliable when applied to vegetation mapping, especially at fine resolutions (Cingolani et al., 2004). In particular, for this analysis, a confusion matrix was computed for both of the maps derived by including or classifying separately the river area (by creating a mask for the channel area) for each image of the historical data set, with the aim of supporting the validity of the latter method (create a mask for the channel area) in enhancing classification accuracy. Since the overall accuracy and the kappa parameter summarize quite well the information provided by the error matrix, these are reported for both processing methods (without and with a mask) for the different image dates considered in this analysis (Table 3.4). The kappa parameter has the advantage that it takes account of the probability of some of the agreements between the original and classified data being due to chance (Mather and Koch, 2011). The example error matrices for the 1966 image (Table 3.3) and the summary of error assessments for all images (Table3.4) show the improvement in accuracy obtained by classifying separately the river channel area and the river floodplain. For the kappa parameter a value of zero indicates

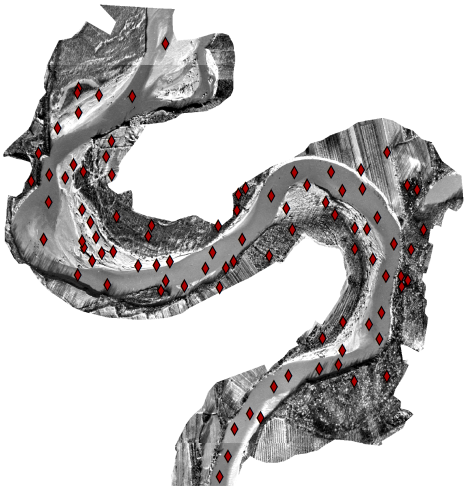

Figure 3.6: Set of points (red diamond) used for computing the confusion matrix. In this example the points lie on the 1966 aerial photograph.

complete lack of agreement between the classification and the test data, while a value of 1 represents the perfect correspondence. According with Montserud and Leamans (1992); Mather and Koch (2011) values of kappa greater than 0.75 and less than 0.4 show, respectively, a 'very good' or a 'poor' classification performance. The entire set of matrixes produced for the accuracy analysis, as well as further information on the computation of the statistics related with the confusion matrix are presented in appendix A.

3.3.5 Analysis of LiDAR data

Analysis of the Lidar data was conducted using the free software FUSION, developed by the US Department of Agriculture, Forest Service, Remote Sensing Applications Center. The analysis extracted properties of the ground surface morphology and the riparian vegetation canopy.

The Lidar data cloud was filtered to detect the ground surface and to generate a digital elevation model (DEM). Fusion uses a hierarchical filtering algorithm proposed by Kraus and Pfeifer (1998) to classify the Lidar points into vegetation and bare ground and then to construct the DEM using the latter points. This technique has been found to be effective where the ground topography is relatively subdued and the vegetation is sufficiently sparse for at least 25% of the returns to reach the ground surface (Kraus and Pfeifer, 1998). A decrease in penetration depth associated with a more extensive vegetation cover and thus the widespread presence of foliage, influences the accuracy of both DEM and canopy structure esti-

(A)	Veg(R)	Sed(R)	Water(R)	Row total
Veg(CL)	29	2	0	31
Sed(CL)	1	27	0	28
Water (CL)	0	1	30	31
Column total	30	30	30	90

(B)	Veg(R)	Sed(R)	Water(R)	Row total
Veg(CL)	25	0	3	28
Sed(CL)	0	16	0	16
Water (CL)	5	14	27	46
Column total	30	30	30	90

Table 3.3: Example of confusion matrixes for the thematic maps derived A) by masking and B) withouth masking the river in the 1966 panchromatic aerial photograph (Figure 3.4). The value proof that the application of the process A) improve the quality of the classification procedure. Veg = vegetation, Sed = bare sediments, R = reference (ground truth) and CL = classified.

	Overall (A)	Overall (B)	Kappa (A)	Kappa (B)
1966	0.96	0.76	0.93	0.63
1970	1.00	0.97	1.00	0.95
1983	0.98	0.72	0.97	0.58
1993	0.96	0.61	0.97	0.42
1997	0.90	0.58	0.85	0.34
2001	0.92	0.92	0.88	0.87

Table 3.4: Overall accuracy and kappa coefficient evaluated to assess the accuracy of the classification processes: A) masking the river channel area and B) including water in the classification of the whole area. For the kappa parameter a value of 0 means absence of agreement between the classification and the test data, 1 represents the perfect correspondence , above 0.75 the procedure performed well and below 0.45 the result should be rejected

mation (Wasser et al., 2013). Both of the required conditions of subdued topography and relatively sparse vegetation cover apply for the study area given the relatively flat floodplain location and an early April survey date, when foliage is absent from the deciduous trees of the riparian forest.

The filtered (i.e. ground surface) points were resampled to a regular 2m grid, by assigning the average value of the returns within each cell, to produce the DEM. A 2 x 2 m resolution was chosen as a compromise between a high map definition and a sufficient number of points within each cell, since the filtered bare-earth points present an average return density of 0.78 per square meter. In order to compare the morphology of different sections of the reach, the longitudinal slope of the floodplain was subtracted from the ground surface elevation. This operation is not trivial when applied to river meanders. As a result of their sinuous course, these rivers have a lower gradient than their floodplain and the gradient changes as meanders evolve. This degree of freedom of meanders (Parker et al., 2007) introduces some difficulties when computing the slope for a meandering river. Moreover, due to their complex geometry, it is not possible to compute the slope as a linear interpolation of the average of the height for different horizontal transects within the active corridor. When the bends migrate laterally they also turn on their axis. The high sinuosity shown by the meander sections under analysis contribute to a reduction (about 2/10000) of the longitudinal slope of the active river corridor, which was estimated around 6/10000. Because of the small longitudinal slope and the short length of the reach, a constant elevation value can be assumed as representative of the elevation of the active corridor. Therefore the median of the elevation frequency distribution for bare sediment (5.54 m) was subtracted from the value of the DEM to generate a DEM of deviations from the median.

The elevation frequency distribution for the study area (Figure 3.7) also shows a bimodal pattern, were the peaks correspond, respectively, to pixels of the DEM which fall into the channel (0 to 2 m range) and those on the floodplain area ($>$ 2 m). This pattern is not representative of the morphology of the entire river corridor, because the Lidar does not penetrate the water and so the true bed morphology of the inundated area is not recorded. Moreover, due to the quite homogeneous colour of the water in the air photographs associated with the 2001 survey, it was not possible to use an optical remote sensed technique to extract the water depth and reconstruct the river channel bathymetry (Marcus and Fonstad, 2008; Bertoldi et al., 2011b). Therefore, the tail of the elevation frequency distribution below 2 m (-3 m when expressed as a relative elevation with respect to the median) was treated with caution in further analyses because of the over-representation of the water surface elevation rather than

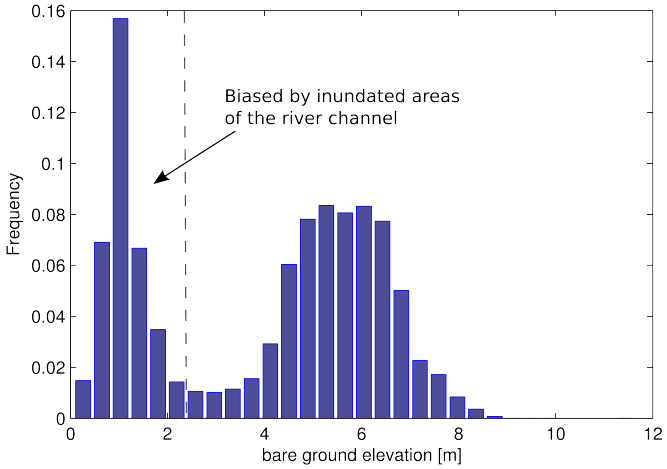

Figure 3.7: Frequency distribution of the DEM within the study area.

that of the inundated river bed within this elevation range. The part of the distribution that exceeds 2 m elevation is almost symmetrical and describes the morphology of the river margins and riparian woodland area.

Information on vegetation structure was extracted by using the points of the raw Lidar data cloud that fell above the bare-earth surface DEM. The vegetation height associated with each point was estimated as the difference between the interpolated ground surface (DEM) and the raw elevations recorded within the Lidar point cloud (see the sketch of Figure 3.8. Because of the low density of points (average horizontal distance between the returns was 0.46 m), these point estimates of vegetation height were organized into a 6m regular grid for further analysis of vegetation properties. The points within each 6 x 6 cell were then used to estimate three properties of the vegetation canopy: height, biomass, and cover density. Vegetation density or cover was computed as the proportion of cloud points within each cell of the 6m square grid that were more than 1.5 m above the estimated ground surface. Introducing this height threshold removed noise from returns close to the ground, while a coarse resolution (compared with the 2m of the DEM) was necessary to have a sufficient number of points within each cell to compute the various vegetation properties with reasonable accuracy. Indicators of the vegetation canopy height and biomass were estimated from the maximum and the average of the point elevation estimates within each cell, respectively. Finally, using the maximum height recorded within each grid cell, it was possible to investigate the distribution of cells with different canopy height ranges.

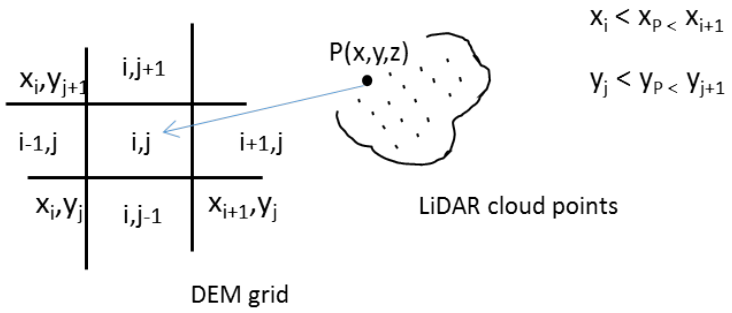

Figure 3.8: Sketch showing the method used to estimate the vegetation height from the raw LiDAR cloud points and the DEM.

The presence of quite steep and high river banks required a new filter operation to avoid classifying ground points that were close to the channel's steep banks as vegetation; since the water surface was well below the bank tops at the date the survey was conducted. This was achieved by estimating land surface gradients from the DEM and generating a new ground surface, where areas showing local slopes greater than 20° were interpreted as steep river banks and so were excluded from the vegetation analysis. This threshold represents a minimum value for the presence of distinct river banks and features exhibiting significantly higher slopes were not met within the study area (Figure 3.9). The above-described thresholds imposed on the surface elevation and on the local slope, allowed the raw Lidar point cloud to be used to extract information on the vegetation canopy structure.

Where it was necessary to compare the Lidar data with that extracted from air photographs, the Lidar data was re-sampled to the same 0.5m grid as the air photographs.

3.4 Results

Analysis of the airborne LiDAR data within the active river corridor highlights interesting properties of the floodplain morphology and vegetation pattern. Having confined the analysis to the unmanaged riparian margin, the information extracted from the Lidar and air photograph data sets can be combined to investigate how vegetation and river processes are related one to another in the planform evolution of meanders.

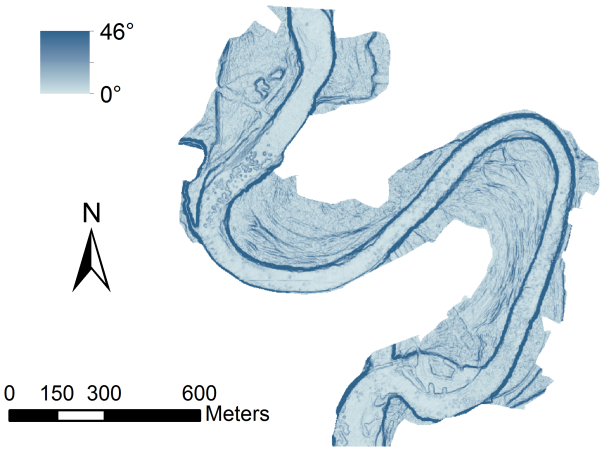

Figure 3.9: Map showing the gradient of the local slopes for the bare ground elevation. High values ($> 20°$) denote the presence of distinct river banks

3.4.1 Morphological structures around a migrating meandering river

The DEM computed from the 2001 Lidar survey reveals a floodplain characterized by a rather complex morphological structure within the study area (Figure 3.10). The river channel is quite well defined by an almost homogeneous grey tone which underlines, as mentioned above, the absence of information on the submerged bed topography. Focusing on the floodplain area which extends from the convex banks, the DEM reveals how the river floodplain is organized in parallel ridges of deposited sediments running parallel to the edge of the convex bend. These ridges are the typical pattern of scroll bars that evolve, with increasing age, into ridge and swale topography (recognizable from the map because of the darker area) as the meanders develop (an example of this structure can be found in Rodnight et al., 2005). The sediment deposition processes that involve the initiation of scroll bars also determine the increasing ground elevation with distance from the river edge. The increase in elevation extends to high elevated flat areas that are largely disconnected from the processes that occur at the river banks and delineate the physical border of the currently active river corridor. These higher areas occur above an absolute elevation of ca 8 m or a relative elevation with respect to the median of ca + 2, 2.5 m.

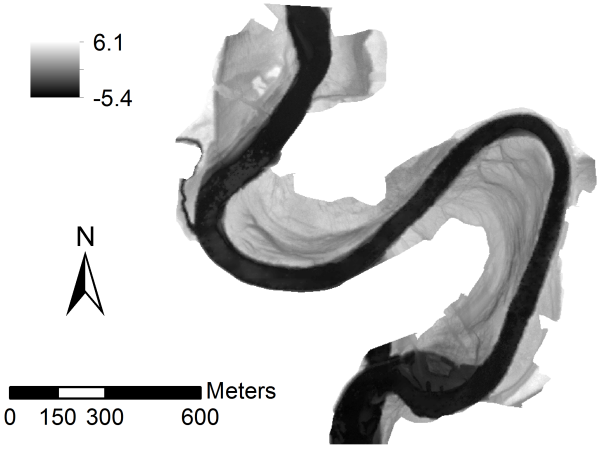

Figure 3.10: DEM detrended for the study area. The submerged channel area is not masked and so the range in elevation represents the full elevation range expressed in the frequency distribution of Figure 3.7. However, most of the topographic complexity in areas where the surface elevation exceeds 2m.

3.4.2 Vegetation structures around a migrating meandering river

Riparian vegetation density within the study area is represented through the spatial distribution of the raw Lidar returns, since this representation indicates all Lidar returns from points above the ground surface described by the DEM (Figure 3.11). An indication of vegetation density is obtained from the spatial distribution of the individual Lidar returns that are above the ground surface as described by the DEM (Figure 3.11). By analysing the Lidar returns within the cells of a 6m x 6m grid, and classifying the largest and average returns in each cell above the DEM surface, broad spatial patterns in vegetation canopy height and biomass are revealed (Figure 3.12 and 3.13, respectively), showing that the vegetation canopy is organized in bands parallel to the edge of the convex river bank, and the height and biomass of each band increases progressively with distance from the river edge, such that the tallest and most mature woodland is located far from the river channel.

The integrated temporal analysis conducted on the historical aerial photographs is mapped in Figure 3.14. This shows a similar spatial pattern in the riparian forest to the vegetation properties extracted from the Lidar data, and indicates that the patterns observed within the riparian forest are strictly related to their age and thus growth stage. Because of the nature of the investigation conducted, the temporal analysis (Figure 3.14) presents riparian structure as a result of the interaction between vegetation and river dynamics along the floodplain throughout the con-

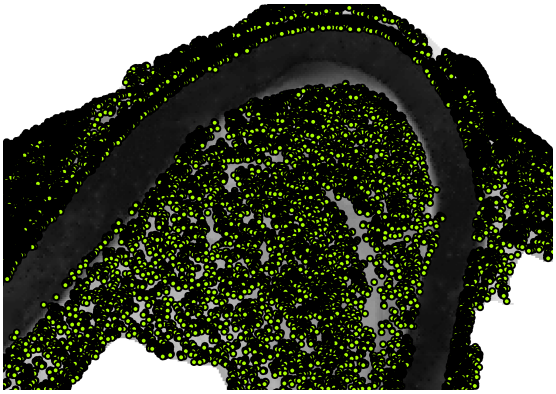

Figure 3.11: Spatial distribution of LiDAR returns (yellow) above the ground surface (grey scale) for a bend of the study area. This allows a qualitative representation of the density of vegetation coverage.

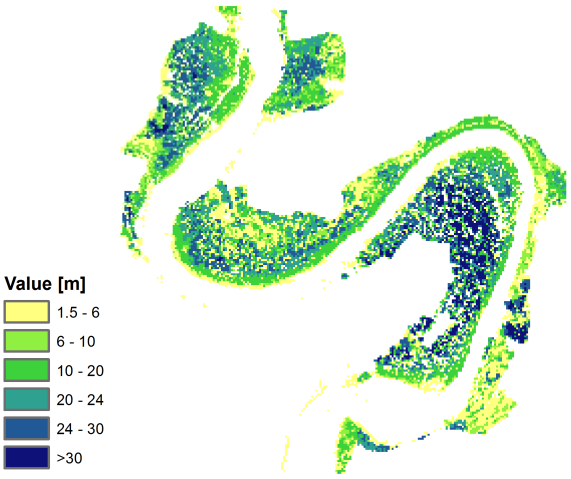

Figure 3.12: Spatial distribution of vegetation canopy height. The height classes are generated from the maximum values of the Lidar returns above the DEM surface within 6m x 6m grid cells.

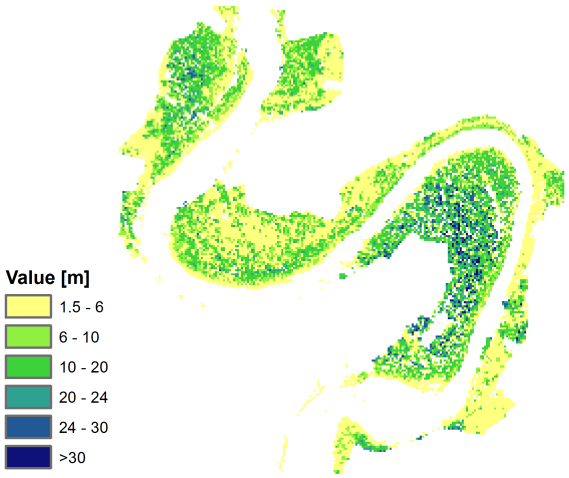

Figure 3.13: Spatial distribution of vegetation biomass, based upon the average values of the Lidar returns above the DEM surface within 6m x 6m grid cells.

sidered period. Specific evidence for this includes dark red patches in the temporal pattern that correspond to colonizing vegetation patches in the historical photographs (e.g. Figure 3.15). The maps obtained for canopy height (Figure 3.12) and temporal dynamics (Figure 3.14), show clearer ridge patterns in the vegetation than the map of vegetation biomass (Figure 3.13) suggesting that the development of understorey vegetation masks the underlying pattern of tree colonisation and growth.

3.4.3 Comparison between vegetation and river morphology

Focusing on natural vegetation and having restricted the study area according to this, we can compare morphological and vegetation structure in order to understand and quantify the role played by vegetation in generating river meander morphology. Moreover, because the river slope is negligible and the height of the canopy was computed with respect to the bare ground, trees and river topography for different sections (downstream or upstream) can be directly compared.

Figure 3.16 illustrates the bed elevation frequency distribution coded according to the elevation distribution of pixels occupied by bare sediments or vegetation (vegetation is discretized according to the height classes introduced in Figure 3.12. The stacked proportional bars (Figure 3.16a) indicate more clearly how the different cover classes are preferentially associated with different elevation ranges than the raw data (Figure 3.16b) (Figure 3.16a). Further discussion on the frequency distribution of different cover type – surface elevation associations will refer to the

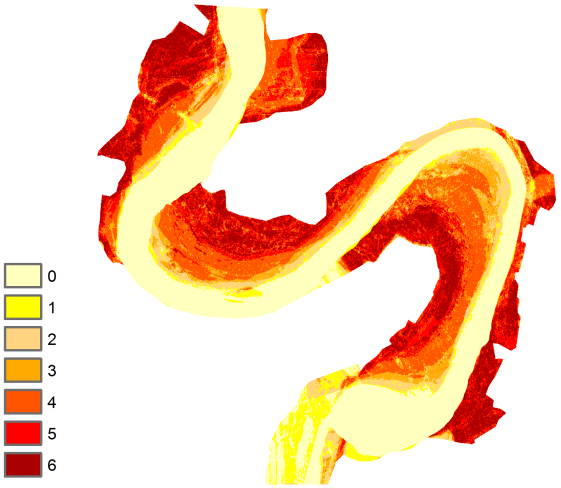

Figure 3.14: Vegetation frequency obtained by overlapping all the classified images (vegetated and non-vegetated pixels): 0 stand for absence of vegetation in a pixel for the whole period considered (1966-2001), on the contrary 6 imply presence of vegetation in all the images analysed.

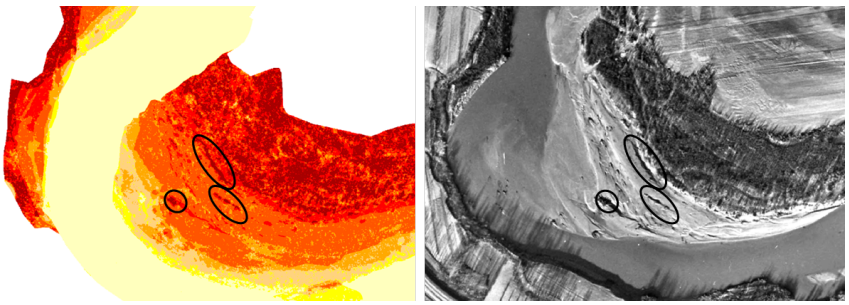

Figure 3.15: Close ups of the upper bend to show how the image analysis captures the initiation and incorporation of scroll bars into the riparian forest. On the left the temporal frequency map of Figure 3.14 and on the right the panchromatic photo for the same area in 1966 (the earliest photographs in the analysis).

portion of the floodplain which has been recently morphologically active (relative elevation ranges from -3 to 2.5 m). The frequency distributions shown in Figure 3.16b and repeated in Figure 3.17 indicate a widely varying proportion of the shortest vegetation height class (1.5 to 6 m). This class has a high frequency relative to almost all other classes at the lowest elevations, where young vegetation is colonising the bare sediment near the low flow channel. However, this shortest class also shows the highest proportions at the highest elevations, close to areas of human disturbance, and also appears in very high frequencies (although lower frequencies than other height classes) in areas of intermediate elevation. The other (taller) vegetation classes, show more distinct trends in frequency with increasing elevation. The second shortest vegetation class (6-10 m) dominates in the zone of the graph where ground elevation is between –2.5 and -0.5 m. Between –1.5 and –1 m elevation, 10-20 m height vegetation shows the second highest frequency, whereas between –1 and –0.5 m, all taller vegetation classes show a high frequency. At elevations greater than –0.5 m, the frequency of 6-10 m vegetation decreases rapidly, whereas all taller vegetation classes show similar frequency. The patterns exhibited by the 6-10 m and taller classes indicate a progressive increase in vegetation height with elevation and the internal variability in vegetation height indicates the complexity of the vegetation canopy, including the influence of the original vegetated scrolls, and the variability in the ability of the Lidar to capture the full vegetation height in early April when leaf cover is very low (this is in agreement with the consideration made by Wasser et al., 2013). However, in general, low estimates of vegetation height (< 6m) are more or less uniformly distributed through most of the floodplain, independently of the relative elevation of the ground, while the Lidar returns from taller vegetation (6 to 30 m) show frequency distribution curves that shift progressively to the right (higher elevation) across the graph shown in Figure 3.17. This behaviour appears clearer when the vegetation classes are merged into three classes (1.5-6m; 6-24m; >24 m) as reported in Figure 3.18. Indeed, this operation contributes, at least partially, to filtering out the uncertainties on canopy height estimates due to the absence of foliage, as already discussed above.

Values obtained from the analysis of vegetation cover temporal dynamics (Figure 3.14) were also associated with the present ground surface (DEM of Figure 3.10) in order to identify any association between riparian vegetation development and the final river morphology. Figure 3.19 shows how the areas representing different stages of the evolution process of the riparian forest (as described by the air photograph analysis) were distributed differently according to elevation of the floodplain. The vegetation classes 0 to 6 represent increasing length/persistence of vegetation

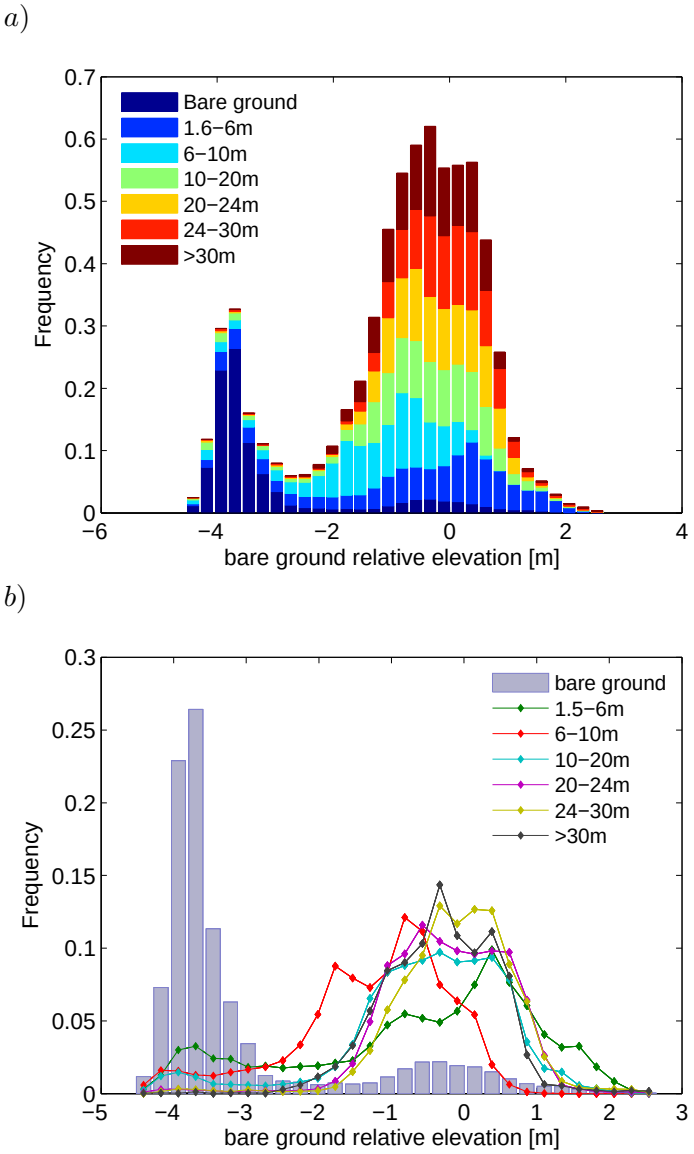

Figure 3.16: Frequency distribution of bed elevation for the study area. (a) with each bar subdivided according to the proportion of pixels occupied by bare ground or vegetation of different maximum height classes and (b) separated distribution curves for bare sediment and each vegetation height class.

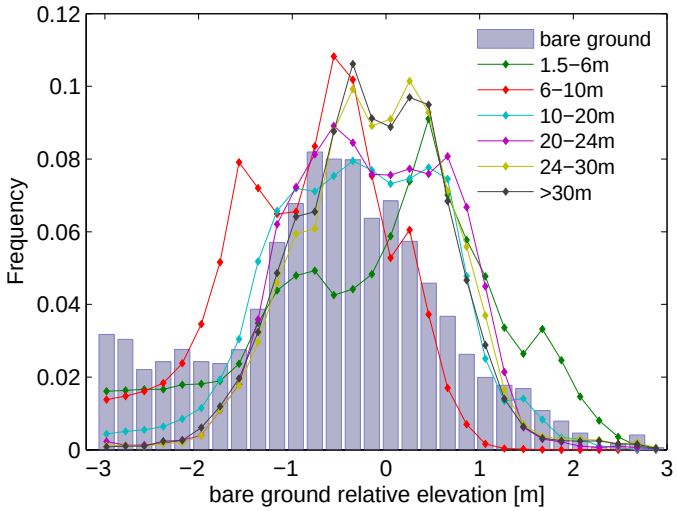

Figure 3.17: Frequency distribution curves of bed elevation for the bare sediment and each vegetation height class within the study area, excluding the area close to and inundated by the river.

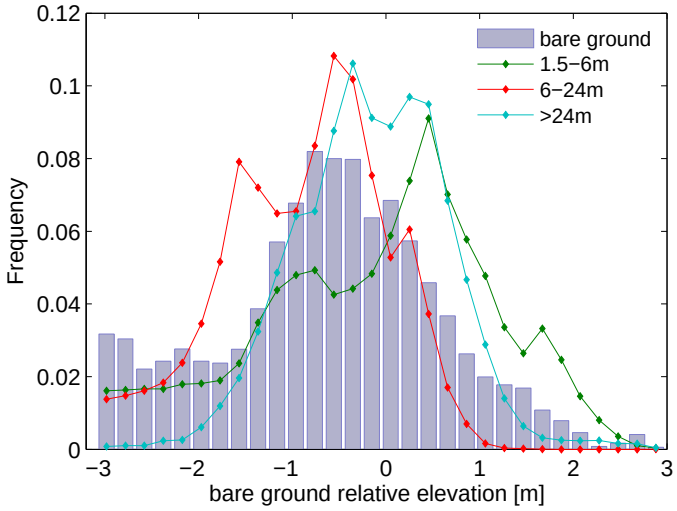

Figure 3.18: Frequency distribution curves of bed elevation for the bare sediment and tree new vegetation height classes with respect to Figure 3.17 within the study area, excluding the area close to and inundated by the river.

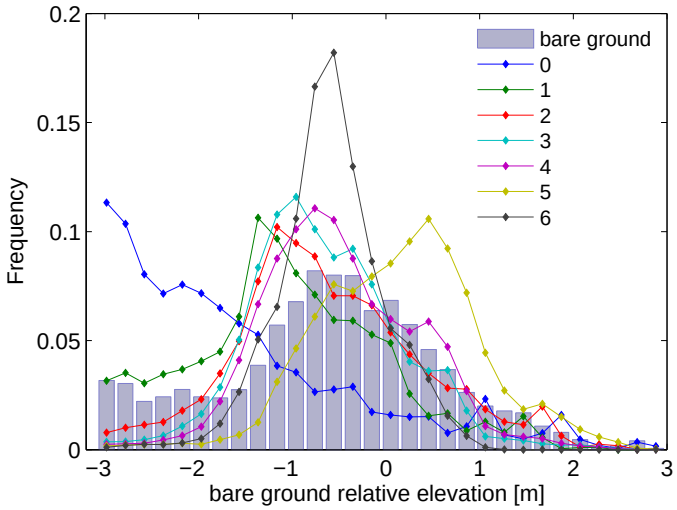

Figure 3.19: Frequency distribution curves of bed elevation for the bare sediments (without the river channel) and vegetation frequency within the study area: 0 means pixel which has never been vegetated and 6 represent a pixel vegetated for the whole period considered. In this plot the channel's area is discarded.

cover from no vegetation in any of the analysed photographs (0) to persistent vegetation cover in all of the analysed photographs (6). The peak of each of the curves for a cover class from 0 to 6 is located in a numerical sequence from the left to the right of the plot, and the frequency of the pixels which did not support vegetation in any of the photographs (value 0) decreases rapidly away from the channel edge as the ground surface elevation increases. In general, areas characterized by the presence of riparian vegetation for most of the dates considered coincide with the highest area of the floodplain, while, areas where vegetation was detected only for few dates are at a relatively low elevation, close to the present river channel. Nevertheless, pixels accounted as vegetated in each of the image analysed (value 6) do not follow this trend, but show a quasi-normal distribution characterized by a peak around the median of the elevation range.

3.5 Discussion

The presence, size and structure of unmanaged riparian vegetation within the study area can be compared with floodplain topography in order to understand how riparian vegetation and river morphology are related to one another in the evolution of river meanders.

Lidar analysis

Results obtained from the analysis of the lidar data show that riparian forest tends to organize in a structure analogous to that observed in the DEM. In particular, by comparing Figure 3.10 with Figure 3.12 a strong relationship between the accretion of the inner bank of the downstream bend and vegetation growth can be inferred, which is in qualitative agreement with observations of the role of vegetation in modifying the flow field and trapping sediments (McKenney et al., 1995; Gurnell et al., 2012; Crosato and Saleh, 2011) and supports the idea that the final floodplain morphology has to be interpreted as the result of a mutual interaction between hydrological conditions, sediments and presence of vegetation (Gurnell and Petts, 2006). However, in the inner bank of the upstream bend the spatial distribution of vegetation shows a less clear pattern than that identified in the downstream bend. Nevertheless, when considering only the morphologically active floodplain within the upstream bend (excluding the stable floodplain/terraces) the vegetation is seen to be aligned in bands parallel to the river edge and with the vegetation height within each band increasing with distance from the current channel position. Overall the vegetation bands are clearly evident and well developed in the downstream meander bend, while this phenomenon is less developed and only clearly evident close to the current channel in the upstream bend. Because of the heterogeneity in tree morphology and age that characterize the canopy of a natural forest (Figure 3.20, Figure 3.21 - Atonarakis et al., 2008), a map obtained by averaging the height of the lidar returns within grid cells may not show a strong spatial pattern (e.g. Figure 3.13). In the present case, this is amplified by the date of the Lidar survey, which was when foliage was absent or at a very early stage of development. Under these circumstances, the Lidar may only rarely record points close to the top of the canopy and the opportunity for the Lidar to penetrate through all levels of the canopy is high.

Image Analysis

Results obtained from the historical analysis conducted using the aerial photographs from different dates (ranging from 1966 to 2001) are consistent with the outcome of the analysis of the Lidar data. In particular, the structure of the present riparian forest and its spatial distribution (Figure 3.12) are reproduced in the map produced by a temporal overlay of classified air photograph images (Figure 3.14). This achievement represents a quite interesting result since it links the existing floodplain morphology and riparian woodland canopy structure with the dynamics of the land coverage through time.

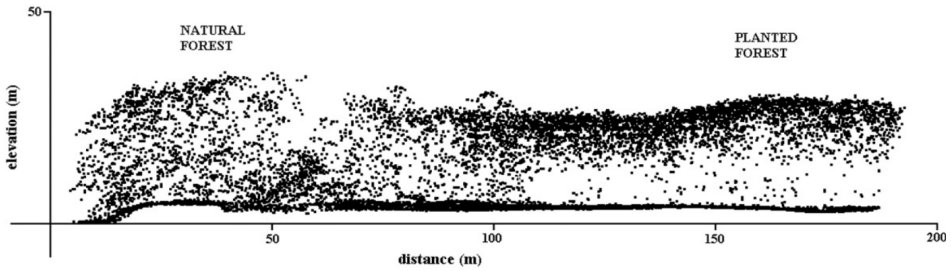

Figure 3.20: Comparison between LiDAR data cloud points for a natural and planted forest (Atonarakis et al., 2008).

Figure 3.21: Example of vegetated ridges and bare swales. Inner bank during the early spring (March), meanders reach of the Taglaimento River, Italy.

Bridging temporal dynamics with the present (2001) morphological and canopy structures

The existence of a relationship between vegetation height and coverage and ground elevation suggests that riparian vegetation influences the processes of deposition of fine sediments, increasing the elevation of the local area (vegetation peak distribution in correspondence of relative elevation higher than -1 m).

Furthermore, the similar pattern shown by the vegetation distribution curves derived (both for canopy height and vegetation dynamics) and the bare sediments (defined as non-vegetated area/pixel) within the inner bank (-2 to 2.5 m) suggests that the morphological structures generated from the interactions between sediments and river flow are organized in a precise spatial pattern. Considering now the high penetration depth of the Lidar return because of the absence of foliage and the high accuracy of the classification performed, that allowed bare ground beneath the trees to be well-detected (see the example of Figure 3.4), the morphological behaviour and associated vegetation development seems to quantitatively support field observations on meandering floodplain structures (Nanson, 1981; Hickin, 1984; Shankman, 1993) that have described the presence of tree-cored ridges with intervening bare swales (as seen in the picture of Figure 3.21).

Moreover, the apparently anomalous pattern that characterized the distribution curve of pixels accounted as vegetated throughout all of the dates considered is probably related with the presence of uprooted wood or pioneer plants presented on the bare gravel of the point bar at the earliest stage of the analysis (see Figure 3.15 and Figure 3.22).

Therefore, by combining the height distribution obtained from the LiDAR analysis with the patterns of vegetation persistence from the analysis of the historical photographic images, it is possible to identify three zones within the study area: the river channel area, the forested area and an intermediate zone that bridges the other two through the initiation and development of scroll bars (Figure 3.23). The three zones can be associated with the type of interactions that take place between sediment flow and woody vegetation. The first (river channel) zone represents the area of the floodplain close to the river channel where, because of consistent solid transport, high tangential stress and frequent anoxic conditions, woody vegetation is presented only as small bushes or is totally absent. The second (forested) zone is characterized by stands of mature trees which stabilize the terrain and interact with the flow field during flood events increasing the deposition of sediment across the land surface in a reasonably extensive way and inducing a general increase in land surface elevation.

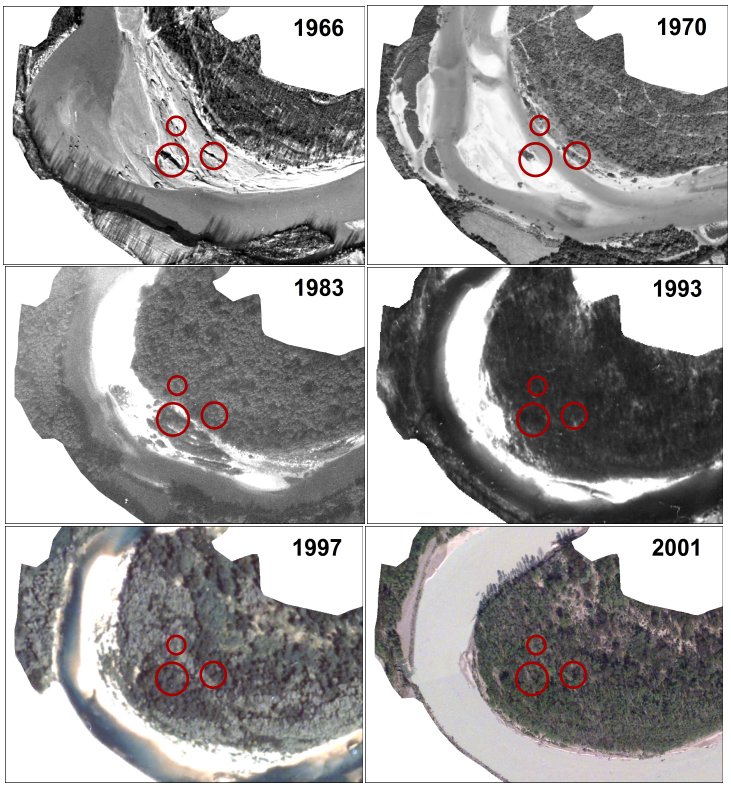

Figure 3.22: Evolution of woody debris and pioneer species through the time period considered in the nalaysis (1966-2001).

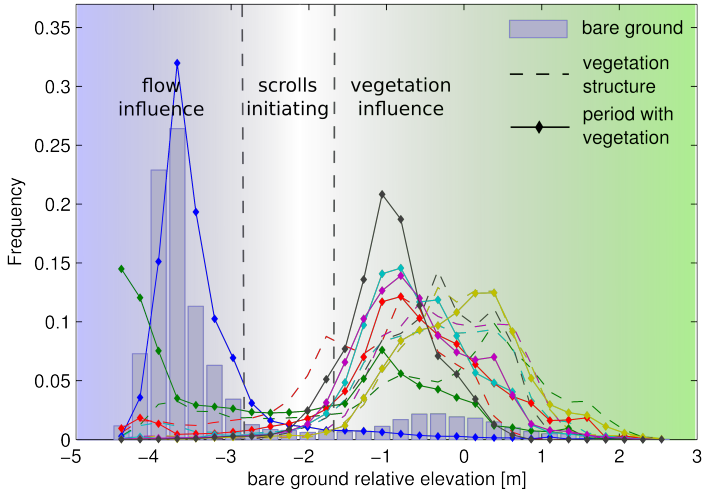

Figure 3.23: Frequency distribution for bare ground (bars) and canopy height (dashed lines) from Lidar data for 2001, and vegetation persistence between 1966 to 2001 (solid line) with respect to the relative elevation of the floodplain within the study area in 2001. The figure is effective in convey the existence of different area of influence characterized by different physical controls: flow (blue area) and vegetation (green area) dynamics.

These two zones are connected through a highly dynamic buffer area, where the mutual interaction between riparian tree species, river flow and sediments is patchy, initiating scroll bar features that trigger accretion processes of the convex bank. This interaction is initiated by the deposition of entire uprooted trees and pieces of wood that become aligned parallel to the river and then sprout to form ridges of shrubs that form areas of high flow resistance and surface roughness (Gurnell et al., 2001).

Finally, it has to be remarked that this section of the Tagliamento River underwent notable channel adjustments (i.e. narrowing and incision; see Ziliani and Surian, 2012). The observed interactions between riparian vegetation and evolving meander morphology might reflect also these processes of channel adjustments together with meander dynamics. Therefore we argue that the quantitative expression of the observed floodplain vegetation and topography patterns may differ from those that might be observed in the case of a freely evolving meandering stream. Nevertheless, the proposed analysis appears to clearly highlight the existence and main features of the three different biophysical zones (river channel area, forested area and an intermediate interaction zone) that characterize the accretion process of meander bends.

3.6 Conclusions

This work has applied remote sensing and image analysis techniques to investigate the relationship between vegetation and river morphology in the evolution of two river meanders. Analysis of Lidar data collected in 2001 has highlighted a strong correspondence between riparian canopy structure and geomorphological features within the floodplain area. In particular, vegetation cover has been found to be distributed in bands according to a ridge and swale pattern, typically initiated by scroll bar formation, which characterises the topography of the convex bank. Moreover, the analysis performed to investigate temporal changes in the extent of vegetation related with river channel lateral migration has further supported the necessity to interpret the final river morphology as the result of a two-way interaction between vegetation pattern dynamics and river processes. The outcomes of the two analyses show that the influence of the river diminishes while the effect due to the presence of trees increases with distance from the contemporary channel edge and this behaviour encompasses a buffer zone where the accretion processes take place. With this analysis we demonstrate how the combination of two different types of remotely sensed data: Lidar and and air photographs can provide important information on the processes of accretion at the inner bank, when applied to the scale of individual meander bends. The analysis can be extended by including the relevant hydrological processes that drive the interaction and associate them with the geometry of the structures observed within the floodplain to investigate the scales of the physical phenomena that are involved.

The present work constitutes a further step in understanding the still not clear biophysical controls of the accretion processes in meander evolution and provides information to support future research in developing bio-morphodynamic models for meandering rivers able to investigate processes of chute cut-off.

Chapter 4

Riparian wood structure and floodplain topography: field measurements in a freely evolving meander bend of the River Tagliamento

The present chapter presents the results of field measurements conducted in a natural meander of the lower reaches of the River Tagliamento, Italy. The aim of this work is to support the findings of the remote sensing analysis (presented in Chapter 3) and to give evidence of the potential of this analysis for providing information for bio-morphodynamics models.

4.1 Introduction

In the last 15 years, field observations have revealed the interactions between riparian vegetation and fluvial processes within the active river corridor, highlighting how these processes are rather complex when investigated at the local scale. At a macro-scale, presence of vegetation along the river edges influences river size and planform evolution essentially by strengthening sediments and modifying river bank stability (Toledo and Kauffman, 2001; Micheli et al., 2004; Allmendinger et al., 2005; Pizzuto et al., 2010). Field work conducted at a smaller spatial scale, has suggested that individual plants or vegetation patches, including wood debris, can trap and stabilize sediments, initiating scroll bars and pioneer landforms (Gurnell et al., 2001, 2005; Corenblit et al., 2009). Moreover, the retention of soil moisture together with organic matter facilitates plant growth or new plant establishment leading to the formation of stable vegetated landforms that determine bank development. In meandering river systems these feedback processes take place within the exposed sediments of the emergent bar in the low flow channel where vegetation species may colonize the exposed sediment (Gurnell and Petts, 2006). Moreover, a

direct relationship between fluvial disturbances (flow events) and the persistence of vegetated landforms exists, for which the longer the pioneer landform evolves and the vegetation establishes the higher the magnitude of the flood event required to remove it or to modify the advancing bank morphology (Corenblit et al., 2007; Gurnell et al., 2012).

Furthermore, analysis of historical sources, particularly information acquired by remote sensing techniques, has revealed temporal dynamics that were previously inferred from field measurements (Zanoni et al., 2008; Garófano-Gómez et al., 2013) and has allowed field analyses to be extended across large areas (Bertoldi et al., 2011a). Conversely, field investigation may support interpretation of analyses of remotely-sensed information (Bertoldi et al., 2011b) and may provide information on physically based relationships involving vegetation dynamics that may then be used to improve bio-morphodynamic models (Perucca et al., 2006, 2007; Crosato and Saleh, 2011). We conducted a field measurement campaign on an evolving natural meander bend of the lower reach of the Tagliamento River (Italy), with the aim of investigating morphological structure and its association with vegetation in order to quantify the linkages between the spatial distribution of vegetation, river flows and the detailed local floodplain morphology. The aims of the analysis are:

i) to detect and quantify the properties of riparian vegetation associated with the accretion process of the advancing bank of a natural meander bend;

ii) to explore relations between flow, vegetation, and sediment transport as potential controls on the observed topographic and vegetation patterns in the advancing channel bank;

iii) to quantify the interlinked processes of opposing bank advance and retreat (accretion and erosion) in an active meander bend over a decadal time scale;

iv) to support the findings of the remote sensing analysis concerning vegetation/topographic structures along the accreting bank with ground data.

4.2 Site choice and Description

Field measurements were conducted in an evolving bend of the lower Tagliamento River, north-east of Italy. In particular, in order to collect data that could be used to rigorously support the remote-sensing analysis presented in the previous chapter, fieldwork should preferably have been

located on the same two meander bends as were analysed in Chapter 3. Unfortunately, there were several constraints that prevented the collection of relevant field measurements at the same two bends utilised in the image analysis. In particular, river engineering interventions implemented in 2003 now protect the outer bank of the upstream bend from erosion, and much of the natural forest within the study area has been replaced with poplar plantations. For these reasons, a site for field measurements was chosen that is located approximately 1km upstream of the original study area, where considerable bend evolution has occurred since 2001. Assuming that the original study area and the upstream site present analogous environmental conditions (Karrenberg et al., 2003) and comparable morphodynamics behaviour, since they have similar planform and channel gradient, fieldwork was conducted on this upstream site to investigate, at the local scale, floodplain and vegetation canopy structure in the inner bank of an evolving meander. In this reach the interaction between sediments and vegetation, particularly black poplar, leads to the formation of pioneer landforms (Gurnell et al., 2005), providing an appropriate field location for investigating these interactions which have been found to play an important role in the evolution of river morphology (Nanson, 1981; Gurnell and Petts, 2006).

The sinuosity of the surveyed bend is about 1.3, which would imply a 'sinuous', rather than 'meandering' channel pattern according to Church (1992). Nevertheless, the expression 'meander bend' is used within the present work for consistency with the wording often used within meander modelling literature.

At the study site, interactions between river flows, sediment dynamics, and colonisation and growth of vegetation, lead to the presence of three distinct zones on the inner bends of freely-developing meanders: (i) a lower zone on point bars, characterized by bare sediments, which often shows extensive deposits of wood and uprooted trees; (ii) an upper zone of mature riparian forest that extends across the floodplain; and (iii) an intermediate and transitional zone that is mostly covered by shrubs and young trees (Figure 4.1 and Figure 4.3).

The coexistence of alpine and mediterranean climate regimes within the Tagliamento basin leads to a flashy pluvio-nival flow regime characterized by very variable flow with rapid rising and falling phases (Gurnell et al., 2001; Tockner et al., 2003). The daily peak oscillations in water level recorded with a 30 minute frequency at the Madrisio gauging station (reported in Figure 4.2 for the period 2001, 2004-2014) illustrate the flashy character of water stage of the Tagliamento river near the study site. This station is part of the river basin monitoring network of hydrometric sensors and it is managed by the Protezione Civile and Ufficio Idrografico of

Figure 4.1: The study area chosen for field investigations, depicted in the most recent aerial photographs (2012).

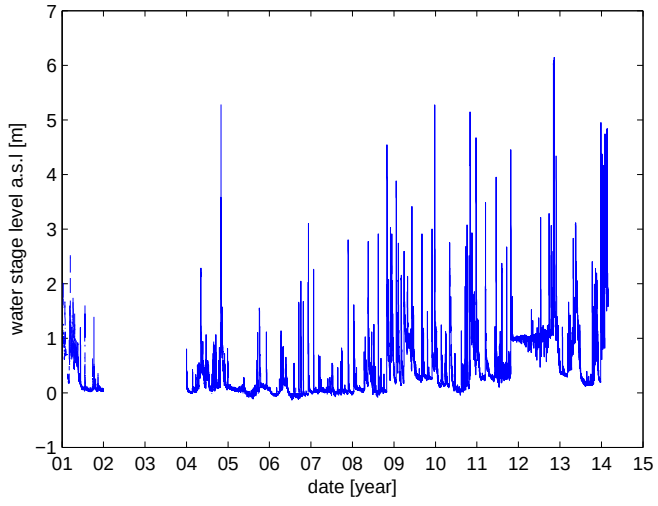

Figure 4.2: Water levels recorded at the Madrisio station (Figure 4.1) since 2001.

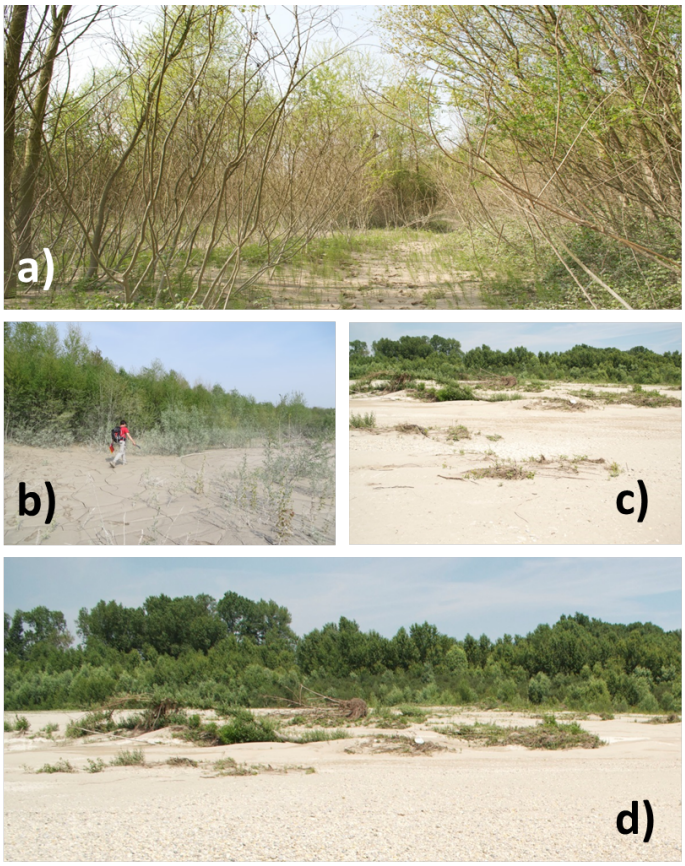

Figure 4.3: Areas under different ages and densities of vegetation within the study area: a) mature vegetation at the highest elevations of the inner bank; b) shrubs located towards the upper part of the point bar; c) deposited wood and uprooted trees on the middle to lower elevations of the point bar; d) exposed, bare sediment towards the toe of the point bar with deposited wood and trees, and then developing woodland at increasing elevations in the background.

the Friuli Venezia Giulia region. Information on the water stage time series is used in the present work, because the complex morphology and the high dynamicity of the river have prevented the development of a reliable discharge rating curve.

4.3 Material and Methods

A combination of topographic surveys, measurements of tree dimensions and age, and analysis of historical flow records allowed relations between the landforms that characterize the accreting bank and flow disturbances to be explored (e.g. Corenblit et al., 2009).

Topographic survey

Information on ground surface elevation was collected for transects perpendicular to the river edge within the inner bank, using a Leica differential GPS (model GPS1200+) and a Leica total station (model TCR705). We applied the RTK (Real Time Kinematic) technique wherever the portion of sky above the instrument was large enough to catch a consistent number of satellites signals, and where these conditions were not met we performed the measurements using the rapid static GPS method. Therefore, the 3D positions of the points that lie on the bare sediments of the point bar were collected using the differential technique (RTK), which provides rapid and accurate (within 1-2 cm) measurements. In contrast, the survey of the ground topography beneath the mature forestry was carried out using the total station. In order to combine data from these two sources, common control points were surveyed. Surveys of each of these common points lasted between 5 and 10 minutes and the huge amount of measurements collected during this time interval (order of 1000) were then post-processed using the Bernese GNSS data processing software developed at the Astronomical Institute of the University of Bern, AIUB (Dach et al., 2007) in order to enhance accuracy up to 10-15 cm. These operations allowed extraction of a complete profile of the inner bank from the river edge through the riparian forest and onto cultivated fields on the floodplain. A preliminary operation was required to correct the raw GPS elevation relative to the WGS84 ellipsoid and to obtain the distance from the geoid (orthometric distance), which represents the mean sea level surface.

The same inner bank profile (transect) was extracted from the DEM estimated from the Lidar survey run in the early spring of 2001 (see Chapter 3). Because bathymetry of the wet portion of the river channel was unknown for both the cases considered (section of 2001 and 2014) the bed

elevation was approximatively reconstructed considering that the typical flow pattern of river meanders, inducing scour on the external bank of the bend and deposit at the point bar, generates a nearly triangular shape of the river channel cross-section (Leopold and Wolman, 1960) with outwards increasing lateral slope. However, detailed measurements collected for the point bar during low water stage were used to partly reconstruct the wet portion of the cross section extracted form the Lidar survey of 2001, inferring that the two sections may present a similar channel bed geometry. Because field measurements were conducted only on the inner bank, the outer bank was reconstructed from the elevation extracted from the 2001 Lidar survey, imposing an analogous slope for the cut bank for the two dates (2001-2014). Considering that conditions in vegetation cover and sediments that constitute the river banks have not changed during the time period considered, the latter appears a reasonable assumption. A more complete characterization of the point bar morphology was obtained by surveying other inner bank profiles along the river bend at different distances from the bend apex, each extending from the shoreline to the beginning of the riparian woodland.

The topographic data were collected following the projection system UTM33 datum ETRF2000 (known as RDN) and converted according to the Italian reference system Gauss Boaga Roma 40, est (zone 2).

The entire set of points collected during the field measurements is presented in Figure 4.4, where it is overlain on the aerial photographs taken in 2012 The surveyed points only partly overlay the 2012 inner bank as a result of the strong lateral migration that has occurred in the last two years. However, this operation provides evidence that the survey was geo-rectified properly. In particular, three features were chosen as reference points: two points close to the outer bank of the downstream meander and a small path that crosses the riparian woodland which was used to survey the ground surface and that it is easily recognizable from the aerial photograph (see Figure 4.1).

Estimation of vegetation canopy characteristics

Tree height and age, together with the vegetation density distribution were estimated in order to provide three-dimensional information on the vegetation canopy structure within the study area. In this operation we included only *Populus nigra* (black poplar). Vegetation spatial distribution was estimated in patches that were chosen along the surveyed transect for their homogeneous vegetation characteristics. The plant density within each patch was estimated by counting the total number of trees within a rectangular quadrat whose dimensions were adjusted according to the size

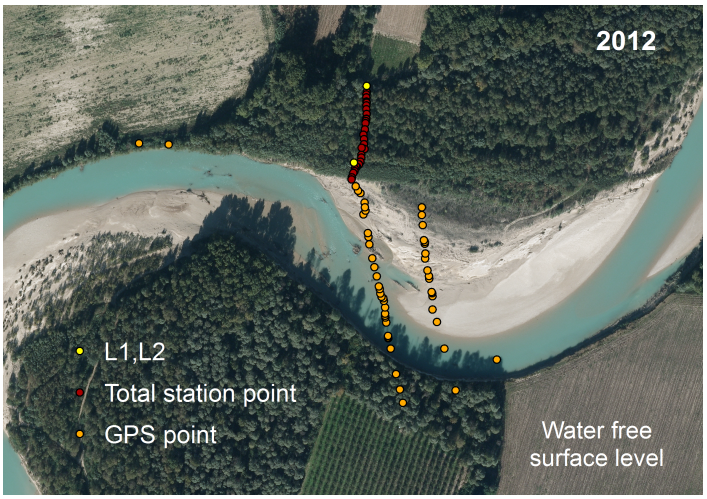

Figure 4.4: Points surveyed during the field workin 2014 superimposed on the most recent aerial photographof the site (2012). L1 and L2 are the two GPS points collected with the static technique used to geo-correct the survey conducted using the total station.

of the trees to ensure a sufficient sample area. Vegetation density values were scaled by the corresponding patch area to provide a density per unit area. Within the area of each quadrat one or more trees, identified as the most mature/tallest, were cored at 1 meter above the ground so that the annual growth rings could be counted to estimate the tree's age, following (Francis and Gurnell, 2006; Moggridge and Gurnell, 2009). The height of each of the cored trees was estimated using a clinometer and their diameter was measured at 1 m above the ground to correspond to the height at which the core was taken. The height, diameter and estimated age of the trees were used to compute a growth curve for Populus nigra at the study site, and to estimate a relationship between tree height and trunk diameter that, together with the growth curve, would allow the height and age of trees to be estimated once the diameter is known.

Analysis of historical hydrological records

Since fluctuations in water stage are fundamental in driving riparian vegetation processes (Mahoney and Rood, 1998; Camporeale and Ridolfi, 2006; Pasquale et al., 2012) the oscillations of the local water level within the period considered in the analysis (2001-2014) were estimated based on the historical water stage records monitored at the Madrisio station, which is located 4 km upstream of the field site (Figure 4.1). The values recorded at this station were correlated with the water level measured at the same

time in the study area during the topographic (4 June 2014) and Lidar (9-13 April 2001) surveys to derive an approximate linear relation between the water stage in the two sections. This approximate relationship allowed a hypothetical water stage time series for the study area to be constructed.

The modes of historical water stage oscillations were also investigated through a Continuous Wavelet Transform in order to explore potential correlations between oscillations related to flow pulses of different intensities and the rates of lateral channel migration observed through the analysis of air photographs.

Simplified analysis of morphological activity

Once the cross section geometry is known and an approximate reconstruction of the water stage time series has been achieved, it is possible to translate the hydrological record into time series of biomorphodynamic relevance. A simplified, quasi 1-D hydraulic modelling approach was used for this, with similar assumptions to those already employed by Bertoldi et al. (2010) to investigate morphological activity in a upstream braided reach of the Tagliamento River. The modelling approach is based on Engelund (1964) and Lotter (1933) and allows the lateral variability of flow parameters across one river transect to be estimated for a given value of the water stage by partitioning the cross-section into vertical strips where local uniform flow conditions are assumed. The above approach can be justified if the following assumptions hold:

- the water level slope is vanishing across the transect (horizontal water surface);
- the longitudinal riverbed slope is constant across the transect;
- the shear stress acting between adjacent vertical strips having different longitudinal flow velocities is negligible with respect to the near-bed shear stress, i.e., with respect to the shear acting between the fluid and a solid surface.

The above method allows the lateral variability of longitudinal flow velocity and local water depth to be estimated across the whole transect for every reconstructed water stage value. Though relying on a series of simplifying assumptions, such information can be used for a first quantitative investigation of the relevant time scales of the processes whereby flow, sediment transport and riparian vegetation interact and give rise to the observed biogeomorphic floodplain patterns.

In order to estimate the time scales of morphological activity, first, the temporal and spatial (across the transect) variability of the water depth

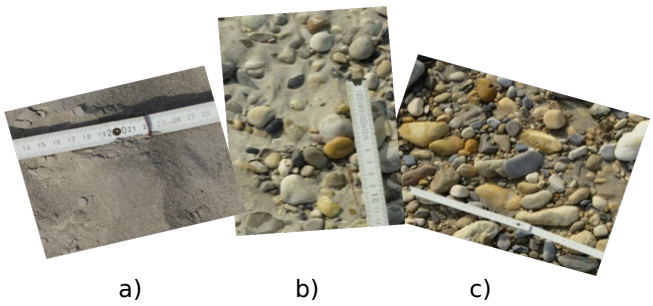

Figure 4.5: Example of sediment grain size surveyed during the field measurements campaign: a) 0.2mm, b) 0.4 cm and c) 2 cm

is computed (i.e., of the inundation dynamics of the different morphological units in which the transect can be conceptually divided - Surian et al., 2009). Second, the lateral variability of the dimensionless Shields parameter θ, which is a commonly used measure of sediment mobility, is computed and can be used as a proxy for detecting thresholds of morphological activity in the system (Surian et al., 2009; Mao and Surian, 2010). In this first analysis bedload is assumed to be the main mechanism for sediment transport, neglecting the influence of riparian vegetation and the role of suspended load. For this reason we set the mobility threshold (θ_{cr}) at the standard value of 0.047 (Meyer-Peter and Müller, 1948). The Shields parameter was computed as

$$\theta = \frac{SD^*}{\Delta d_s^*} \tag{4.1}$$

where S represents the longitudinal slope of the reach evaluated along the channel axis ($S \simeq 0.0009$ in this case), Δ is the relative submerged sediment density (set to the conventional value of 1.65), while D^* is the water depth which was computed as the difference between the free water surface elevation, estimated using the water stage recorded at the Madrisio station, and the ground elevation for each point of the cross section collected during the field work. The diameter representative of the sediment size d_s^* was chosen for the different zones of the cross section in accordance with field observations as 2 cm, 0.4 cm and 0.2 mm (see images of Figure 4.5). The use of * indicates a dimensional parameter.

This analysis is based on three main simplifying hypothesis: (i) the water level time series has been reconstructed through relation (4.3) that is based on only two data points; (ii) the analysis refers to a fixed cross-sectional topography, while the meander bend has been consistently migrating within the considered time period; (iii) the quasi-1D hydraulic

model cannot account for the whole complex hydrodynamic patterns that characterize the flow in a meander bend. Nevertheless, the validity of this simplified approach can be justified for the present analysis, where the aim is to attempt a first quantification of the relevant time and space scales of the process of bend accretion and floodplain pattern development, and not to provide a quantitative detailed modelling of the hydro-morphodynamics of that specific meander bend. The validity is supported by: (i) strong nonlinearities in relation (4.3) should not be expected because of the relatively small distance between the Madrisio gauging station and the study area, and related small size of the additional contributing catchment to the study area with respect to Madrisio; (ii) while the cross-section has been evolving morphologically, it sounds reasonable to assume that its shape and size should not have changed dramatically, with the main expected differences between 2004 and 2014 being an extension of the accreting vegetated floodplain region and an increase in the bed scour close to the outer bend region because of increased channel curvature; (iii) the main shortcoming of the adopted quasi 1D hydraulic model is the impossibility of accounting for transverse flows associated by centrifugal effects and topographic steering that are known to be relevant in meander bends, while the model is however able to describe the outward increase of the streamwise velocity component at least at a first approximation.

Remote sensing

A set of aerial photographs (see Table 4.1), covering a time period from 1993 to 2012, was assembled in order to quantify river channel planform dynamics at the study site. To this aim, river banklines were digitized in each of the aerial photographs and the distance between river banks (inner, outer) for two consecutive dates was used to provide an estimation of the lateral migration rates which were computed as follows

$$MR = \frac{A_i}{L_i}, \tag{4.2}$$

where A_i and L_i represent respectively the area included between the inner or outer bank of two consecutive dates and the length of the shifting bend. Because the most recent aerial photograph available for the analysis referred to the 2012, the present convex and cutting banks were approximately detected on the basis of information gathered in the field and later corrected by using a Landsat image from April 2014. In order to be able to compare the different dates, as for the analysis reported in the previous chapter (Chapter 3), all the images were geo-corrected to a common coordinate reference system: the Italian national projection system Gauss Boaga Roma 40 for the zone 2 (est).

Year	Type	Scale	Resolution (dpi)	Pixel size (m)
1993	A, B/W	31,807	1200	0.80
1997	A, C	28,119	800	0.70
2001	O,C	-	-	0.50
2006	A	18444	600	0.85
2007	A	18084	600	0.86
2009	A	17489	1800	0.26
2012	O,C	-	-	0.21

Table 4.1: Details of the dataset used for the historical analysis. O = Orthophoto, A = aerial, B/W = black and white, C = coloured.

Moreover, evolution of deposited wood into vegetation patches was tracked from the set of available images. In particular we identified pieces of wood deposited in 2001 and followed their evolution through images from different dates until 2012 (the most recent high resolution image available for the area). Later the positions of these features were located in the field and the diameter of the tallest tree within each feature was measured. Furthermore, the DEM generated from the Lidar survey conducted in 2001 was used to obtain information on the initial geometry (in 2001) of the same transect that was surveyed in the field campaign.

4.4 Results

This section presents the outcomes of the analyses in relation to the objectives of this Chapter. Data collected in the field is investigated to quantitatively describing the inner bank structure, including both topographic pattern and riparian forestry characteristics. This is combined with historical hydrological data and remotely sensed data to investigate the temporal evolution of the river banks.

4.4.1 Field observations of topographical and vegetation patterns

Figure 4.6 shows a comparison of the same transect in 2001 and in 2014. Data from 2001 were extracted from the LIDAR survey, while data from 2014 were obtained from field work combining GPS- and total station-surveyed points. As already reported for other meander bends (Nanson, 1980), the collected data for year 2014 revealed an inner bank characterized by a rather complex topographical pattern. The external portion of the transect close to the eroding bank (i.e., approximately between the lateral distances 0 and 120m) has the typical cross-sectional shape for an active meandering channel bend, with a lateral slope that is increasing

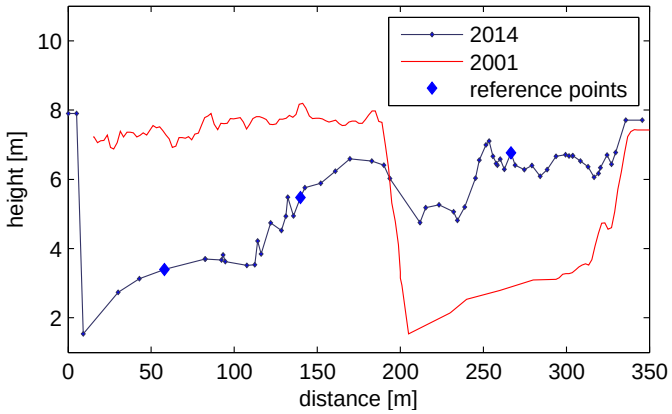

Figure 4.6: Comparison between the cross section obtained from the field measurements (2014) and that extracted from the DEM (2001).

towards the cut bank (e.g. Seminara and Solari, 1998). Further inward, the 2014 transect displays a series of overlapping bed oscillations at two different spatial scales: two large scale oscillations occur at the scale of the wetted channel width: smaller scale oscillations, in the form of a ridge/swale sequence are superimposed and occur in the most inner vegetated region (230-330m) with wavelengths of tens of meters (Figure 4.6). Figure 4.7 presents an enlarged snapshot of Figure 4.6 in order to better highlight the ridge/swale sequence, denoted by R/S. The same features cannot be detected in the 2001 cross-sectional profile, because the inner bank was much less developed and the cultivated, managed land area was much closer to the active river section compared to more recent years (see also Figure 4.15 for an aerial view).

Figure 4.8a and Figure 4.8b show, respectively, the growth curve and the regression relations between tree height and diameter computed using the field measurements. An almost linear relation can be inferred between plant height and diameter, while the growth curve can be used to convert estimates of tree height derived from remote sensing analysis (e.g., from the analysis of LIDAR data presented in the previous Chapter 3) into estimates of vegetation age.

From field observations and the analysis of aerial photographs, riparian vegetation appears to be organized in a hierarchical structure which, according to the tree evolution stage, reflects different spatial patterns (see the qualitative illustration in Figure 4.9). Along the area close to the wet river channel (approximate lateral distance between 120 and 230m) vegetation is mainly composed of dead wood and uprooted trees, while from 230m onwards the ground is essentially covered by riparian wood-

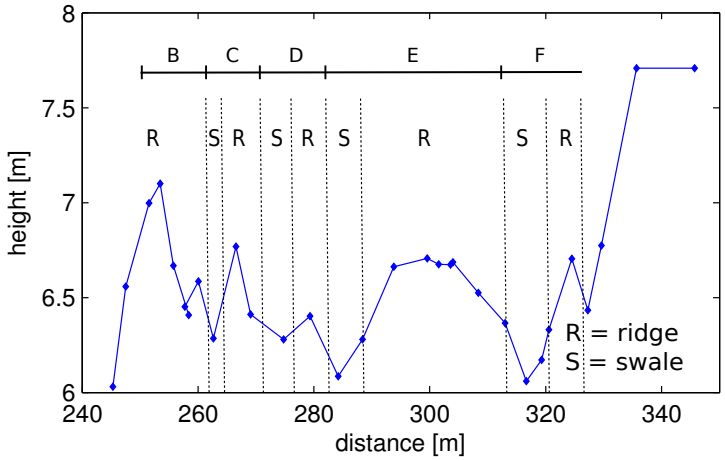

Figure 4.7: Cross section topography of the portion of the study area covered by mature vegetation.

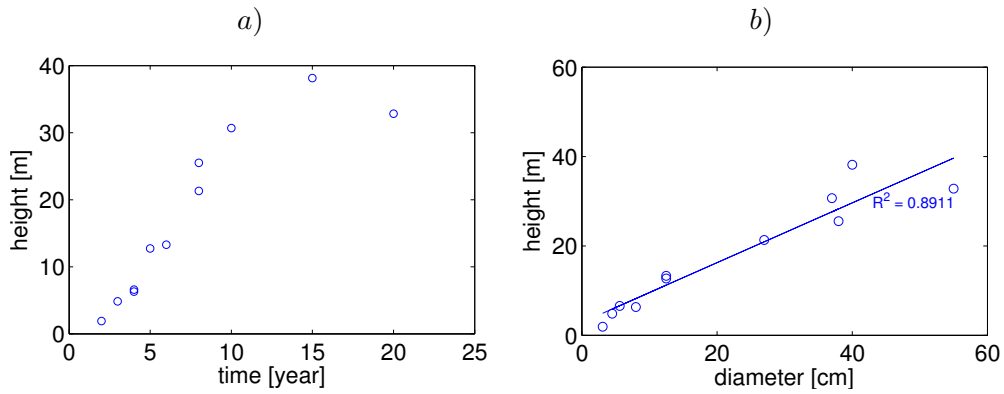

Figure 4.8: a) Growth curve and b) linear regression relationship between height and diameter for the riparian vegetation (specifically P. nigra) within the study area.

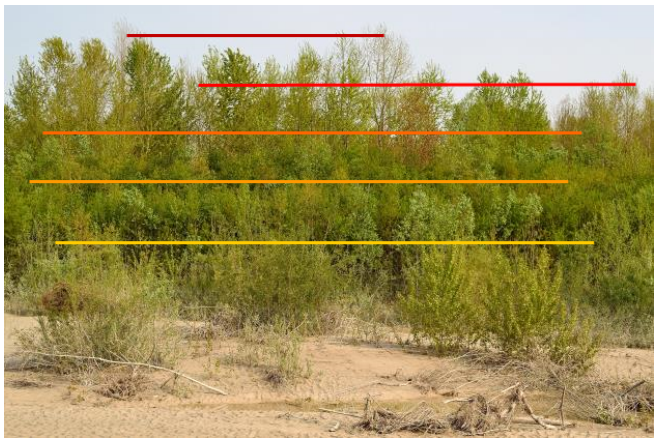

Figure 4.9: Riparian canopy spatial distribution. Vegetation organized in a hierarchical structure with tree height increasing with distance from the river edge.

Diameter Class	Diameter [cm]
1	3
2	7.5
3	15
4	25
5	40

Table 4.2: Diameter of each class used for the estimation of vegetation biomass (Figure 4.10).

land. In the intermediate region, the vegetation is dominated by patches of bushes (trees in their early stage of growth). Moreover, the bushes and trees within the woodland are organized according to their age in bands parallel to the river edge, presenting a density distribution that is different for each band. Figure 4.10 shows the frequency distribution of trees of different diameter (i.e. age) (the value of each class is reported in Table 4.2) for the whole sequence of ridges and swales denoted as B to F in Figure 4.7. A clear difference is evident between ridges and swales, with ridges characterized by a much higher density of larger (greater diameter) trees compared to swales that appear as small channels that are relatively free of vegetation.

Coupling the topographical and riparian vegetation measurements allows quantification of vegetation properties within the meander bend cross section inferred from the remote sensing analysis of the previous chapter (Chapter 3). In particular, and with reference to Figure 4.6, three main zones can be identified, characterized by distinct topographical and vegetation properties: (i) the non-vegetated river bed (lateral distances 0-

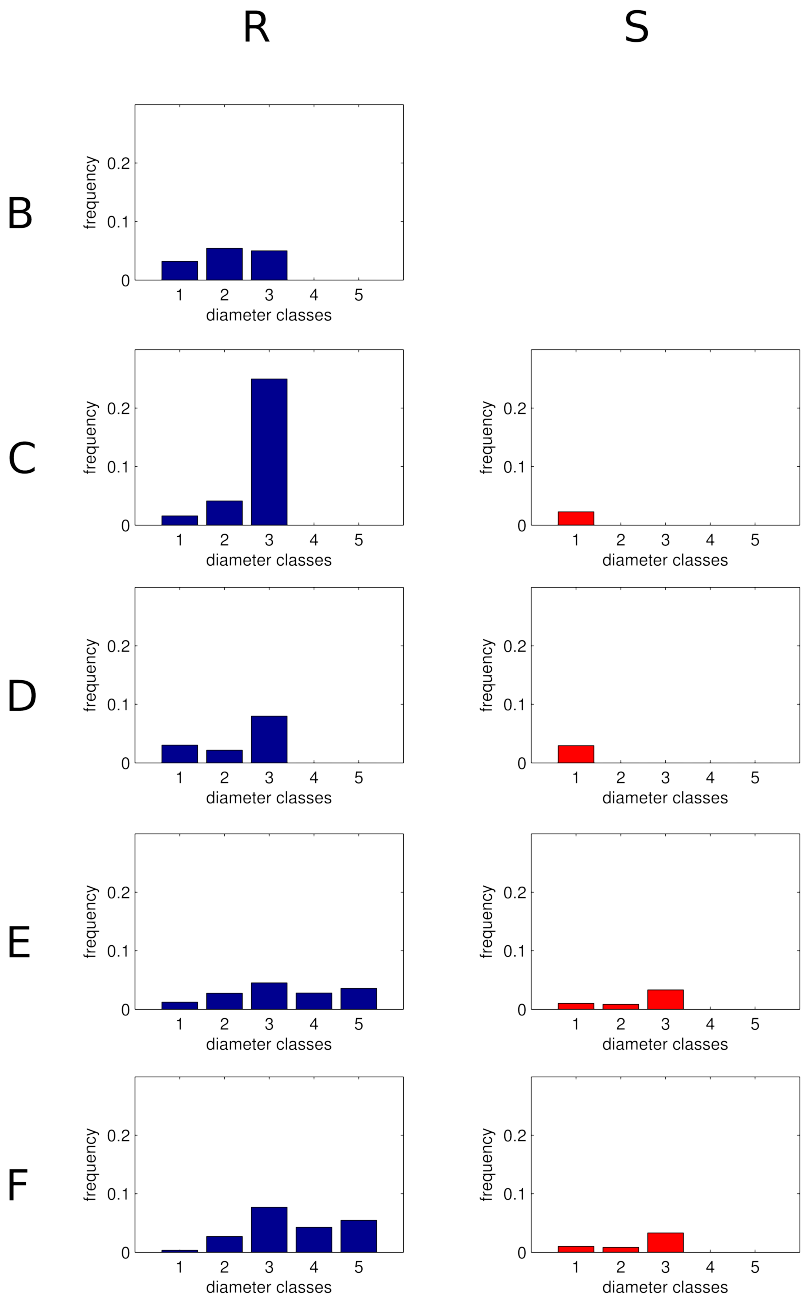

Figure 4.10: Riparian canopy spatial distribution. Vegetation organized in a hierarchical structure with tree height increasing with distance from the river edge.

120m), (ii) the point bar with pioneer plant species, (120-230m) and (iii) the mature forest area (230-330m). The river bed shows a regular profile with outward increasing lateral slope, while the point bar and mature forest portion of the transect are characterized by overlapping bed topography oscillations at two different scales, which are reflected by analogous fluctuations in the age/height/diameter and density of the riparian trees (specifically P. nigra). The point bar is mainly occupied by deposited uprooted trees and colonizing herbs and grasses, while the density of trees in the mature riparian forest is characterized by small scale transverse oscillations that reflect the topographical patterns of ridge/swale sequences (an example is reported in the pictures of Figure 4.3).

4.4.2 Quantitative analysis of the interplay among flow, vegetation and sediment transport

The linear relation derived between the water level $h_{madrisio}$ recorded at the Madrisio station with reference to a local datum and the water level h_{bend} (measured above the mean sea level) in the study area, based on the data collected during the field work and extracted from the 2001 LIDAR-derived DEM, reads:

$$h_{bend} = 1.3756\, h_{madrisio} + 2.1756\ . \tag{4.3}$$

This relation was used to reconstruct an approximate time series of water stage in the study area for the period 2004-2014, i.e. the period for which a continuous record was available at Madrisio. The reconstructed water stage time series is reported in Figure 4.14.

By associating the water levels on the graph of Figure 4.14 with the elevation of the surveyed points on the cross section from the field investigations (Figure 4.6), it was possible to obtain a first quantification of the dynamics of inundation and of morphological activity at the study area. Figure 4.11 displays the 2014 transect geometry (green line; the same as that reported in Figure 4.6) together with the percentage of time, with respect to the 2004 – 2014 period, during which each point of the transect would have been submerged on the basis of the 1D hydraulic modelling approach.

The three different zones previously detected display rather different properties in terms of their inundation dynamics. Only the most external portion of the non-vegetated river bed (roughly the first 25 m from the eroding bank) is predicted to be wet for more than 50% of the considered time period. The inundation duration of the whole region, including its innermost part, is greater than 10% over the 2004-2014 decade. The duration of inundation for the point bar region colonized by pioneer trees

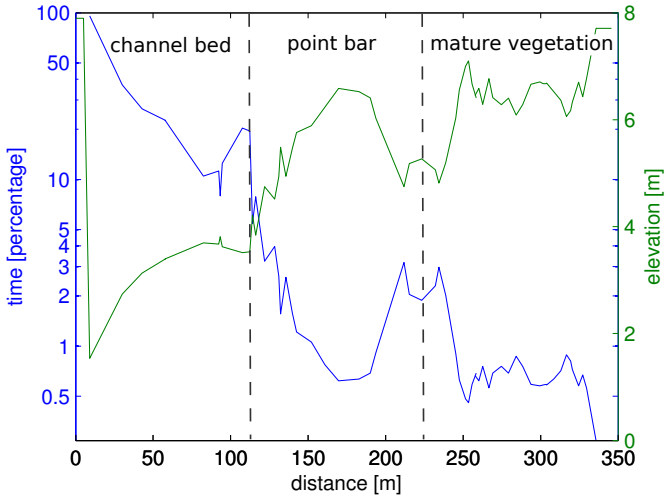

Figure 4.11: Time period (express as a percentage) for which a chosen point along the cross section would have been submerged during the time interval covered by the hydrological dataset.

ranges between 5% and 10% of the whole decade, which is considerably lower than the unvegetated riverbed and shows some variability related to the large scale topographic oscillation associated with this part of the point bar. Finally, the inundation duration of the innermost portion of the transect, the mature forest area, is much more regular compared to the other two regions and spans less than 5% of the reference period used for this analysis, corresponding to the largest flood events.

The difference in inundation dynamics among the three regions is even clearer in the plot reported in Figure 4.12, which shows a duration curve of the local water depth values predicted at three lateral locations representative of the three different biomorphodynamic regions of the transect. The analysis shows how the three different areas have been submerged with a temporal frequency that changes by an order of magnitude between each area (see Figure 4.12).

Following the analysis of the period of time for which each area would have been inundated, a similar analysis investigated the different durations of expected morphological activity for each of the three regions in which the transect has been partitioned. The result is reported in Figure 4.13a,b. In Figure 4.13a the value of the surface sediment size surveyed during the field campaign is used to compute the Shields mobility parameter, while in Figure 4.13b the representative diameter of the gravel fraction that characterizes the surface of the innermost part of the non-vegetated bed region has been used. The two diagrams provide complementary in-

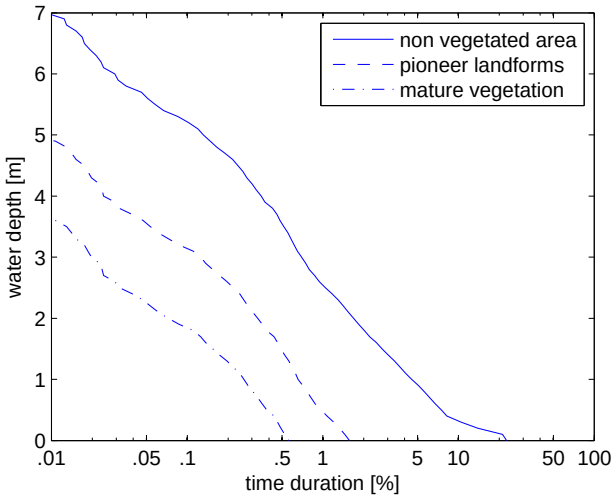

Figure 4.12: Percentage duration of local flow depth values predicted over the considered time period (2004 – 2014) for each of the three lateral locations chosen as representative of the three zones in which we subdivided the cross section: non vegetated river bed, point bar with pioneer species and mature forest area.

formation. Figure 4.13a indicates that at the representative location, the representative surface sediment for the river bed, point bar and mature forest can be locally transported for 2.2%, 1.2% and 0.6% of the time period, respectively. These numbers show a rather different proportion if compared with those related to the differences in inundation dynamics for each region. This is related to the fining of the surface sediment towards the accreting part of the transect. It also appears that the expected values of the Shields parameter increase rapidly with water depth in the innermost region (mature forest) where typical values of suspended sediment transport are achieved ($\theta > 0.2$), while more limited values characterize the unvegetated bed region, where local conditions mainly correspond to bedload transport of the representative sediment size ($\theta < 0.15$).

A much stronger difference, analogous to that characterizing the inundation dynamics appears instead in Figure 4.13b, where the same sediment size has been used (ds=0.02m). This indicates that in the innermost region (mature forest) conditions for gravel bedload transport are met only for a duration of 0.12% of the whole period of analysis, i.e. for about 5 days over 11 years. Figure 4.14 reports the height threshold value for water elevations able to transport sediment for the different zones within the study area.

The analysis of vegetation dynamics in the evolving river transect was carried out by locating the position of deposited trees detected on the 2001

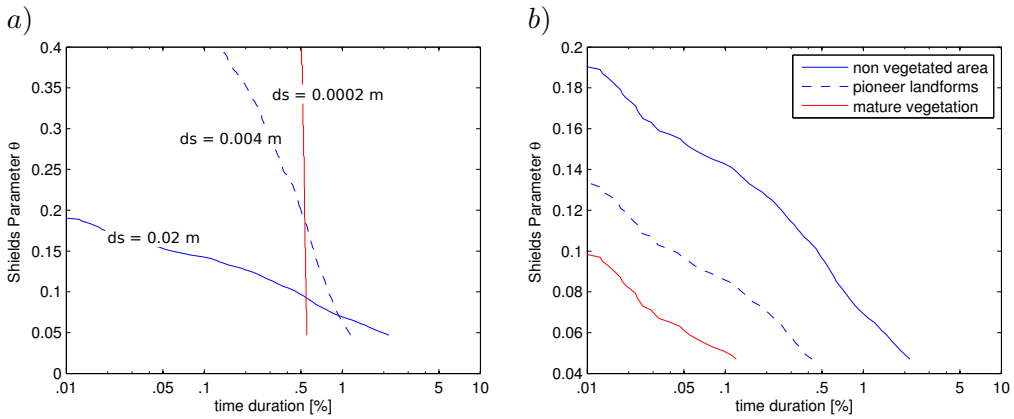

Figure 4.13: Percentage duration of expected morphological activity in the considered time period (2004 – 2014) estimated using a) the value of sediment size surveyed during the field campaign and b) imposing a constant value (0.02 m), for each of the three lateral locations chosen as representative of the three zones in which we subdivided the cross section: non vegetated river bed, point bar with pioneer species and mature forest area.

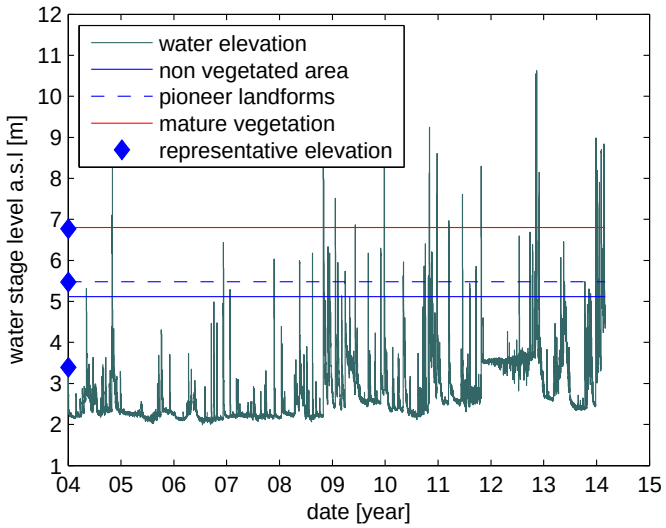

Figure 4.14: Threshold value of free water surface elevation for the three different zones: channel bed (no vegetated area), point bar (pioneer landforms) and inner bank (mature vegetation). Water levels exceeding the height threshold for a zone result in morphological activity.

point	Coordinate East	Coordinate North	Diameter [cm]
P1	2363376.146	5075476.023	15
P2	2363359.365	5075489.862	19
P3	2363346.626	5075448.742	10
P4	2363290.626	5075463.721	24

Table 4.3: Coordinate in UTM ETRF 2000, 33, of the points tracked for different dates and the correspondent tree diameter measured during the field campaign.

aerial image in the field, and by measuring the diameter of the largest tree at the same location (as an indicator of patch age).

By tracking the evolution of deposited wood through time (position reported in Table 4.3), it was possible to show that in general vegetation farther from the river edge has grown faster than the vegetation that was partially submerged in 2001 (see Figure 4.15 and Table 4.3 Coordinate in UTM ETRF 2000, 33, of the points trucked for different dates and the correspondent tree diameter measured during the field campaign). However, values reported in Table 4.3 for the different points show that trees at position P4 have grown much more than the trees located at points P2 and P1 although P4 is closer to the river edge and therefore exposed to higher stress condition (a longer anoxia period and elevate shear stress values) especially in the early phases of growth (see Figure 4.15). This may indicate that the influence of river processes on the riparian vegetation does not depend only on the position of the tree along the transversal transect (close or far from the non vegetated river bed) as it has been typically assumed when modelling riparian vegetation dynamics (Perucca et al., 2006; Camporeale and Ridolfi, 2006), but more specifically on the relative location of the deposited tree with respect to the flow pattern associated with the river bend. Indeed, as it is possible to observe from the sequence of images in Figure 4.15, the point bar portion located upstream of the bend apex is mainly covered by bare sediments, while in the point bar region downstream of the bend apex, vegetation is rather homogeneously covering the ground. However, tree diameters reported in Table 4.3 show that the trees surveyed at locations P3 and P4, even being rather close (about 20m) one another, present a different rate of growth. A possible interpretation is the streamline convergence that is expected downstream of the bend apex (Zolezzi et al., 2012b; Frascati and Lanzoni, 2013), which dissipates flow energy, thus generating low velocity areas that may protect the growth of trees at the downstream end of the point bar at its innermost side.

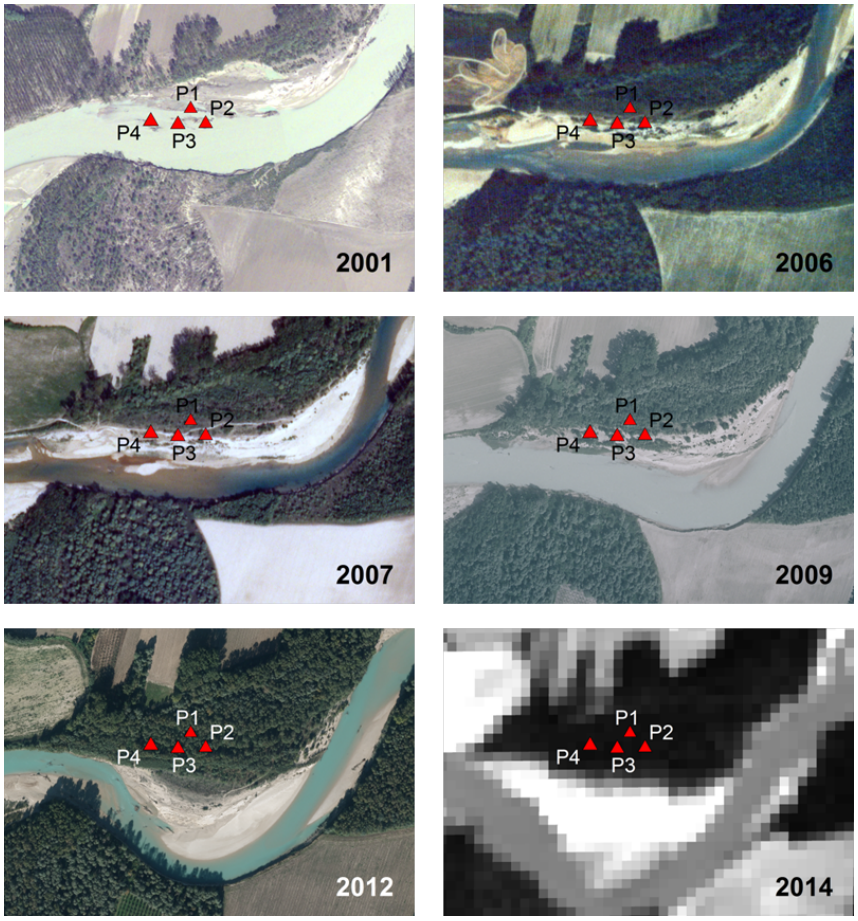

Figure 4.15: Position of the tracked points P1,P2,P3,P4 reported in Table 4.3 during different phases of the evolution process. Aerial photographs from 2001 to 2012, Landsat image from 2014.

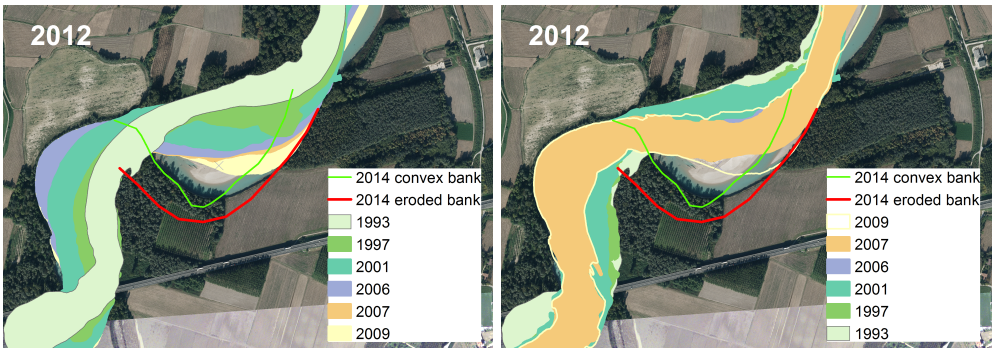

Figure 4.16: Area eroded and deposited estimated using the aerial photographs available from 1993 to 2009.

4.4.3 Temporal erosion and accretion dynamics in the evolving meander bend

Images obtained by overlaying river channels from different dates (Figure 4.16) allow the estimation of the lateral migration rates for the cut bank, when the images are overlain chronologically, and for the accreting bank, when the inverse order is applied. Results expressed in m/year and are reported on the water stage graph in relation to the time interval for which the migration rates were computed (Figure 4.17), so that it is possible to visually associate lateral migration rates with the water stage pattern of that period. A clear difference emerges between both erosion and accretion rates computed before and after 2008, with rates of migration of both banks being much higher after 2008.

The comparison of the 2014 and 2001 transects reported in Figure 4.6 also provides evidence of the cumulative processes of outer bank erosion and of inner bank accretion that took place at the outer and inner bank, respectively. From this comparison, it emerges that the meander bend evolution has eroded an estimate cumulative sediment volume of 1250 m^3/m and deposited a cumulative sediment volume of 550 m^3/m.

Results from the wavelet analysis, performed on the historical hydrological dataset recorded at the Madrisio station, are reported in Figure 4.18. From the observation of the contour plot (b) and the Global spectrum (c) two main frequencies arise: one with period of around 30 days and the other characterized by a period of 130 days. More interesting is the Scale-Averaged Wavelet Power for the frequency interval that includes the two detected, globally dominant water stage oscillation frequencies, i.e., 30-150 days: Figure 4.18d shows quite clearly a marked increase in water stage variability after 2008.

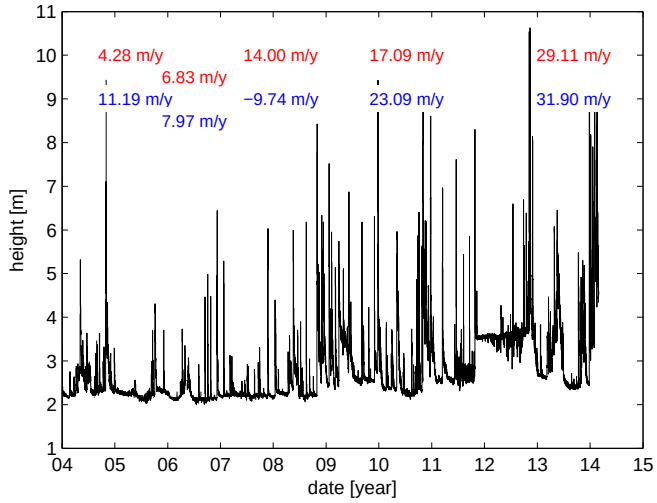

Figure 4.17: Value of lateral migration rates computed for the cutting (red) and convex (blue) bank. The migration rate is expressed in meters per year considering the distance along the trajectory perpendicular to the bend apices. The external bank is always eroded while for the inner bank positive/negative values corresponds to accretion/erosion, respectively. Each couple of values is reported in correspondence of the related time interval.

4.5 Discussion

Topographic and riparian vegetation patterns in accreting meander banks

Field observations confirm that patterns in riparian vegetation and bed topography have mutual relations, in qualitative agreement with the outcomes of the remote sensing analysis of Chapter 3.

At a given time, the cross section profile changes according to the properties (mainly the spatial pattern distribution) of the vegetation: a sharp profile associated with bare ground (river bed, Figure 4.3d), pioneer landforms associated with the presence of large woody debris (river point bar Figure 4.3c,b) and more regular, small-scale oscillations within the establishing vegetation cover (inner bank, Figure 4.3a). The mutual feedback between topography-vegetation giving rise to the observed patterns is also supported by the analysis of vegetation density within the vegetated area, which quantifies the presence of vegetation on ridges, while swales are characterized by the almost complete absence of vegetation (Figure 4.10 and Figure 4.3a). These results are consistent with field observations of the influence of riparian structures on floodplain planform

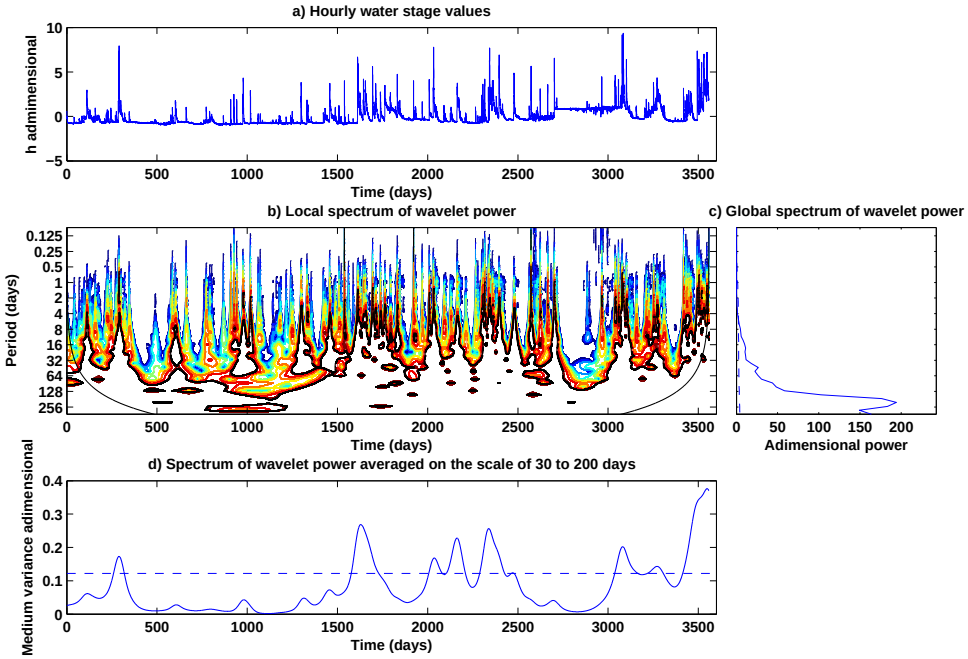

Figure 4.18: Wavelet analysis of the historical river stage record (2004-2014) at Madrisio. (a) Normalized water stage time series; (b) contours of the wavelet power spectrum of the normalized water stage. The area below the thin continuous line is less significant because it is subject to the influence of boundary conditions; c) global power spectrum that coincides with the Fourier Transform; d) variance variation for the frequency ranges from 30 to200 days.

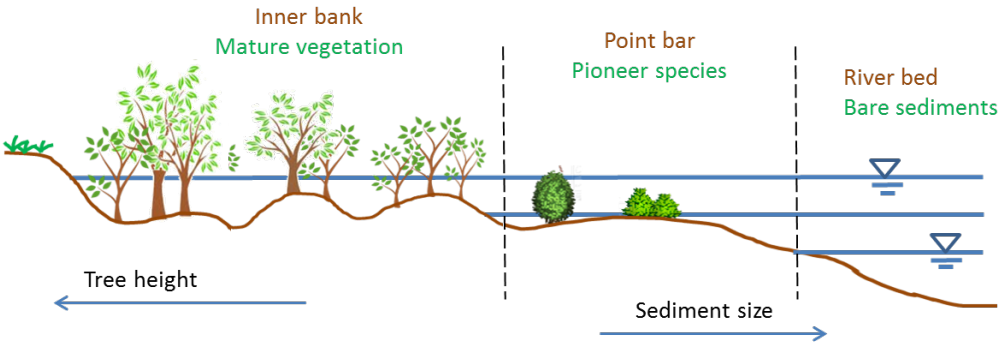

Figure 4.19: Conceptual scheme of the inner bank showing morphological and riparian canopy structures.

(Hickin, 1974; Gurnell and Petts, 2006) and the conceptual models that have been developed to investigate the interaction between vegetation and river morphology (McKenney et al., 1995; Grenfell et al., 2011).

Such mutual interaction produces patterns, which are suggested to be organized at two different spatial scales. Investigations of river cross section geometry for two different dates (2001 and 2014) have indeed highlighted the presence of complex morphological associated with the accretion processes (Figure 4.6). Two macro oscillations (point bar and old bank) scale with the channel width can be detected and several random variations characterized by a smaller spatial scale. However, these apparently irregular oscillations display a quite regular pattern of alternate ridges and swales typical of scroll formation in meandering rivers (Nanson, 1980). In particular, these features are related with the presence of riparian vegetation that, interacting with the flow and sediment, leads to the formation of scours (swales) and deposits (ridges) around trees or dead wood. The existence of these patterns was already well known from the studies of Nanson (1981); Hickin (1984) but the quantification of the vegetation and topographic properties, as well as its spatial scales (micro and macro) don't seem to have been quantified in previous works. The spatial scale of the macro-oscillation approximately coincides with the scale of the streamwise vegetation age/ topographic bands detected from the remote sensing analysis (about 80-100 m).

Figure 4.19 shows how the cross section can be partitioned in three main zones characterized by interaction among flow, vegetation dynamics and sediment transport occurring at different time scales and producing different type of patterns and where the dominant biophysical processes are different. Vegetation growth and decay, for similar soil and plant species conditions, is related to the temporal dynamics of water

level oscillations within the flooded area (anoxic periods, shear stress or low moisture for the roots), vegetation is organized spatially (along the transversal coordinate) according to the water stage (Nanson and Croke, 1992; Décamps et al., 1994; Bendix and Hupp, 2000). Indeed, Figure 4.11 shows different time persistence of inundation periods for the different elevation zones of the inner bank profile (reference elevation associate to the points reported in Figure 4.6). Moreover, the different time scales presented in Figure 4.11 highlight a substantial differences between the different areas which lead to a different spatial organization of the riparian trees along the transect. Evidence of this can be found by comparing this latter graph with the growth curve reported in Figure 4.8a, considering that young vegetation (< 2 years) is less resilient to frequent stress condition and needs dryer periods to grow. Evidence of interaction with sediment transport is provided also by Figure 4.13.

It can be conjectured that micro-oscillations are related with complex 3D patterns (secondary flows, as hypothesized by Nanson and coworkers) while macro-oscillations, scaling with the average wet channel width, may be associated with larger scale flow patterns, with a less local, 'bulk' effect of vegetation on the flow dynamics.

Finally, it must be noted that, as already observed by Ziliani and Surian (2012), the surveyed reach has been subject to channel adjustment, leading mainly to incision, as it appears in Figure 4.6, where there is a surface in the outer bank (recent terrace) higher than the surface in inner bank (floodplain). As discussed also in Chapter 3, such overall adjustment is likely not to significantly affect the main outcomes of the present work, at least qualitatively, though a quantitative inspection of its role certainly deserves future investigations.

Implications for modelling the planform evolution of single-thread channels

Increasing awareness of the need to develop planform evolution models able to incorporate the different dynamics of the advancing and retreating banks has highlighted a substantial knowledge gap on the interactions between vegetation and fluvial processes that complicate the development of physically-based models (see Chapter 2).

The quantitative characterization of the advancing bank dynamics indicates several key ingredients for those model developments:

- need to incorporate flow unsteadiness as different time scales are present in terms of inundation dynamics and morphological activity of the wet channel, eroding and accreting bank. Besides highlighting the major time scales of flow unsteadiness for a given river system,

the variance plot of the constructed water level data (Figure 4.18d) reveals that the river stage has been markedly increased in the last decade, showing an earlier time period characterized by lower variance and another more recent period by increased oscillations. This latter result can be related to the values estimated for the migration rates for the two banks (see Figure 4.17);

- need to account that different processes may be more relevant in different regions of a cross section;

- unsteadiness does not only refer to flow and inundation but also to channel geometry (ex. observed oscillations of the width of the active main channel). These are partially quantified through the analysis of the aerial images. By comparing the decoupled analysis of the banks migration rates with the changes in the degree of flow stage oscillations, a relation between the intensity of the erosion (high variance fluctuation) and accretion (low variance fluctuation) migration rates can be hypothesized. Nevertheless, according to the graph, the low variance period that may correspond to the vegetation recruitment phase is not enough for bank advance (e.g 50-1500 days, around 10 m/y), but it requires the low phase to be followed by variations in water level (interaction between vegetation, river flow and sediments) as has happened during the last 4 years (from 2000 to 3000 days). This consideration is in agreement with other observations that have been made on the interaction between sediments and vegetation in generating river morphology (Hupp and Osterkamp, 1985; Francis, 2007; Hupp and Rinaldi, 2007).

4.6 Conclusions

Results obtained from the present analysis, together with the analysis of Chapter 3, highlight how the combination of different techniques (field investigation, remotely-sensed image processing and analysis of historical time series data) may help in quantitatively investigating the biomorphodynamics of lateral migration of meander bends. Moreover, from the investigation of the cross section topography and historical water stage we identified some macro oscillations associated with different time periods that in turn influence the vegetation spatial distribution. Two levels of organization of the inner bank morphology arise: one (macro variation and channel width) dependents on the water stage, the other determined by the presence or absence of vegetation and its interaction with the water flow (micro variation). Possible dynamic relations linking the patterns at

the two scales still need further explorations.

Furthermore, the existence of three zones within the inner bank was detected independently from three different analysis: from the analysis of the historical hydrological data as difference water persistence time-length above the ground and, more qualitatively, from the observation of the cross section topography. Interestingly the same result was found previously as result of a combination of analysis of Lidar data and historical aerial photographs.

Moreover, the analysis shows how the information collected in the field to characterize the riparian canopy structure complete the remote sensed analysis conduced and reported in the previous chapter. For instance the growth curve of the analysis on vegetation properties can be used to convert maps showing the tree height distribution with tree age and, conversely, to interpret the values in the persistence map in order to estimate the height of the riparian canopy. Therefore, from the analysis of aerial photographs of an evolving vegetated meander where vegetation species are known, it would be possible to characterize at each date the canopy structure.

In this approach a first attempt to quantify lateral migration rates for the convex and cutting bank in a actively evolving meander bend has also been proposed. Although under hyper-simplified hypothesis, the founding provides information on the evolution trend and, thanks to the analysis of the signal of the river stage, allow to correlate the intensity of the lateral migration with the temporal variation in water height level.

Analogously the findings of this analysis provide a solid base for future research in developing bio-morphodynamic models that aim to reproduce and investigating the accretion processes at the inner bank in meandering river planform evolution.

Chapter 5

Modelling vegetation feedbacks on river meanders evolution: an insight into the accretion processes

In this chapter a simplified bio-morphodynamic model is proposed to investigate for the lateral migration of a meandering river bend. The main novelty compared to previous works is twofold: i) the accreting and the eroding banks evolve under the effect of different processes and ii) the interplay between bank accretion and riparian vegetation dynamics is modelled explicitly, albeit in a simplified way. The adopted strategy is explicitly based on the knowledge developed from the analysis presented in the previous chapters. Data from field investigations and historical hydrology records (already introduce on the previous chapter) was used as input in a final application that allows a preliminary, qualitative validation of the proposed model.

5.1 Introduction

Riparian vegetation within the active river corridor, interacting with river processes, acts as a 'river engineer' in controlling river channel morphology and planform evolution (McKenney et al., 1995; Gurnell and Petts, 2006; Bertoldi et al., 2011b). In particular, for the case of river meanders, vegetation associated to point bar development and subsequent formation of scrolls has been denoted as fundamental in river channel lateral migration (Nanson, 1981). At the same time, the reinforcing action operated by the root system on bank sediments increases their resistance to the erosion processes, and thus influence the migration rates of the inner and outer banks of meander bends and induce morphological changes at both local (cross-section) and reach scale (Allmendinger et al., 2005; Braudrick

et al., 2009).

Most of the models that have been developed to describe lateral meanders migration are based on the simplified bank erosion law proposed by Hasegawa (1977) and Ikeda et al. (1981) - HIPS model, under the fundamental assumption of constant channel width in time, implying the same migration rate for the two opposite banks. Uncertainty in the application of these models, essentially especially related to the lack of physical bases for the lateral migration coefficient E, has motivated recent research efforts aimed at addressing the separate dynamics of each river bank, and the interaction between the channel and its floodplain. These efforts, however have mainly focused on modelling bank erosion/failure mechanisms (Motta et al., 2012b) and the effect of floodplain erosional heterogeneity on lateral migration (Güneralp and Rhoads, 2011). Only recently, bio-morphodynamics models have associated river migration rates with vegetation biomass lateral dynamics to investigate the interplay between riparian vegetation and meanders planform evolution, and vice versa. (Perucca et al., 2006, 2007).

The novel framework proposed by Parker et al. (2011) introduced a new perspective in modelling meandering rivers, by addressing the lateral migration of inner and outer banks separately. This concept of separately evolving banks underpins channel width adjustment as a dynamic balance between the accretion and erosion processes that occur at the inner and outer bank, respectively. Following this approach,Eke et al. (2011, 2014) were able to model river meanders evolution introducing closure relationships for both the migration of the advancing and cutting bank, accounting for the sediment exchange between the two bank regions and the channel region.

An intriguing issue emerging from the modelling work of Eke and Parker (2011); Eke et al. (2014) and from the recent experimental work of van Dijk et al. (2013) is the way channel width adjusts in time in response to a dynamic 'dialogue' between the two banks. In this respect, both analyses put forward arguments supporting a '*bar push*' or a '*bank pull*' driven width adjustment. Despite these recent improvements, however, existing modelling studies haven't explicitly addressed yet the biophysical processes of flow-sediment-vegetation interaction likely controlling the development of floodplain patterns and channel morphology within the advancing bank region, with the majority of studies being biased towards the bank erosion mechanism.

Due the complexity of the involved physical processes, an hybrid reductionist–holistic model to describe such patterns in relation to vegetation dynamics could provide better understanding of the physical controls of the meanders planform evolution (Seminara and Bolla Pittaluga, 2012).

Following this idea a bio-morphodynamic model has been developed that couples a minimalist approach for the interaction between riparian vegetation and river processes with a non linear analitical model for morphodynamics of a meander bend. The model proposed is used to: i)investigate the bio-physical controls of inner bank accretion, ii) quantitatively asses the role of river- and vegetation-induced processes on the developing riparian patterns and iii) quantify channel width temporal variation in a free migrating meander.The model is applied to idealized cases and then it is preliminarily validated by using the data collected during the field measurements presented in Chapter 4.

5.2 Method

In order to achieve the objectives listed above, the bio-morphodynamic model is kept at the lowest possible level of complexity and in its first stage of development the interactions between ecological system and flow dynamics have been investigated at the cross section scale.

It is useful to first broadly illustrate the adopted modelling strategy before providing a detailed description of the proposed bio-morphodynamic model. Because river morphodynamic processes occur on a timescales usually larger than those of riparian vegetation evolution, biological dynamics and river morphology are here modelled accounting for such timescale difference (Figure 5.1). Under this fundamental assumption, the temporal evolution of the system is analyzed sequentially, and the input hydrograph is suitably thresholded in order to distinguish between high flows, which are related to channel bed morphodynamics, and low flows, when riparian vegetation evolution occurs. The interaction between flow and vegetation is modelled converting the water stage time series into a stepwise sequence of steady states whereby a local uniform flow is assumed at each stage (see paragraph 5.2.4). In turn, the presence of vegetation within the inner bank affects sediment mobility, determining the width of the morphologically active portion of the cross-section, and therefore creating a feedback effect on river bed morphology. Under the hypothesis of local uniform flow conditions, a simplified relation is used to describe the sedimentation processes induced by the interaction between riparian plants and the flow field (see paragraph 5.2.1). The transverse bed profile in the active river channel is obtained by applying an analytical morphodynamic model of flow and bed deformation in constantly curved channels (Seminara and Solari, 1998, see paragraph 5.2.5). An estimate of the eroding bank retreat rate over one flood event (see paragraph 5.2.2) is obtained through a first application of the bend morphodynamic model (solid line in Figure 5.1): this allows to

adjust the active channel width, which corresponds to the new hydraulic conditions (dashed line in Figure 5.1). The morphodynamic bend model is applied a second time under the assumption of equilibrium conditions for the representative discharge value chose for each high flow event. The final outcome therefore results from a reciprocal exchange of information between these two models at the different time-steps (see Figure 5.1). It is worth to notice that the model allows sediments at the inner bank to be either eroded or deposited. The different components in which the model is structured are detailed below. In particular, since the morphodynamic models adopted in the analysis are derived from a common framework, this will be first introduced and afterwards the specific solutions will be described.

5.2.1 Modelling the mutual interaction between vegetation dynamics and river processes

River processes constitute fundamental controls on riparian vegetation dynamics, including the provision of nutrients and water to support vegetation growth, the availability of exposed sediments for the colonization of pioneer species and the erosion of vegetated area. River processes therefore affect in a variety of ways the dynamics of riparian vegetation. On the other hand, the interaction of riparian species with the flow field and the sediments affects river channel morphodynamic, altering erosion processes and inducing sediment deposition (vegetation-induced processes). Figure 5.2 illustrates a sketch of the modelling framework, along with the definition of the most relevant geometric and hydraulic parameters. The vegetation biomass is represented through the dimensionless parameter b, which measures the local biomass density and ranges from 0 to 1. Moreover in Figure 5.2 h^* and η^* denote the water free surface and the ground surface elevation, respectively; while D^* represents the channel water depth. The variables referred to an orthogonal reference system (s^*, n^*, z^*), in which s^* is the longitudinal (streamwise) coordinate, n^* represents the transversal coordinate orthogonal to s^* and z^* is the vertical axis orthogonal to the plane where the axis s^* and n^* lie, and pointing upwards. Hereafter a superscript asterisk will indicate dimensional variables. The quantities introduced are used in the formulation of the meander bend morphodynamic sub-model described in 5.2.5.

River controls on riparian vegetation dynamics

The effects of river-induced processes on riparian vegetation have been summarized using the vertical distribution curve of the local maximum

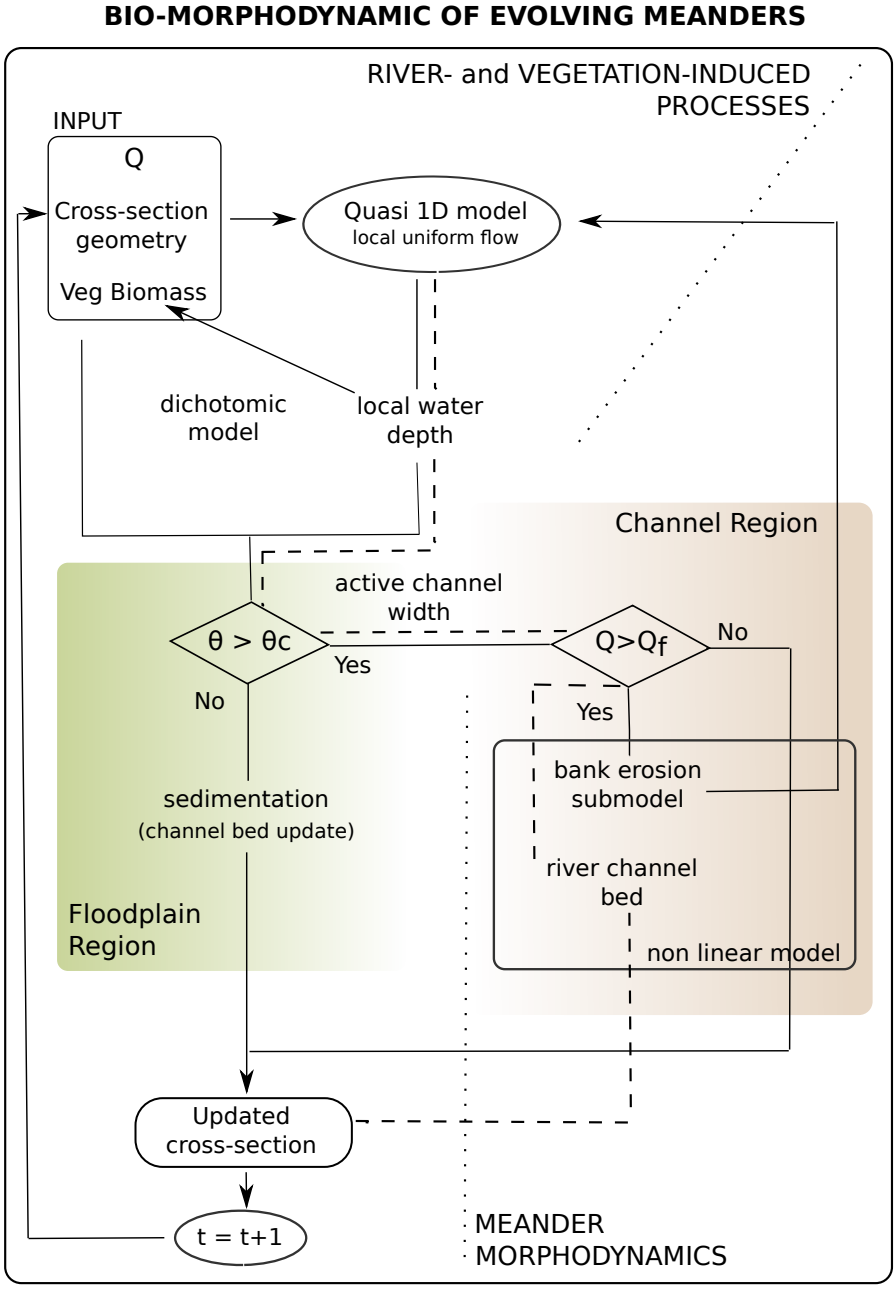

Figure 5.1: Flow chart of the bio-morphodynamic model developed. For the case of formative flood ($Q > Q_c$), a first application of the bend morphodynamic model (solid line) estimate bank retreat and allow channel width adjusting (dashed line). The bend morphodynamic model is recall, a second time, to compute the new channel bed. The procedure is iterate at each time step.

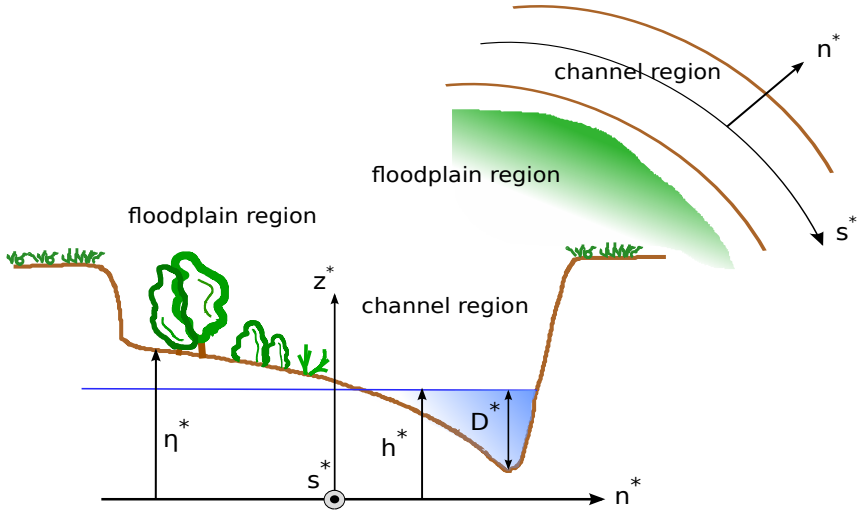

Figure 5.2: Sketch of the constant curvature meandering channel and notations. A star denotes dimensional variables.

biomass density proposed by Marani et al. (2013):

$$b_{eq}(\eta^*) = 2\left[exp(\lambda_1(\eta^* - z^*_{b0})) + exp(-\lambda_2(\eta^* - z^*_{b0}))\right]^{-1}, \tag{5.1}$$

where η^* is the ground elevation, and λ_1, λ_2 quantify the rates with which fitness decays far from its maximum, which is reached in correspondence of the optimal elevation z^*_{b0}. This latter refers to ideal conditions of moisture availability expressed as distance from the water table (assumed horizontal along the section), and can be changed opportunely to model different groundwater conditions or different types of vegetation. The value obtained from the relation (5.1) is then rewritten as

$$b_{eq}(\eta^*) = \frac{b_e q(\eta^*)}{b_{eq,max}}, \tag{5.2}$$

with $b_{eq,max}$ the maximum value of b_{eq}, to obtain a normalized value of biomass ranges from 0 to 1. Moreover, the introduction of the parameters ($\lambda_{1,2}$) allows to account for two hydrological mechanisms that affect vegetation: the destructive action of the river flow and the control of sediment moisture due to the water table depth. Increasing in λ values denotes more specialized vegetation, able to grow up to an optimum biomass only in a narrow range of bed elevation. As a result, the curves that can be obtained by varying the values of λ_1, λ_2 and z^*_{b0} are comparable with the three type of curves proposed by Perucca et al. (2006) for the biomass den-

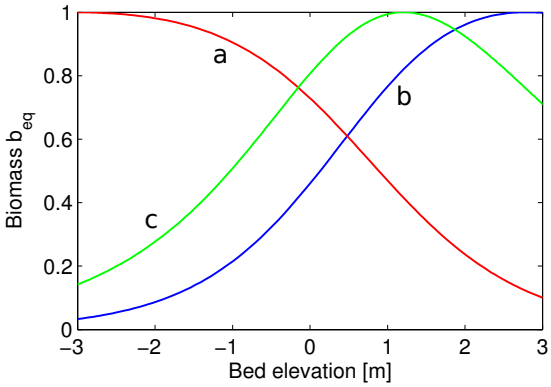

Figure 5.3: Example of distribution curves for biomass density varying the coefficient $\lambda_{1,2}$ in equation (5.1): a) $\lambda_1 = 1.1, \lambda_2 = 0.02$; b) $\lambda_1 = 0.1, \lambda_2 = 1.0$; c) $\lambda_1 = 0.4, \lambda_2 = 0.7$; with $z^*_{b0} = 0.7\ m$.

sity (see figure 5.3), showing that, despite defined for meanders in tidal environment, the law (5.1) fits well also for the case of fluvial meanders.

In order to model the temporal evolution of the vegetation biomass over the cross-section, we adopt the dichotomic model proposed by Camporeale and Ridolfi (2006). Vegetation growth during the exposed period ($h^* < \eta^*$) is modelled as function of moisture availability through the equation (5.2); vegetation decay during the wet period is related with the negative effects induced on the riparian species by the flow (e.g. uprooting, anoxia, burial). Influence of such hydrological forcings on the biomass temporal evolution is therefore modelled through the following equations:

$$\frac{db}{dt^*} = \sigma_1 b^{m_1}(b_{eq} - b)^{m_2}, \qquad h^* < \eta^* \tag{5.3}$$

$$\frac{db}{dt^*} = -kb^{m_3}(h^* - z^*_b) \qquad h^* >= \eta^* \tag{5.4}$$

where b is the vegetation biomass, t^* is time, b_{eq} represents the maximum vegetation biomass (derived from the equation (5.1)), the so called 'carrying capacity', h^* is the water level, η^* is the ground surface and m_1,m_2,m_3 are species-dependent coefficients, while σ_1 and k represent, respectively, the growth and decay rates. Since the two latter parameters also depends on the characteristics of the species and on the environmental conditions field informations are fundamental for the correct set up of the model. Although model parameters might simulate the behaviour of different species, their effect have not been investigated in this work ($m_1 = m_2 = m_3 = 1$).

Vegetation feedbacks on flow and sediment transport

As described in Chapter 2, the interaction between riparian vegetation and over-bank flow associated with soil reinforcement operated by plant's root system represents a fundamental mechanisms in the evolution of the floodplain and in the lateral migration of river banks. In particular, pioneer plants that colonize the inner bank or the presence of deposited dead wood along the river affects the depositional and erosional patterns initiating pioneeristic landforms that, for the case of river meanders, can evolve in scrolls formation (Nanson, 1981; Gurnell et al., 2001; Nakayama et al., 2002).

In order to quantitatively reproduce these effects in the model, two hyper-simplified equations have been proposed. The first accounts for the active role played by riparian plants in inducing sedimentation, and it reads

$$\frac{d\eta^*}{dt^*} = \lambda^*_{sed} b D^*_0, \tag{5.5}$$

where λ_{sed} is the deposition rate expressed in mm/day, b is the overall biomass and D^*_0 is the local water depth. In equation (5.5) the deposition rate, expressed through the coefficient λ_{sed}, can be estimated from field/laboratory observations (e.g. Welling and He, 1998; van Dijk et al., 2013).

The reduced sediment mobility due to root system development is accounted for by modifying the threshold value for which sediments can be transported accordingly with

$$\theta_c = \theta_{cs} + \theta_{cv} b^{\alpha_t}, \tag{5.6}$$

where θ_{cs} is the threshold value for the incipient movement of the grain for the case of bare sediments (typically taken as 0.047), θ_{cv} represents the increase of stability due to the presence of trees' roots and α_t is a coefficient that depend on the roots properties of the species considered. In this work α_t has been set to 0.6 in order to obtain a sediment reinforcement effect stronger during the initial stages of the evolution of the riparian biomass. The relation (5.6) indicates that the soil resistance to erosion, measured through the critical Shields parameter for sediment motion θ_c, increases nonlinearly with increasing biomass b, with a faster increase for relatively lower values of b. The parameter α_t in equation (5.6) has been chosen in the range 0.5 - 1 in accordance with Bertoldi et al. (2014) while a value of 0.3 has been assumed in this first model development for θ_{cs}, which would imply a maximum increase of the critical Shields parameter for sediment motion θ_c up to the theoretical value of 0.347 when $b = 1$. It is important to note however that the condition $b = 1$ is almost purely theoretical and

never reached, with typical peak b values around 0.4, with a correspondent soil reinforcement characterized by $\theta_c = 0.19$ which appears in accordance with the values proposed by Bertoldi et al. (2014).

Furthermore, changes in roughness associated with the presence of vegetation were accounted by varying the Strickler coefficient according to the following linear relation:

$$k_s^* = k_{sg}^* + (k_{sv}^* - k_{sg}^*)b \tag{5.7}$$

where k_{sg}^* (assumed about 35 $m^{1/3}s^{-1}$) and k_{sv}^* are the Strickler coefficients associated with the bare sediments and ground with fully developed vegetation, respectively. In the present analysis the latter value was assumed about 20 $m^{1/3}s^{-1}$, which is higher than what suggested by Bertoldi et al. (2014) in order to account for the reduce effect on flow resistance due to the patchy distribution that characterizes colonizing vegetation within the inner bank. Moreover, the roughness estimated according to equation (5.7) was converted to the Chezy coefficient in order to be consistent with the following analysis (see paragraph 5.2.5)

5.2.2 Bank erosion submodel

Outer banks in meandering rivers typically present a cohesive top layer often related to the presence of vegetation and a non-cohesive bottom layer (Lauer and Parker, 2008). The action of fluvial erosion on the lower layer undermines the upper one leading to its failure. Presence of block of cohesive sediments at the toe of the bank increases the resistance of the bank to the erosion, reducing its retreating rate (Parker et al., 2011). The whole process is often modelled using an erosion coefficient; the rate of lateral erosion ζ^* for the external bank is modelled, following the established approach proposed by Motta et al. (2012b), through the excess shear stress relation

$$\zeta^* = M^*(\tau^* - \tau_c^*), \tag{5.8}$$

where τ^* is the longitudinal shear stress computed at the toe of the external bank, τ_c^* represents the critical stress threshold for the sediment transport and M^* is the lateral migration coefficient that depends on the physical characteristics of the river bank (sediments and presence of vegetation) and can be estimated through field measurements (Darby et al., 2007; Constantine et al., 2009; O'Neal and Pizzuto, 2011). Including relation (5.8) in the model, it has been implicitly assumed that material eroded at the outer bank is immediately transported out of the section. This assumption allows to keep valid the hypothesis of non permeable conditions at the external border used by most analytical morphodynamic models.

5.2.3 Flow unsteadiness

Quantitative bio-morphodynamic models for the study of the mutual interaction between vegetation and river processes crucially need to account for temporal variability of streamflow (Camporeale and Ridolfi, 2006, 2010). On the other hand, analytical solutions for flow field in meandering rivers have been almost always derived for an ideal channel fed with a 'formative' constant discharge. For a given streamflow time series, the proposed modelling approach first identifies a discrete number of 'formative events'. This is achieved by thresholding the series with a value that is obtained as a percentage (α) of the maximum discharge value $\bar{Q}^*$ of the analyzed record, such that

$$Q_f^* = \alpha_Q \bar{Q}^*. \tag{5.9}$$

For each formative event a 'representative', constant discharge value was chose. Having neglected the unsteady effect the morphodynamic submodel developed cannot presently account for differences in intensity and duration of the event. Afterwards, the quasi 1D hydraulic submodel 5.2.4 is applied to determine the portion of the morphologically active cross-section over which the bend morphodynamic submodel is applied.

5.2.4 Quasi 1-D hydraulic submodel

Fluctuation in streamflow, required for vegetation dynamics, was modelled using a quasi 1-D hydraulic model over an assigned morphology. In this phase (see Figure 5.1) channel bed morphodynamycs and lateral bank migration are not modelled and changes in bed elevation are restricted to the depositional processes induced by the interaction between vegetation and flow during the submerged period (according with equation 5.5).River channel flow field and water stage is estimated for each discharge value by partitioning the cross-section into vertical strips where local uniform flow conditions are assumed (Lotter, 1933; Engelund, 1964). This approach is valid under the assumption of: i) horizontal water surface, ii) constant longitudinal slope across the transect and iii) negligible shear stress between adjacent strips with respect to the shear force acting at the near-bed surface (the same modelly tool is used also in Chapter 4).

Lateral variability of both longitudinal flow velocity and water depth, estimated across the whole transect by applying this method, are used as input for the biological model (5.3)-(5.7). Moreover, the portion of the morphologically active cross-section which formative conditions (Q_f) is established considering the local values of Shields parameter (see previous chapter) that exceed the critical value estimated through relation (5.6).

The above model was first used, in absence of erosion processes (fixed

initial bed), to check the validity of the physically-based relationships proposed in section 5.2.1 to describe the mutual interaction between river and biological processes. The case of a free river bar in a channel subject to fluctuation in water discharge that, thanks to periods of low flow, allow the colonization of the exposed sediments and vegetation growth, appears suitable for our purpose. The latter case of study was informatively used to investigate the impact of river flow disturbance, moisture supply and other hydrological aspects on the lateral biomass distribution.

5.2.5 Meander bend submodel

For every 'formative' event in the analysed hydrological record, the meander bend submodel is applied over the morphologically active portion of the cross section, i.e. the region for which

$$\theta(n) > \theta_c(n); \tag{5.10}$$

where $\theta(n)$ is computed through the quasi-1D submodel described in Section 5.2.4 (see Figure 5.1) and $\theta_c(n)$ is obtained through (5.6) and accounts for the effect of laterally variable soil resistance to erosion due to vegetation. Note also that the lateral variability of the Shields parameter $\theta(n)$ also incorporates the role of vegetation through its effect on the flow roughness (5.7). Equation 5.10 is therefore also used to determine the value of the cross-sectional active width and its temporal variability.

The meander bend morphodynamic sub-model consists of a 3D nonlinear model for the flow and bed deformation in a bend of constant curvature, in close analogy to the one proposed by Seminara and Solari (1998), which here is slightly adapted to account for the lateral roughness variability associated.

The meander bend sub-model considers the steady flow of a constant discharge Q^* in a curved channel characterized by an initial width $W^* = 2B_0^*$, radius of curvature R^* and cohesionless bed. The curvature of the channel axis is defined as $\mathcal{C}^* = R^{*-1}$ and assumed constant along the longitudinal coordinate. The variables that characterize the flow field are referred to an orthogonal reference system (s^*, n^*, z^*), where s^* is the longitudinal (streamwise) coordinate, n^* represents the transversal coordinate orthogonal to s^* and z^* is the vertical axis orthogonal to the plane where the axis s^* and n^* lie. In particular, U^*,V^*,W^* denote, respectively, the longitudinal, transverse and vertical components of the local velocity vector $\mathbf{U}^*$ averaged over turbulence, D^* is the local flow depth, h^* is the free surface elevation (see Figure 5.2). Furthermore, following this reference system, we denote by U_0^*,D_0^* and C_0 the average speed, depth and friction coefficient that characterize the uniform flow that would occur in

a straight reach of longitudinal slope S_0 with the same discharge, width and sediment size of the bend under analysis. It is convenient to cast the mathematical problem in a dimensionless form; therefore we introduce the following dimensionless variables

$$(s^*, n^*) = B_0^*(s, n) \tag{5.11}$$
$$z^* = D_0^* z \tag{5.12}$$
$$\mathbf{U}^* = (U^*, V^*, W^*) = \quad U_0^*(U, V, W) \tag{5.13}$$
$$(h^*, D^*) = D_0^*(h, D) \tag{5.14}$$
$$P^* = \rho U_0^{*2} P \tag{5.15}$$
$$\nu_T^* = (\sqrt{C_0} U_0^* D_0^*)\nu_T \tag{5.16}$$
$$\mathbf{q}^* = (q_s^*, q_n^*) = (q_s, q_n)\sqrt{g(\rho_s - \rho)/\rho d_s^{*3}} \tag{5.17}$$

where B_0^* represents the initial width of the channel, P^* is pressure, ν_T represents the local value of the eddy viscosity, q_s^* and q_n^* are, respectively, the longitudinal and transversal component of the unit sediment rate vector $\mathbf{q}^*$, g is gravity acceleration, ρ_s and ρ are water and sediment density, respectively, and d_s^* is the sediment grain size (assumed uniform). The notation reported above allow us to write the governing equation for the longitudinal and transverse momentum along with the continuity for the fluid and sediments in their dimensionless form as follows:

$$\beta\sqrt{C_0}(\nu_T U_{,z})_{,z} = NP_{,s} - NC_0\beta + VU_{,n} + \beta WU_{,z} + \nu N\mathcal{C}UV \tag{5.18}$$
$$\beta\sqrt{C_0}(\nu_T V_{,z})_{,z} = P_{,n} - \nu N\mathcal{C}U^2 + VV_{,n} + \beta WV_{,z} \tag{5.19}$$
$$V_{,n} + \nu N\mathcal{C}V + \beta W_{,z} = 0 \tag{5.20}$$
$$P_{,z} = -\frac{1}{F_0^2} \tag{5.21}$$
$$q_{n,n} + \nu\mathcal{C}Nq_n = 0 \tag{5.22}$$

where a comma indicates the partial derivative. In equations (5.18)-(5.22) $\mathcal{C}$ is the dimensionless channel axis curvature, ν is the curvature ratio and N the longitudinal metric coefficient due to the curvilinear system adopted; which are defined as

$$\mathcal{C} = \frac{R_0^*}{R^*}, \quad \nu = \frac{B_0^*}{R_0^*}, \quad N = \frac{1}{1 + \nu n\mathcal{C}}. \tag{5.23}$$

Due to the hypothesis of constant curvature, longitudinal derivatives have been neglected in transversal momentum equation (5.19), the continuity equation for the liquid (5.21) and solid (5.22) phase, while $\mathcal{C}$ assumes an unitary value. Furthermore, several dimensionless parameters have been

introduced in the system of equation (5.18)-(5.22), namely, the half-width to depth ratio β, the Froude number F_0 and the friction coefficient C_0. They are defined as

$$\beta = \frac{B_0^*}{D_0^*}; \tag{5.24}$$

$$F_0 = \frac{U_0^*}{\sqrt{gD_0^*}}; \tag{5.25}$$

$$C_0 = \left[6 + 2.5ln\left(\frac{D_0^*}{2.5d_s^*}\right)\right]^{-2} \tag{5.26}$$

In this analysis we will assume the channel wide enough to ignore the hydrodynamic influence of the near-bank regions on the central portion of the channel and the flow and the bed topography patterns slightly perturbed with respect to the flow an bed topography in the reference straight channel; this is related to the typical shallow-water condition and to the 'weak curvature' common in natural meandering rivers, quantified by the relations

$$\beta >> 1 \quad \nu << 1. \tag{5.27}$$

The governing equations (5.18)-(5.22) are associated with the following boundary conditions:

$$U = V = W = 0 \qquad (z = z_0) \tag{5.28}$$

$$U_{,z} = V_{,z} = W - \frac{V}{\beta}\frac{dh}{dn} = 0 \qquad (z = h) \tag{5.29}$$

$$V = q_n = 0 \qquad (n = \pm 1). \tag{5.30}$$

The first condition introduces the local value of the conventional reference level z_0 at which the no-slip condition is imposed; the second condition imposes that the shear stress must vanish at the free surface and the requirement that the latter has to be a 'material' surface (i.e. moving with the fluid); the third condition requires that the side walls must be impermeable to flow and sediments.

In order to close the mathematical problem, two further closure relations are needed for ν_t and q. Following the approach proposed by Seminara and Solari (1998), ν_t is defined as:

$$\nu_t = U(n, \xi)D(n)\mathcal{N}(\xi), \tag{5.31}$$

where U is the longitudinal flow velocity, $D(n)$ is the local depth , ξ is the normalized vertical variable defined as $\xi = (D(n) + z - h(n))/D(n)$ and

$\mathcal{N}(\xi)$ is the vertical distribution of the eddy viscosity, which reads (Dean, 1974):

$$\mathcal{N}(\xi) = \frac{k(\xi)(1-\xi)}{1 + 2A\xi^2 + 3B\xi^3}; \tag{5.32}$$

in which k is the von Karman's constant and $A = 1.84$, $B = -1.56$.

Sediment transport (bed load) is determined by local flow conditions and its direction deviates from the direction of the average bed shear stress because of gravity action associated with a laterally sloping bed. Such effect is well known to play a crucial role on the definition of the transversal bed slope. Therefore, assuming such deviation to be a small number, the bed load rate vector (q_s, q_n) can be written as:

$$(q_s, q_n) = \Phi(\theta)\left(1, \frac{\tau_n}{|\tau|} - \frac{r}{\beta\theta}\eta_{,n}\right) \tag{5.33}$$

where r is an empirical constant ranging about 0.6 (Talmon et al., 1995), $\eta = h - D$ is the dimensionless bed elevation, Φ is the dimensionless bed load function for which several semiempirical formulas are available in literature and mainly depends on the local value of Shields stress θ for bed load-dominated river channels: θ is defined as

$$\theta = \frac{|\tau|^*}{(\rho_s - \rho)g d_s^*} \tag{5.34}$$

The problem formulated above is subject to the integral constraints stipulating that flow and sediment discharge must be constant along the entire reach. In dimensionless form they read:

$$\int_{-1}^{1} D dn \int_{\xi_0}^{1} U d\xi = 2, \qquad \int_{-1}^{1} \Phi(\theta(n)) dn = 2\Phi_0(\theta_0), \tag{5.35}$$

where the subscript '0' refers to the reference condition in the straight reach.

In order to find a solution for the above problem, the following general perturbation approach can be employed (e.g. Seminara and Solari, 1998)

$$U = \check{u}(n)\mathcal{F}(\xi) \tag{5.36}$$

$$V = \check{v}(n)\mathcal{F}(\xi) + \nu V_1(n, \xi) \tag{5.37}$$

$$H = h(n) + \nu\check{h}(n) \tag{5.38}$$

$$D = D_0(n) + \nu D_1(n) \tag{5.39}$$

in which $\mathcal{F}$ is a function for the vertical profile of the streamwise flow velocity, and $\check{v}$ denotes the local distribution of the secondary flow induced by

curvature, with vanishing vertical average. The solution is found through a classical procedure for which only the essential steps are recalled here.

At the leading order, $\mathcal{O}(\nu^0)$, the structure of $\mathcal{F}$ is obtained by means of an iterative procedure to solve the streamwise component of the momentum equation (5.18), rewritten in terms of the vertically re-scaled coordinate system (s, n, ξ). Using (5.31) and (5.32), the function $\mathcal{F}$ presents the classical logarithmic profile corrected by a 'wake' function (see Figure 5.4a) and reads:

$$\mathcal{F} = \frac{\sqrt{C_0}}{k}\left[ln\frac{\xi}{\xi_{0S}(n)} + A\xi^2 + B\xi^3\right]; \tag{5.40}$$

where ξ_0 is the normalized form of the conventional non-slip reference level. By imposing that the function $\mathcal{F}$ integrated along the water depth has to assume unitary value, ξ_0 reads

$$\xi_{0S} = \frac{\xi_0}{D_0(n)} \tag{5.41}$$

$$\xi_0 = exp\left(-\frac{k}{\sqrt{C_0}} - 0.777\right) \tag{5.42}$$

The transverse component of the Reynolds equations (5.19), at the order $\mathcal{O}(\nu)$ suggests to set

$$\frac{dh_1}{dn} = \frac{F_0^2 a_1(n) D_0(n)}{\beta\sqrt{C_0}} \tag{5.43}$$

$$V_1 = \frac{\check{u}(n) D_0(n)}{\beta\sqrt{C_0}}\mathcal{G}(\xi, n) \tag{5.44}$$

where the function $\mathcal{G}$ represents the vertical structure of the secondary flow related with the centrifugal effect under constant curvature (e.g. Rozovskij, 1957), and it can be obtained by solving the following differential system:

$$\left[\mathcal{N}(\xi)\mathcal{G}_{,\xi}\right]_{,\xi} = a_1(n) - \mathcal{F}^2(\xi, n); \tag{5.45}$$

$$\mathcal{G}|_{\xi=xi_0} = \mathcal{G}_{,\xi}|_{\xi=1} = 0; \tag{5.46}$$

where a_1 describes the transverse inclination of the water free surface which satisfies:

$$\int_{\xi_0}^{1} \mathcal{G}(\xi, n) d\xi = 0. \tag{5.47}$$

An example of the function $\mathcal{G}$ for a fixed position along the transect is reported in Figure 5.4b.

The morphodynamic problem for a bend of constant curvature just formulated can be solved at different levels of complexity. Zolezzi and Seminara (2001) obtained a linearized solution, while Seminara and Solari (1998) were able to derive a nonlinear solution.

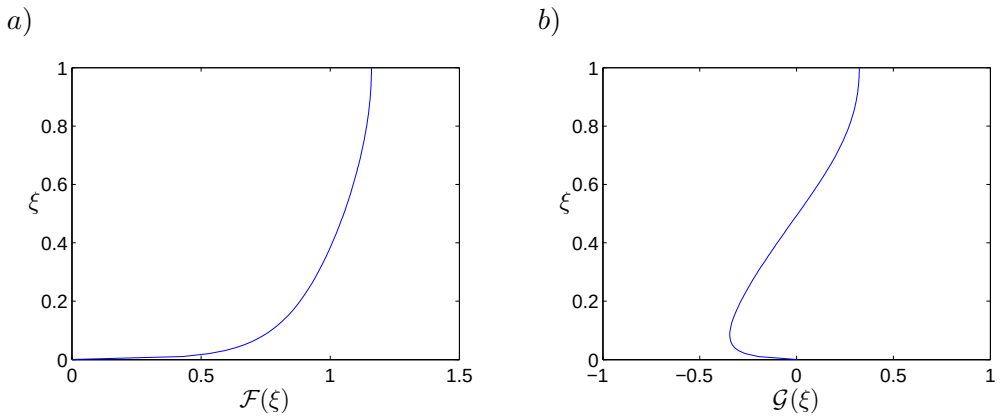

Figure 5.4: Example a) of the vertical distribution of the functions $\mathcal{F}(\xi)$ and b) of the vertical distribution of the function $\mathcal{G}(\xi)$ that describes the secondary flow component, for a fixed position along the transect. The value of the friction coefficient C_0 is set equal to 0.008.

Linear solution

Following Zolezzi and Seminara (2001) a linearized solution for the depth-average form of the problem (5.18)-(5.22) is derived for the case of constant curvature channel, by assuming that the perturbations of water depth and velocity are 'small' quantities relative to the uniform reference flow. By neglecting any variation along the channel axis, the solution proposed by Zolezzi and Seminara (2001) can be written as:

$$(U, V, H, D) = (U_0, 0, H_0, D_0) + \nu(u, v, h, d) \tag{5.48}$$

$$(u, v, h, d) = \left[0, 0, \left(\bar{h_1}\mathcal{C} + \bar{h_2}\mathcal{C}' + \bar{h_3}\mathcal{C}''\right), \left(\bar{d_1}\mathcal{C} + \bar{d_2}\mathcal{C}' + \bar{d_3}\mathcal{C}''\right)\right] n + \left(\hat{u}, \hat{v}, \hat{h}, \hat{d}\right) \tag{5.49}$$

with

$$(\hat{u}, \hat{h}, \hat{d}) = \sum_m (u_m, h_m d_m) sin(M_m n), \qquad \hat{v} = \sum_m v_m cos(M_m n) \tag{5.50}$$

becomes for the case $m = 1$ (first transverse Fourier mode):

$$(u, v, h, d) = \left(0, 0, \bar{h_1}, \bar{d_1}\right) n + (\hat{u}, 0, 0, 0) \tag{5.51}$$

with

$$\hat{u} = \sum u_m sin(M_m n) = \frac{b_1 + a_2 b_4 - a_2 F_0^2 b_2}{a_1}, \tag{5.52}$$

where $M_m = 1/2(2m+1)\pi$ and the coefficient $\bar{h_1}$ and $\bar{d_1}$ of equation (5.51) are

$$\bar{h_1} = b_2 \qquad \bar{h_1} = F_0^2 b_2 - b_4 \tag{5.53}$$

The coefficients a_i and b_i are the coefficient of the depth averaged linear system derived for the solution and they depend on the parameters that define the reference uniform flow (see Zolezzi and Seminara, 2001).

Non linear solution

The fundamental difference between the 'classical' linear meander solution described in the previous Section and the nonlinear solution of Seminara and Solari (1998) is that this latter work assumes that the lateral bed slope is a small parameter, which does not necessarily imply that the amplitude of the water depth and velocity perturbations are 'small', especially when the channel is wide and shallow enough. The perturbation of the water depth is therefore modified compared to the classical linear approach such that the reference flow becomes a *locally* uniform flow in a straight channel with slowly-varying unknown water depth $D_0(n)$.

Let us then briefly recall how to determine the function $D_0(n)$ that describes the lateral variation of the water depth at the leading order. We first expressed the different term above introduce as function of the unknown term $D_0(n)$. At the leading order the streamwise component of the Reynolds equations allows to determine the function $\breve{u}(n)$ introduced in equation (5.39), describing the slowly varying uniform flow velocity in the straight reference channel as

$$U = D_0(n)^{1/2} \mathcal{F}(\xi). \tag{5.54}$$

Moreover, at the leading order, the continuity equation for the solid phase (5.22) imposes that the transverse sediment rate must vanish for each point of the cross section. Therefore, by substituting the structure individuated for V_1 and U, equations (5.44) and (5.54), respectively, into equation (5.33), the relation for the unknown function $D_0(n)$ proposed by Seminara and Solari (1998) can be written in the form:

$$\frac{dD_0(n)}{dn} = -\frac{\nu\sqrt{\theta_0}}{r\sqrt{C_0}} \frac{\mathcal{G}(n)_{,\xi}}{\mathcal{F}(n)_{,\xi}} |_{,\xi_0} D_0^{3/2}. \tag{5.55}$$

having defined $\tau = (\tau_s, 0 + \tau_n')$ with

$$\tau_n' = \frac{D_0(n)}{\beta} \mathcal{N}(\xi_0) \breve{u}^2 \mathcal{G}_{,\xi}|_{\xi_0} \tag{5.56}$$

$$\tau_s = \sqrt{C_0} \mathcal{N}(\xi_0) \breve{u}^2 \mathcal{F}_{,\xi}|_{\xi_0} \tag{5.57}$$

The form of equation (5.55) denotes that the transverse bed variation is characterized by an increasing outward slope and that its amplitude increases linearly with channel curvature, through the parameter ν, and the square root of the Shields parameter. Because the functions $\mathcal{F}$ and $\mathcal{G}$ depend on the transverse coordinate n, the equation (5.55) can not be solved analytically. Therefore, the solution can be found by numerically integrating equation (5.55) using a trial by error method that assigns an initial condition in terms of the unknown function D_0. The final solution is obtained by imposing that the lateral variability of the water depth satisfies the integral constraint on the liquid flow discharge expressed in equation (5.35).

Non linear solution with transverse roughness variation

The non linear model for the evolution of the channel bed was then modified in order to account for the change in flow resistance associated with the presence of vegetation within the evolving inner bank. The local water depth, obtained from the quasi 1-D hydraulic model (paragraph 5.2.4) accounts for the vegetation effects through relation (5.7). It was used to compute the value of the friction coefficient C_0 (5.26) at each position of the cross-section. The new equation for the vertical distribution of the uniform flow component $\mathcal{F}(\xi)$ then reads

$$\mathcal{F} = \frac{\sqrt{C_0(n)}}{k}\left[ln\frac{\xi}{\xi_{0S}(n)} + A\xi^2 + B\xi^3\right] \tag{5.58}$$

with the normalized form of the conventional non-slip reference level given by

$$\xi_{0S} = \frac{\xi_0}{D_0(n)}; \tag{5.59}$$

$$\xi_0 = exp\left(-\frac{k}{\sqrt{C_0(n)}} - 0.777\right). \tag{5.60}$$

In the light of this, also the longitudinal component of the bed shear stress τ_s (5.57) varies along the transect according with the relation:

$$\tau_s = \sqrt{C_0(n)}\mathcal{N}(\xi_0)\breve{u}^2\mathcal{F}_{,\xi}|_{\xi_0} \tag{5.61}$$

Under such condition, the effects induced on the river bed morphology due to channel curvature are associated, through a 'bulk' effect expressed by a modified coefficient C_0, with the modification of the flow field induced by riparian vegetation. On the other hand, vegetation success and growth is

conditioned by the secondary flows that, modifying the river channel bed, allow bare sediments to be colonized during the low flow. Therefore, this rather simple feedback mechanism built-in the developed model allows to link biological dynamics with morphological processes.

5.3 Results

The Results Section is organized in four parts. Section 5.3.1 presents at its beginning the four streamflow time series that have been used as input data for all the analysis included in this Chapter, discusses their significance, and afterwards presents a model application to the idealized case of a straight channel (limit case of vanishing curvature) without introducing any specific channel bed morphodynamic submodel. In this way bed evolution is purely depositional, through equation (5.5) and no possibility of bed scouring is foreseen. Such oversimplified, even unrealistic test case is chosen with the sole aim to investigate the sensitivity of the adopted submodel for riparian vegetation dynamics (Section 5.2.1) to the choice of the several model parameters on which it is dependent.

Section 5.3.2 then focuses on the meander bend morphodynamic submodel presented in Section 5.2.5: it reviews the main outcomes of the linear and nonlinear solutions and compares the classical nonlinear solution with that obtained by allowing a lateral variability of the friction coefficient. The lateral evolution of a meander bend cross-section with constant curvature is then analysed in Section 5.3.3 under three of the adopted flow hydrographs introduced in Section 5.3.1. The results of this analysis allow several answers to the research questions posed in Chapter 2, particularly in relation to the bed topography and vegetation patterns developing in the advancing bank and in the floodplain as well as to the temporal dynamics of the morphologically active channel width.

Finally, the results of a qualitative comparison between the outcomes of the proposed model with the field and remote sensing observations performed on the meander bend of the Tagliamento River (Chapter 4) is presented in Section 5.3.4.

5.3.1 Riparian vegetation dynamics in response to hydrological forcings

Different hydrological patterns were used to assess and quantify the influence of the main hydrological forcings on river channel morphodynamics, in a natural evolving meander. To this aim, first we investigated a case in which river water discharge oscillates with regular frequency (time between two consecutive flood event about 1 year) and constant amplitude,

as reported in Figure 5.5. For this case formative condition are associated with the maximum value of discharge (420 m^3/s). Then we relaxed the regularity of the events by assigning a random distribution (in magnitude and time) of floods that realize as instantaneous increment in water discharge (Figure 5.5b), investigating the effect of each discharge value above the 273 m^3/s. The first and the latter data set allowed to investigate the effect of temporal variability in discharge formative value and of formative discharge fluctuation (without raising/decreasing phases), respectively. Therefore, once identify the influence of these two hydrological flow properties, these characteristic were merged in a new hydrograph reported in Figure 5.5c (formative discharge threshold imposed equal to 236 m^3/s). Finally, the historical hydrological dataset used for the analysis of the field data presented in the previous chapter(Chapter 4) was used to provide a first validation of the model, accounting as 'formative' the flood above 570 m^3/s. For all the four tests, the discharge threshold used to define formative conditions was computed by imposing the coefficient α_Q of the equation (5.9) about 0.4.

An example of the river cross-section morphology and biomass distribution resulting from simulating the mutual interactions between vegetation and river hydrology using the quasi 1-D model presented in Section 5.2.4 is reported, for the study case of a sinusoidal cross-section and selective vegetation ($\lambda_1 = 0.3$,$\lambda_2 = 1$ and $z_{b0} = 0.7$), in Figure 5.6a. The initial cross-section transverse profile (black thick line) was approximated through a sinusoidal shape which can be considered as loosely representative of the hypsometric curve of a straight reach of a channelized river with alternate bars (Colombini et al., 1987). In addition, Figure 5.6b shows the positive trend showed by the average value of river bed vertical accretion (black line) and vegetation biomass (red line) associated with the imposed water surface fluctuation (blue line). Despite a net increase in biomass growth with respect to the initial phase, there is a decrease in vegetation biomass at each flood event. On the other hand, having neglected the presence of erosional processes and as consequence of the sedimentation induced by the action of the vegetation on the over-bank flow field, the channel bed keeps increasing its average elevation. In the figures 5.6a and b, the green line represents the maximum biomass density distribution, *carrying capacity* (5.2), at the beginning (a) and along (b) the simulation respectively. This value, depends only on the distance of teh ground surface from the water table (see equation (5.1)). It shows a slight variation in correspondence of the first and the fourth flood event, around the 200th and 1300th day of the simulation. The transversal variation of the river channel bed responsible of these small fluctuations is reported in Figure 5.6a with a black thin line together with the final lateral distribution of

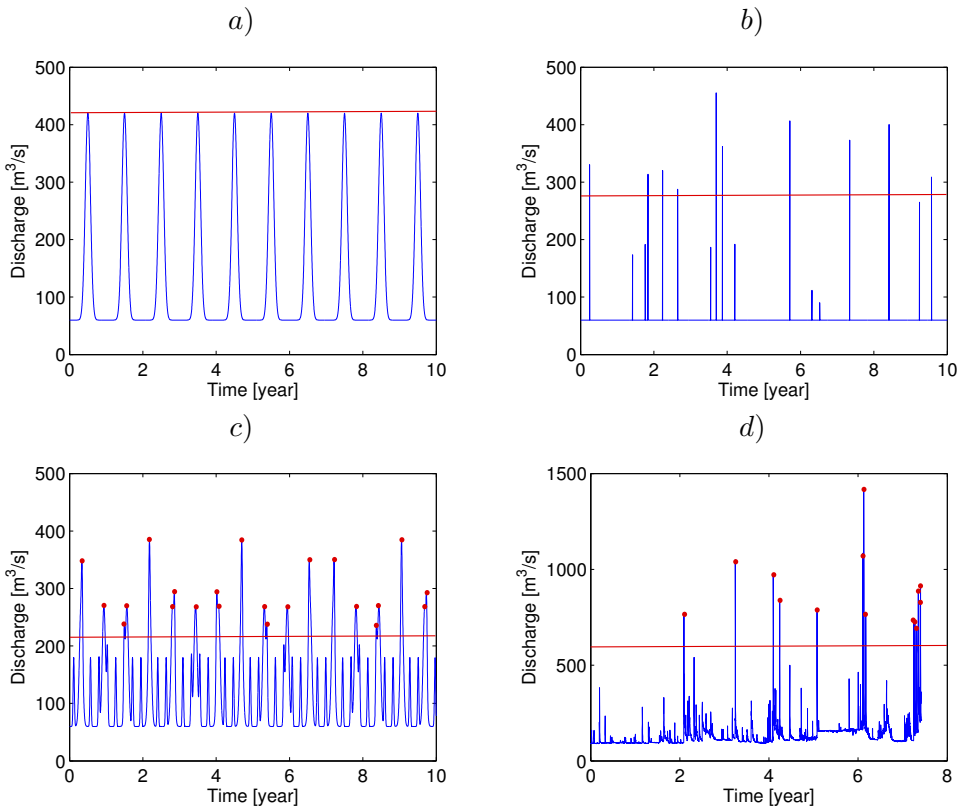

Figure 5.5: Flow discharge series used in the analysis (blue line) and associated threshold value (red line) used to define formative conditions. For the case of a) regular oscillation with constant amplitude the threshold value coincide with the formative discharge, while for b) instantaneous discharge variation each event above the red line is considered formative. For the mixed cases: c) oscillation with different peak values and d) real historical hydrological dataset the pick of each flood above the threshold value has been chosen as formative discharge (red circles).

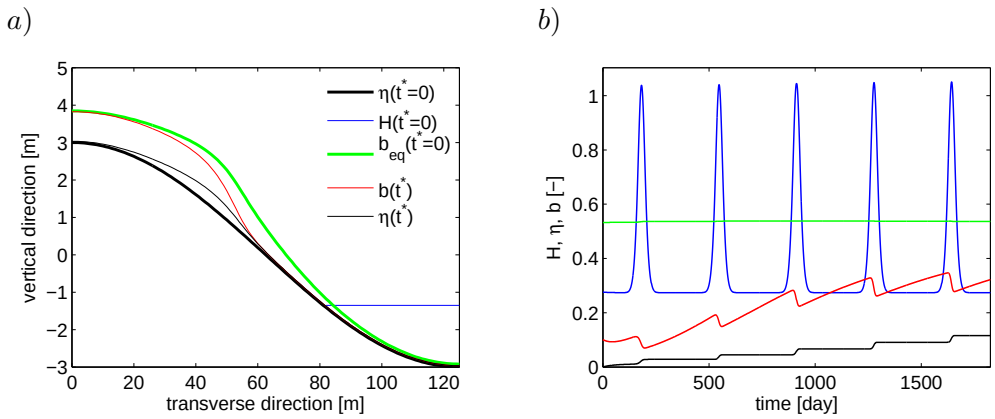

Figure 5.6: Example of the solution obtained by coupling the quasi 1D flow model (Section 5.2.4) with the riparian vegetation submodel (Section 5.2.1) idealized as loosely representative of the hypsometric curve of a straight reach of a channelized river with alternate bars, initial $\eta(t^* = 0)$ and final $\eta(t^*)$ bed profiles: a) evolution of the cross section, b) temporal evolution of the normalized main quantities. In both panels, the initial bed elevation $\eta(t^* = 0)$ is denoted with a thick black line, the free surface elevation h with a blue line and biomass at the beginning of the simulation $b_{eq}(t^* = 0)$ with a green line, ($\lambda_1 = 0.3$, $\lambda_2 = 1.0$ and $z_{b0} = 0.7$); the updated bed elevation (black thin line) and overall biomass b (red line). Other parameters: $\lambda_{sed} = 6 \times 10^{-3}\ m/day$, $\sigma_1 = 0.005\ day^{-1}$, $k = 0.017\ day^{-1}$ and $m_1 = m_2 = m_3 = 1$.

the overall biomass across the transect.

Because vegetation, by affecting flow resistance, induces sediments deposition (Hickin, 1984; McKenney et al., 1995), we investigated changes in vegetation biomass temporal dynamics associated with flow disturbance capacity and moisture sediment availability by varying, the parameters σ_1 and k of equation (5.3) and (5.4), as suggested by Gurnell et al. (2012). Results of this operation are reported, in terms of biomass transverse average value, in Figures 5.7a,b. The sensitivity analysis was then extended including other two important hydrological aspects, namely, the time interval between two consecutive flood events (Figure 5.7c) and the water base discharge value (Figure 5.7d).

Depending on the environmental conditions that affect plants growth (Figure 5.7a), vegetation biomass can grow very fast and reach a nearly equilibrium condition ($\sigma_1 = 0.008$) or growth can be slower and slower leading to reduce, progressively, the amount of overall biomass achievable. In the case of hostile environment ($\sigma_1 = 0.001$), 'negative' effects due to river flow action are predominant and vegetation drastically reduce its presence within the inner bank area. Similar results can be obtained by increasing river flow disturbance capacity accounted through the k parameter in Figure 5.7b. This latter case highlights the strong influence

of river-induced processes on vegetation during its early phase, which decreases with increasing trees age. Good environmental conditions for vegetation growth are represented by the slope of the ascending phase of each curve (see figures 5.7a and b), with high slope values corresponding to suitable environment for vegetation growth. Fixing the growth rate during the simulation (constant slope in the graph of Figure 5.7c) implies to consider stable environmental conditions for vegetation growth. Curves obtained from changing floods frequency, with each event presenting analogous disturbance capacity and under the hypothesis of stable environmental condition, show a constant small variability in final vegetation biomass production (Figure 5.7c).

Figure 5.7d summarizes the results proposed in Figures 5.7a,b. It shows that minimum water level variation in the river channel promotes riparian vegetation growth (higher moisture supply due to an increasing in water table elevation) for base discharge value less than 50% of the maximum discharge value considered in the analysis. Further increasing of the flow discharge that feed the channel determines, first, anoxic condition of the root system and, for even higher discharge values, the erosion of the vegetated area or trees uprooting, leading to an abrupt diminishing in the presence of riparian vegetation. The extreme case for which the whole cross-section result always submerged (dimensionless disharge value unitary in Figure 5.7d) determines a channel entirely constituted of bare sediments.

5.3.2 Comparison between the meander bend morphodynamic submodels

A preliminary study was conduced to quantify the differences between the solutions for the flow field and bed topography resulting from the application of the three meander bed morphodynamic models described in Section 5.2.5: namely one linear (Zolezzi and Seminara, 2001) and two non linear models, which are based on Seminara and Solari (1998) and on an extension of the latter, which was suitably modified to account for the lateral variation of the friction coefficient within the cross-section area. In particular, we focused on the prediction of the transversal distribution of the water depth and of the longitudinal component of the shear stress, being this what ultimately determines the lateral evolution of the external bank (see Section 5.2.2). Figure 5.8 shows the variation of the water depth along the transect, as predicted by the three moorphodynamic models applied. The straight dashed line denotes the linear solution, while the curved solid line represents the solution obtained by including the non linear effects. The comparison between this two curves highlights the

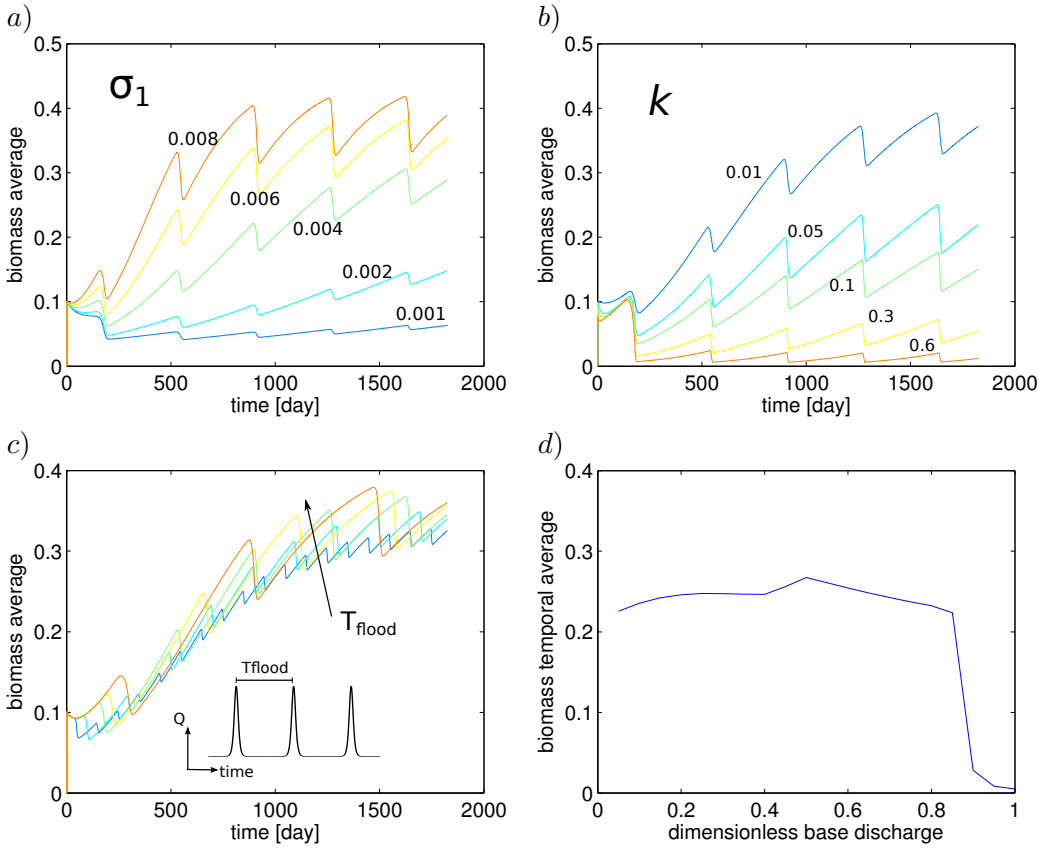

Figure 5.7: Influence of main model parameters on the overall biomass temporal distribution in a channel with an initially sinusoidal cross-sectional shape. Default parameters are as follows: the base discharge 100 m^3/s and the hydrograph consists of an identical sequence of identical floods with peak $Q = 1600\ m^3 s^{-1}$ occurring once a year. Values of the other parameters are $z_{b0} = 0.7$, $\lambda_1 = 0.3, \lambda_2 = 1.0$, $m_1 = m_2 = m_3 = 1$, a) $k = 0.017\ day^{-1}$, b) $\sigma_1 = 0.005\ day^{-1}$, c) and d) $k = 0.017\ day^{-1}$, $\sigma_1 = 0.005\ day^{-1}$ Panel a) examines the sensitivity of the cross-sectionally averaged biomass growth to σ_1; panel b) the sensitivity to k; in panel c) and d) what varies is, respectively, the period between consecutive flood events and the base discharge values.

well known effect whereby simplifications introduced in deriving the linear solution lead to underestimate the water depth at the inner bank ($n = -1$) and, to overestimate it at the outer bank ($n = 1$), with respect to the predictions of the non linear theory. Moreover, the result obtained accounting for a lateral variability of the friction coefficient C_0 (red solid line), due to the presence of laterally variable vegetation biomass within the inner bank, slightly diverge from the non linear solution computed assuming the same roughness along the entire cross-section. The reader may have noticed that the y axis of figure 5.8 is reported with the values inverted. This strategy allow to interpret the plot of the water depth lateral variability as the transverse variation of the channel bed that results to be in equilibrium with the flow conditions and the river geometry (i.e curvature), because of the typically small value of the lateral slope of the water free surface, for which $\eta = H - D$.

Comparing transverse variation of flow properties (namely, longitudinal components of the flow velocity and of the near-bed shear stress) allows to understand the role of the non linear effects on the flow velocity (Figure 5.9a) and on the shear stress (Figure 5.9b). Of particular interest is their behaviour at the lateral boundaries ($n = \pm 1$) of the transect. The sinusoidal structure imposed to the velocity component to solve the flow field in the linear model leads to an oscillation around a reference value, occurring in the middle of the cross-section $U(n = 0) = 1$; Figure 5.9a. Figure 5.9a shows a high difference in predicting flow velocity by using a linear and non linear solution (dashed and solid line, respectively), with a substantial overlapping of the solutions obtained by applying the two non linear models, in analogy to what observed in the bed transverse profile of Figure 5.8.

Results obtained from the analysis of the longitudinal shear stress component (Figure 5.9b) presents a different trend from that observed in the lateral distribution of the river bed and of flow velocity patterns. In this case, indeed, the linear solution (dashed line) differ slightly from the non linear one (solid blue line) far from the river banks, but the two solutions strongly diverge while approaching the channel boundaries ($n = \pm 1$). Moreover, differently from what happened for the longitudinal velocity component U, the inclusion of the transverse variation of C_0 reduces the predicted value of shear stress (solid red line) at the inner bank ($n = -1$) and increase it in proximity of the outer bank ($n = +1$). The transverse location where the two nonlinear solutions intersect, as well as the gap between the values predicted at the banks, may vary subject to the reference flow and to the curvature ratio.

For the sake of completeness, we reported in Figure 5.10 an example of the transverse variation of the $\mathcal{G}$ (equation 5.46) in the non linear models,

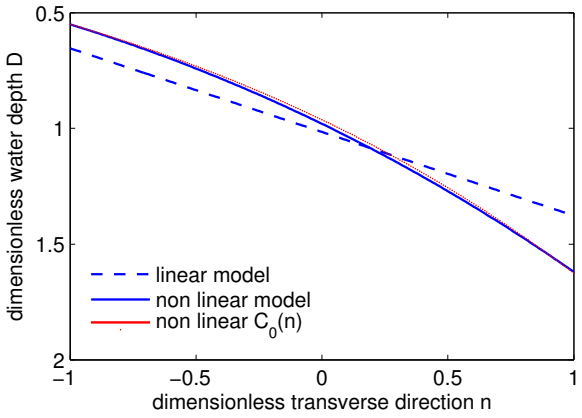

Figure 5.8: Comparison between the transverse variation of the water depth D_0 predicted from the three different bend morphodynamic models: linear model (dashed line), non linear model (solid line) and non linear model accounting for transverse variability of the friction coefficient C_0 (dotted line); $\beta = 11$, $\theta = 0.14$,$ds = 0.007$, $\nu = 0.5$.

with constant (solid line) and variable (dashed line) friction coefficient C_0. The vertical structure of the secondary flows does not present significant changes across the transect in agreement with Seminara and Solari (1998), and the contribution given by a variable friction coefficient seems to be almost imperceptible. In light of this latter consideration, and considering that the predicted values of the water depth (Figure 5.8) and the longitudinal component of the flow velocity U (function of D_0 and $\mathcal{F}$ - Figure 5.9a) are pretty similar for the two non linear models, the differences in shear stress value (Figure 5.9b) can be related with the variation of the friction coefficient in the relation (5.61).

In the following we will use the non linear solution that accounts for a variation of the friction coefficient value along the transect, in order to model the biomorphodynamic processes associated with the lateral migration of the river banks of a constant curvature bend.

5.3.3 Biomorphodynamic of a laterally migrating meander bend

Figure 5.11a shows several stages of a thirty year simulation of the lateral evolution of a constant curvature meander bend in presence of riparian vegetation under periodical discharge variation (Figure 5.11b). At the very beginning of the simulation the channel presents a rectangular cross section included between the two banks (positioned at -50 an 50 m) and characterized by a flat bottom (0 m elevation). After the first formative event (formative discharge assumed for this case coincident with the

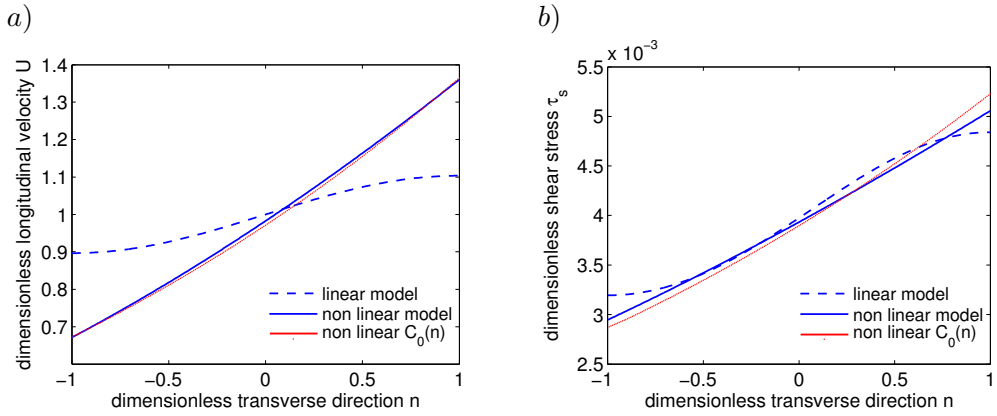

Figure 5.9: Transverse profile of a) longitudinal flow velocity U and b) longitudinal bed shear stress τ_s obtained with the three different bend morphodynamic sub-models, linear (dashed line), non linear (solid blue line) and non linear with lateral variation of the coefficient C_0 (solid red line); $\beta = 11$, $\theta = 0.14$,$ds = 0.007$, $\nu = 0.5$.

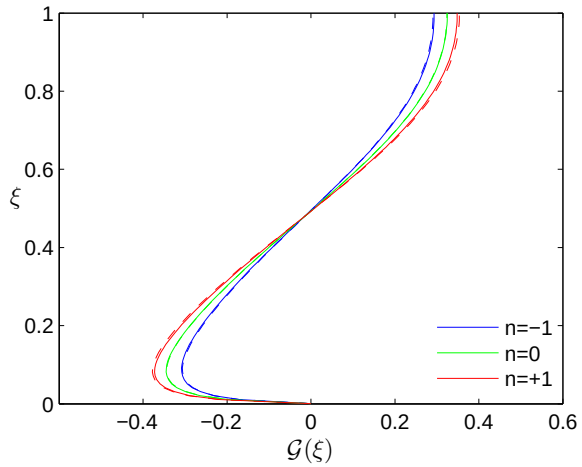

Figure 5.10: Example of lateral variation of the $\mathcal{G}$ function, which represents the vertical profile of secondary helical flows in a bend of constant curvature. The three lines refer to the inner bank ($n = -1$), the middle of the channel ($n = 0$) and the outer bank ($n = 1$) for the case of constant coefficient C_0 (solid lines) and variable along the transverse coordinate (dashed lines).

peak of each flood event), the flow field induced by channel curvature (scour/deposit at the outer/inner bank) modifies the transverse inclination of the river bed, generating the classical cross-section of a meander bend (see section t_0 in Figure 5.11a). Since the latter represents the first physically meaningful configuration of the evolution processes we prefer to omit the starting, arbitrary rectangular geometry from the plot of Figure 5.11a. During low flow, following the first event, riparian vegetation colonizes the exposed sediments of the channel bed and consolidate the ground through its growth. The subsequent increase in water stage due to a new flood event determines sediments deposition together with plants removal in the vegetated area. When the formative discharge is reached (maximum discharge value), bank retreat is computed and the channel bed is updated according to the new value of the morphologically active width and the simulation procedure is repeated for all the events of the considered hydrograph (Figure 5.11b). Temporal oscillations in channel width and in the longitudinal shear stress values at the toe of the external bank during the simulation are reported in Figure 5.11b. Bank erosion, initially increases channel width, which further promotes channel narrowing. The model suggests that such temporal oscillation is intrinsically associated with flow unsteadiness. This is how the mechanism generates: increasing channel width due to erosion processes reduces the water depth, extending the portion of cross section available for vegetation recruitment and brings the water table to a suitable elevation for vegetation growth. Considering the stabilizing role played by vegetation, this mechanism leads to progressively reduce the morphologically active channel width under formative conditions. This 'dance' (already argued by Nanson, 1981) between the two river banks is well reproduced by the curve of Figure 5.11b, which consists of a sequence of red and green segments. Active channel widening due to the erosion of the outer bank during the event's peak is reported with an almost vertical segment (red line), while the accretion process is associated with a loss of active area (green dashed line). The temporal oscillations of the channel width are in turn associated with progressively appearing spatial oscillations of the ground surface that characterizes the accreting bank (Figure 5.11a), which is the result of these mutual interactions, namely, active channel narrowing/widening and sedimentation processes.

By observing the curve of Figure 5.11b the processes described above seems to produce a channel width that oscillates around a steady state after the third flood event. Moreover, the cross-section profile at the end of the simulation (t_{END}) shows two distinct regions (length around 90 m) that identify the new constituted inner bank and the active channel width (see figure 5.11b). This qualitatively agrees with the field observations

presented in chapter 4. Furthermore, the final cross-section presents a transverse profile similar to that have been observed by Camporeale and Ridolfi (2010) in their model.

Further analysis were conduced to assess the impact of different hydrological and biological forcings in order to identify the physical controls of the morphological pattern observed in the field (see chapter 4). In light of the results showed in Figure 5.7 two contrasting biological scenarios were chosen to simulate the condition of suitable environment for riparian vegetation growth ($k = 0.015$) and the extreme case in which high flow disturbance prevent vegetation biomass development ($k = 0.7$). In the following, these two cases will be associated with the letter A and B, respectively. It is acknowledged (Gurnell et al., 2001; Braudrick et al., 2009; Perona et al., 2012) that two relevant parameters for the formation of morphological structures associated with the interplay between riparian vegetation dynamics and river hydromorphodynamic processes are flow magnitude and floods time frequency. However, it is important to consider also that vegetation-induced river processes (i.e. sedimentation) depends on the duration of the period in which trees are partially wet. Therefore, we investigated separately the effect of such hydrological controls by using the simplified hydrographs reported in Figure 5.5 a and b, which are identified in the analysis as 1 and 2, respectively. In particular, hydrolograph 1 (Figure 5.5a) shows a periodical oscillating pattern characterized by constant peak value which was chosen as formative discharge to update the river morphology. The rising and decreasing phase allow to model river- and vegetation-induced processes. Figure 5.5b presents hydrograph 2, where floods magnitude and temporal frequency are both generated randomly. In this case the absence of a transitional phase between low flow and high discharge was designed on purpose to isolate the flow influence on vegetation and vice versa. The two properties could be analyzed together in the more complex hydrograph 3 (Figur 5.5c). Results obtained are reported in the composite Figure 5.12 and Figure 5.13 showing all the possible combinations of environmental conditions (A-B) and forcing hydrograph (1-2-3), i.e., A1,.., B3. In particular, Figure 5.12 shows the cross-section profile (brown thick line) and the related vegetation biomass (green thin line) at the end of the simulation, after ten years of bio-morphological changes. Figure 5.13 presents the time series morphologically active width and of the predicted longitudinal shear stress at the outer bank ($n = 1$) for each formative flood.

Simulations conduced for the case of vegetated channels, (column A on Figure 5.12) have revealed the formation of two distinct zones within the cross-section area: one higher elevated zone colonized by vegetation (on the left) and the other characterized by bare sediments (on the right).

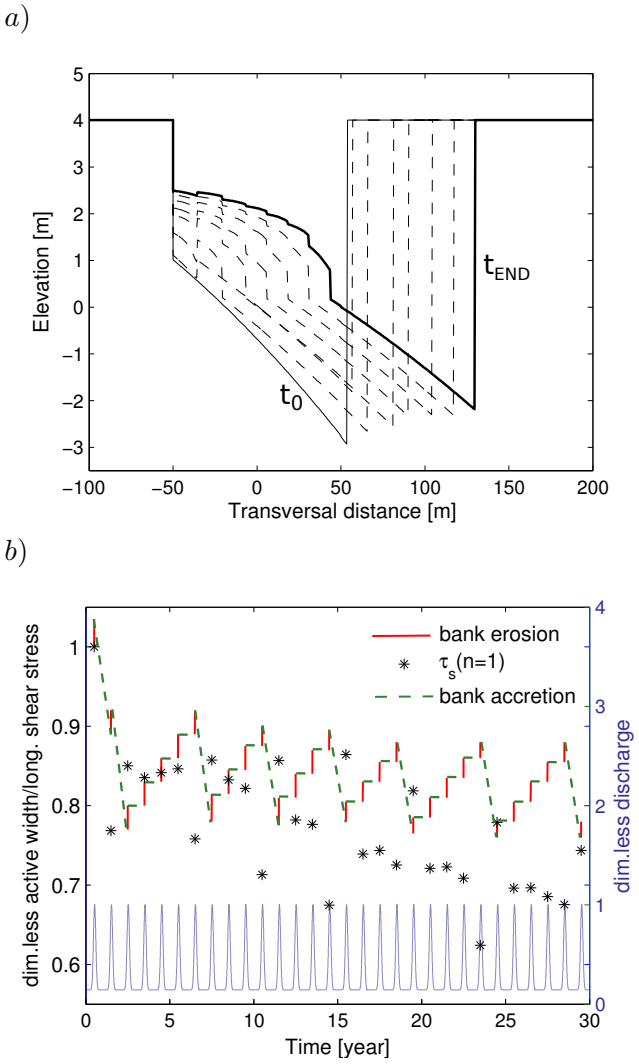

Figure 5.11: Cross section temporal evolution: a) transverse channel bed elevation and b) fluctuation of the morphologically active channel width due to the erosion processes that occur at the outer bank (red line) at each flood event because of the shear stress value (denoted with an asterisk) and the accretion of the inner bank (dashed green line). Active channel width and longitudinal shear stress are made dimensionless using their initial values, water discharge is denoted with a light blue line and it is represented scaled by its maximum value.

Considering the architecture of the model applied, the latter zone represents the portion of the morphologically active river cross-section during the last flood and therefore the present channel, while the first identifies the new constituted inner bank. This separation appears less marked on figures B2 and B3 (column B) and it vanishes completely in the first case (B1) where the role of vegetation is almost negligible. Moreover, in each pair AB, vegetation success and growth is associated with a narrower active channel with respect to the case of less developed vegetation biomass (see different plots reported in Figure 5.13). This first comparison highlight the strong influences of river- and vegetation-induced processes in driving morphological changes.

The vertical comparison between the results presented in Figure 5.12 shows that different hydrological disturbances imply differences in the development of the inner bank ground surfaces, providing evidence that fluctuations in flood magnitude associated with a gradual variation of the water stage are two fundamental ingredients for the formation of complex morphological pattern within the advancing bank area (A3). The lack in one of these two components, indeed, determines more simplified patterns (A2,A1) or smoother ground surfaces when vegetation growth is strongly inhibited (B1,B2 and B3). Moreover, panel A2 reveals that fluctuations in flood magnitude controls the lateral oscillation of the ground surface at the inner bank, while sedimentation induced by vegetation during the over-bank flow increases inner bank elevation, separating it from the active channel (panel A1).

Further analysis showed that the differences in channel cross-section observed are associated with different temporal evolutionary path of the active channel width and with the erosional power, as reported in Figure 5.13.

Figure 5.13, panel A1 shows channel narrowing phases (dashed green line) alternated in time with widening phases (red line) in terms of both width and near-bank shear stress value. According to the result presented in figure 5.11b (which refers to the same simulation over a period of 30 years) this oscillation seems to occur around an equilibrium, steady state value that corresponds with the formation of an inner bank surface scaling with the active channel width. On the other hand, when vegetation removal prevents the accretion of the inner bank, the channel keeps increasing its active width, and progressively looses its erosional power (Figure 5.13, panel B1).

Variation in flood magnitude which characterizes panels A2, A3, B2, B3 in Figure 5.13, is reflected in increasing the channel width (black thin line) that is not directly related with the erosion of the outer bank during a flood event (red line), like for the cases commented above. Consid-

ered that in the model both the inner and outer bank can erode, this behaviour can be explained with the lost of a portion of the inner bank that is morphologically active under the flow conditions imposed by a certain flood event. This does not happen for the cases A1, B1 (periodical floods with constant magnitude) because the discharge that generated the inner bank (stable area) had never been overcome during the simulation. Moreover, the erosion at the inner bank determines a less regular pattern in both active channel width and near-bank shear stress temporal fluctuations. Interestingly, a more regular oscillation is recovered in panels A3, B3 (random oscillation of the hydrological pattern), where these three mechanisms (outer bank erosion, inner accretion and erosion at the inner bank) alternated in generating river morphology. In particular, in presence of less developed vegetation biomass (B3), the active width seems to diverge, while for the other case (A3) the role of vegetation is to constrain the evolution of the active channel width.

5.3.4 Application to a meander bend representative of the lower Tagliamento River

A find scenario was built with the aim to explore the predictions of the proposal model when applied to a real case. It must be stated that, because of the many adopted simplifications, a close correspondence with the field observations could not be expected. The performed application is therefore expected to be a 'realistic' one, rather than aiming at closely reproducing the dynamics of a specific bend. The cross section, the hydrograph and vegetation processes have been chosen to match as much as possible the conditions met in the bend of the Tagliamento River where field observations took place (Chapter 4).

To this aim, we used the data collected during the field campaign (see chapter 4). In particular, we assumed a selective vegetation biomass ($\lambda_1 = 0.6$; $\lambda_2 = 6$) with optimum at $z_{b0} = 4.8\ m$. Vegetation growth rate was estimated from the growth curve extracted from biomass measurements at a value of $9 \times 10^{-2}\ day^{-1}$, while the decay coefficient k was reasonably set at $0.014\ day^{-1}$. The grain size dimension used was that of the active channel, estimated around $0.04\ m$ and assumed constant. The initial domain was set such that the river bank reached the elevation of $8\ m$ as estimated from the topography measurement, the slope for the river reach was estimated about 0.001 and as hydrological input was chosen the historical hydrological data set (Figure 5.5d) already used for the analysis presented in the previous chapter (chapter 4). The erosion coefficient M was imposed equal to $1 \times 10^{-}6\ m^3/s$, the critical value for the shear stress was set at $10\ N$ and the coefficient accounting for

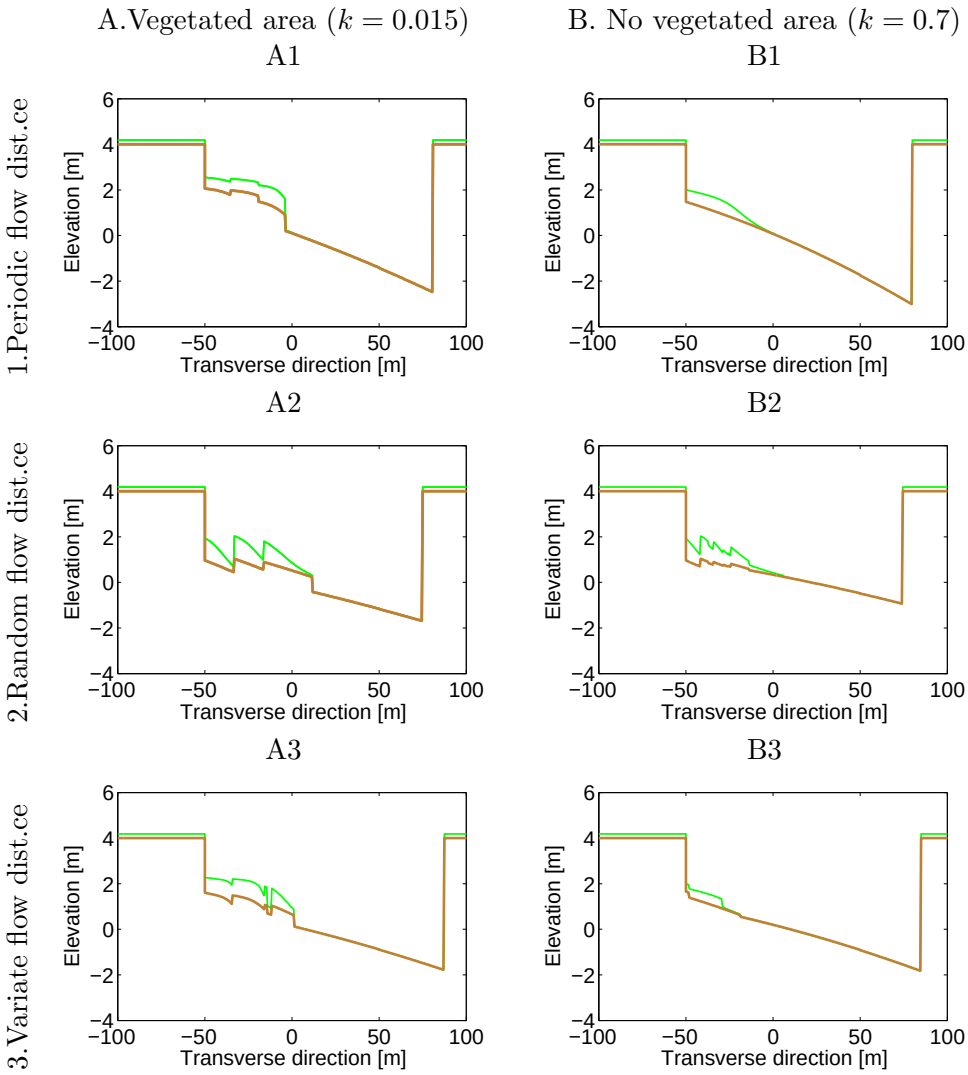

Figure 5.12: Cross section temporal evolution for different hydro-biological scenarios: A and B denote, respectively, suitable environment for riparian vegetation growth ($k = 0.015$) and the extreme case in which high flow disturbance prevent vegetation biomass development ($k = 0.7$). Each case has been investigated using different hydrographs, namely, 1 presents periodic oscillating pattern characterized by constant peak value, 2 where flow magnitude and temporal frequency are both generated randomly and 3 its a more complex hydrograph that include characteristics of 1 and 2. The panels A1,..., B3 show all the possible combinations of environmental conditions (A-B) and forcing hydrograph (1,2,3).

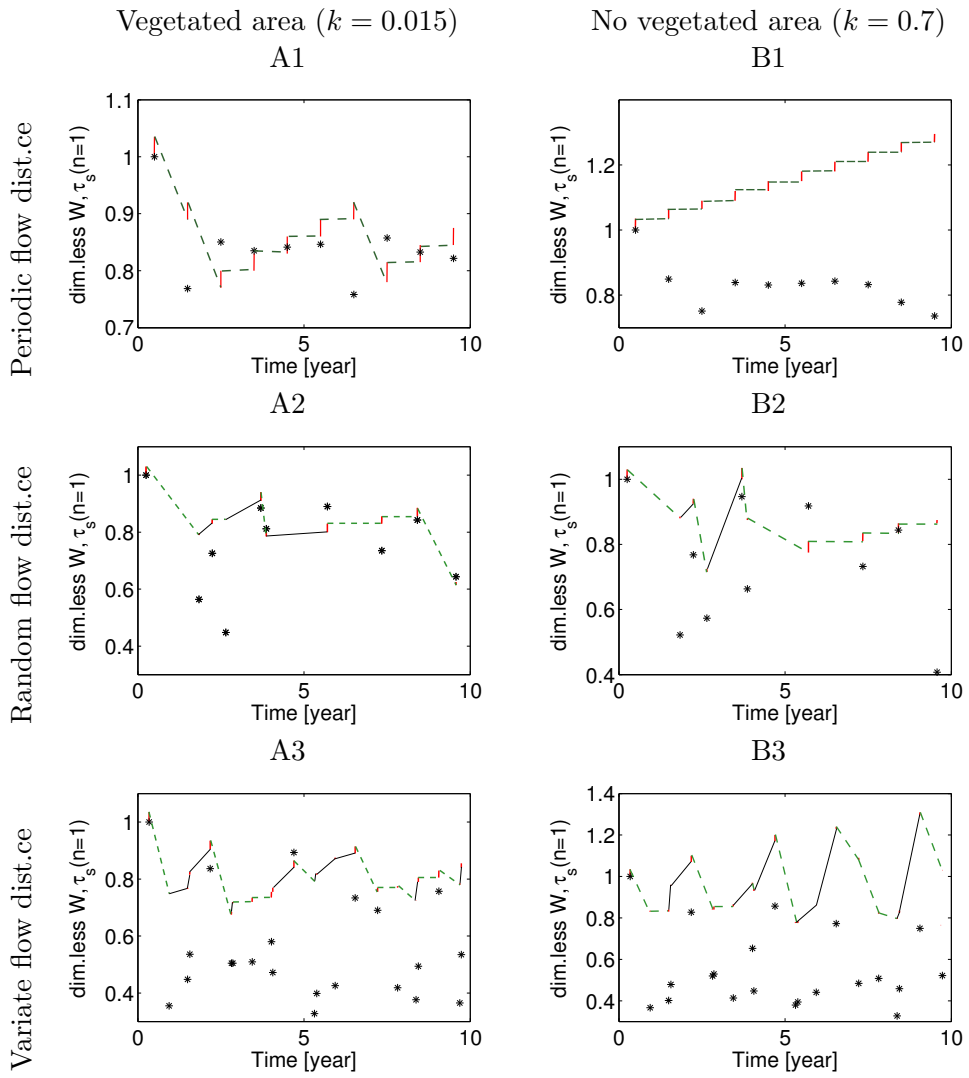

Figure 5.13: Fluctuation of the morphologically active channel width and correspondence value of the near-bank shear stress for different hydro-biological scenarios: A and B denote, respectively, suitable environment for riparian vegetation growth ($k = 0.015$) and the extreme case in which high flow disturbance prevent vegetation biomass development ($k = 0.7$). Each case has been investigated using different hydrographs, namely, 1 presents periodic oscillating pattern characterized by constant peak value, 2 where flow magnitude and temporal frequency are both generated randomly and 3 its a more complex hydrograph that include characteristics of 1 and 2. The panels A1,..., B3 show all the possible combinations of environmental conditions (A-B) and forcing hydrograph (1,2,3).

vegetation-induced deposition at 5.8×10^{-3} m/day The result obtained is reported in form of cross-section (brown line) and related vegetation biomass transverse distribution (green line) in Figure 5.14a. Following the same procedure applied above, the final cross-section is associated with a graph showing channel width (red/green line for erosion/accretion) and shear stress (asterisk) variation through out the simulation time and the related flow disturb (blue line); see Figure 5.14b.

Figure 5.14b shows clearly a narrowing effect due to the low magnitude of the events that occurred in the first four years, that allow the presence of suitable conditions (water table depth and flow disturbance) for riparian vegetation success and growth. On the other hand, after the sixth year, frequent floods of increasing magnitude promote bank erosion (red line) inducing channel widening.

Interestingly the model was able to describe overall bank accretion similar to that observed in the field and to reproduce the three zones such as determined from topography measurements (see Figure 5.15). In particular, river channel area extends from -150 to -40 m, the area farer from the river edge from -10 to 50 m an the area in between from -40 to -10 m. Moreover, the area located far from the river edge presents several oscillations of the ground surface, denoting a strong similarity with the topographical signature of the study case of chapter 4 of the present thesis.

5.4 Discussion

Results obtained through the proposed simplistic biomorphodynamic model show the validity of using an hybrid numerical and analytical model in simulating bio-morphological interactions (Seminara and Bolla Pittaluga, 2012) in advancing meander bends. The proposed method indeed allows to reproduce ground topography and riparian vegetation pattern similar, at least qualitatively, to those observed in the field (see chapter 4 and also Rodnight et al., 2005; Rozo et al., 2012) that can be argued to underpin the further development of scroll bars (Figure 5.14).

It is worth discussing the results of the present Chapter in the light of two main focuses: i) the possibility to reproduce spatial patterns of ground topography and riparian vegetation along the inner, accreting meander bank and ii) the properties and controlling factors of temporal width variations associated with the dynamic evolution of a meander bend.

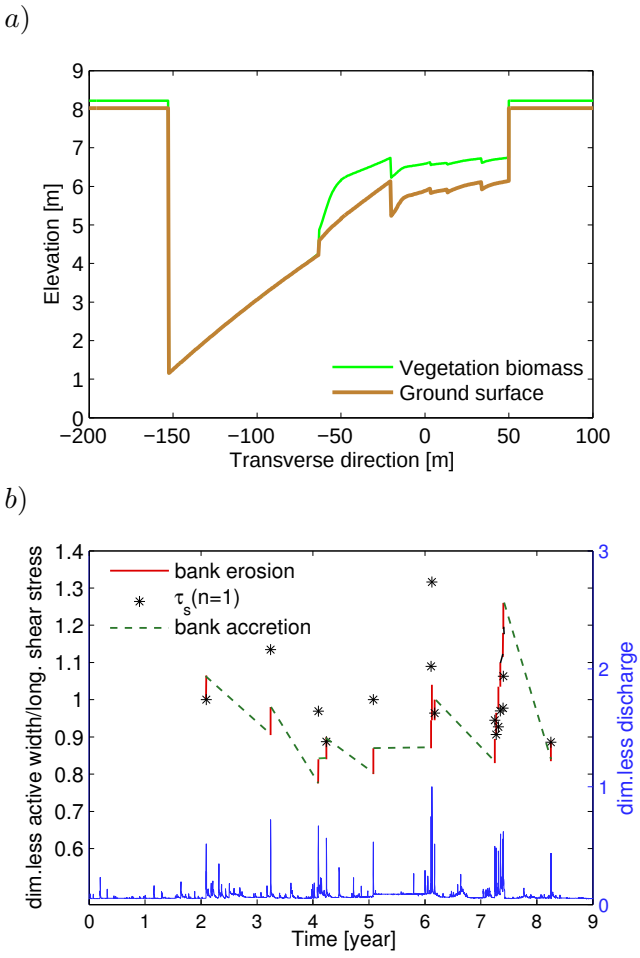

Figure 5.14: Cross section temporal evolving: a) transverse channel bottom elevation and b) fluctuation of the morphologically active channel width due to the erosion processes that occur at the outer bank (red line) at each event (light blue line) because of the shear stress value (asterisk) and the accretion of the inner bank (dashed green line). Active channel width and longitudinal shear stress are made dimensionless using their initial values, water discharge is represented scaled by its maximum value.

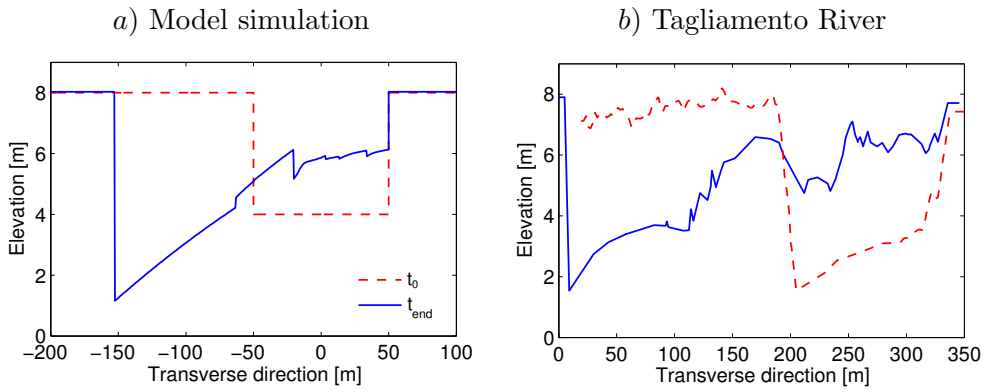

Figure 5.15: Comparison between initial (red dashed line) and present (solid blue line) geometry between a) model output and b) real cross-section of the Tagliamento River. Input data for the simulation, as well as the cross-section profiles (b) were estimated from the analysis conduced in chapter 4.

Morphological and vegetation patterns

Different combinations of the external hydrological and ecological forcing effects are predicted to result into different morphological and vegetation patterns at the inner bank. In particular, the different model runs point out the existence of two accretion mechanisms that, by cooperating, generate complex landforms within the inner bank area: lateral and vertical accretion. The transverse oscillation of the ground surface of the convex bank is due to the oscillation in river discharge that, as commented above, determines when the bank will extend or retreat. This variation leads to a new configuration of the point bar that modifies the inner bank profile. The other mechanism consists in vertical accretion due to the deposition induced by the interaction between vegetation and the flow field during over-bank flow. Presence of riparian trees or dead wood, modifying scour and deposit pattern initiate complex landform that evolve in a ridge and swales topography (Nakayama et al., 2002; Gurnell et al., 2012). However, the assumption of a continuous transverse vegetation biomass distribution prevented the possibility to catch this local flow field variation and, therefore, to describe the small-scale oscillations of the ground surface and of vegetation biomass within the inner bank.

Figure 5.7d denotes that the persistence of high flow for long periods of time determine the absence of vegetation. This is in agreement with the definition of channel subarea given in the previous chapter that distinguishes the three regions within river cross-section according to their time scale of inundation.

Temporal oscillations of the active channel width

Analysis of width temporal variation shows that the presence of vegetation within the inner bank prevents the occurrence of the 'runaway widening' mechanism, for which the eroding bank retreats much faster than the opposite bank can advance. This result is in agreement with laboratory experiments in which the development of a stable meander have required the use of cohesive material (van Dijk et al., 2013) or live alfalfa sprouts (Braudrick et al., 2009; Tal and Paola, 2010) to limit channel widening. Moreover, this represents an interesting achievement because in all the analyzed cases, constraint in channel width was due to accretion processes that occurred at the inner bank rather than in increasing erosion resistance, as the erosion coefficient M was kept constant in the different simulation runs.

Furthermore, results obtained shows that river channel width does not only depend on the presence of vegetation but also by the characteristic of the hydrological disturbance. This appear quite evident by observing the case of vegetated floodplain under periodic floods characterized by same magnitude. For this case, indeed, the erosion that occurs at the outer bank during the flood event increases the channel width, and this decreases, in turn, the river water stage. This allows vegetation to colonize the newly exposed sediments and growth, thus stabilizing the ground. Therefore, in absence of higher discharge the inner bank keeps advancing, thus reducing the channel width until the occurrence of a new flood competent to produce channel widening through erosion of the outer bank. This process is well recognizable in the oscillating pattern of figure 5.13A1 and it is in agreement with the field observation (Nanson, 1981) for which the outer bank move and the other tries to catch it up periodically. Moreover, the channel undergoes widening via right (outer) bank pull that induce narrowing processes toward bar push, as pointed out by Eke et al. (2014) who applied a more simplified closure relation to describe inner bank advance.

The simulation carried out with varying flood magnitudes revealed a less regular pattern of width oscillations (see Figure 5.132,3). In this cases, indeed, an increase in water discharge may lead to portion of the inner bank becoming morphologically active during the flood and therefore can be eroded. Such morphological activity is related to sediment mobility, which is influenced by the soil reinforcement provided by vegetation, the higher the biomass value, the higher the magnitude of the flood event required to activate erosion processes at the inner bank. This latter result is in accordance with the concept of 'fluvial biogeomorphic cycle' individuated from field observation on the landforms created by vegetation hotspots by Corenblit et al. (2007) and so, further supports the adequacy

of the developed model to reproduce, at least qualitatively, observed biophysical dynamics.

Finally, it is worth noting that variation in active channel width seems to be related not only with the maximum discharge value that flowed into the channel, but also with the time interval with which this occurred (see differences in Figure 5.12 and 5.5).

5.5 Conclusions

The present work, by separately modelling the evolution of the inner and outer bank of a meander bank and explicitly accounting for the active role of riparian vegetation in the advancing bank, constitutes a novel step in understanding biophysical interactions controlling fluvial processes of meander evolution.

The model is a first, biophysically based attempt to overcome the simplifying hypothesis of constant channel width on which meander migration models have been traditionally based. Differently from the closure for bank erosion and deposition proposed by Eke et al. (2014), which is based on the framework for self evolving bank of Parker et al. (2011), in this approach inner bank advancing is related with vegetation dynamic on the point bar accounted for through physically-based relationships for vegetation biomass dynamics. Despite the simplified closure used to describe vegetation-induced deposition and the continuous transversal distribution of the vegetation biomass, results obtained are encouraging of the model adequacy to reproduce observed processes.

The following main research needs can be formulated referring to the main simplifying hypothesis of the present Chapter, both in relation to the hydro-morphodynamic sub-models and to the vegetation dynamics sub-models.

- Accounting for the non stationary term in the sediment continuity equation (5.22) will relax the hypothesis that river channel bed adjustment occurs under equilibrium formative conditions. Such improvement will allow to model river morphology at each time step and for each discharge value, thus allowing to fully incorporate the effect of flow unsteadiness in the model predictions.

- Besides flow unsteadiness, also morphological unsteadiness likely affects the river bed response during formative events, like that related with the temporal oscillations of the active width. A simplified analytical modeling of such effect on river bed response would allow to build a more complete morphodynamic modeling approach.

- Extension of the model from cross-section scale to the reach length is required to include a more detailed description of spatially distributed meander dynamics under unsteady flow conditions. This step crucially requires to account for a coherent sediment budget at the reach scale, for instance through the sediment continuity criteria present in the modeling approach of Parker et al. (2011).

- Vegetation induced processes, mainly, sediment strengthening and deposition should be modelled accounting for variation of vegetation properties within their age.

- The sensitivity analysis made on the effect of the different parameters that can be changed in the model highlight the need to gain quantitative knowledge on vegetation properties when modelling bio-morphological interaction in a specific case. Despite most of these can be estimated through field measurements (i.e. growth rate, transverse biomass distribution; see Chapter 4) several parameters are difficult to be estimated in particular those related to sediment deposition (λ_{sed} in equation 5.5), to the effect of trees roots on soil reinforcement (equation 5.6) and to the vegetation decay rate during the submerged period (k parameter in equation 5.4).

Results obtained in this phase of the analysis underline the necessity of a multidisciplinary approach to investigate bio-morphological processes (Camporeale et al., 2013) and further suggest that model application has to be supported by field investigation. Overall, the model gave evidence of the potential of hybrid models in deep understanding the physical controls of the bio-morphological processes at the advancing bank that govern the planform evolution of river meanders.

The next Chapter 6 addresses one of the required improvements to the present modeling analysis. Namely it considers that temporal width oscillations emerging from both the modeling (this Chapter) and empirical analyses (Chapter 4) may induce changes in river bed instability and flow pattern (Repetto et al., 2002; Luchi et al., 2011). This effect may be particularly relevant when widening or narrowing phases occur at the same time scale of that of bed level adjustments. For these reasons, Chapter 6 represents a first attempt to model the effect of width unsteadiness on the curvature-induced flow and bed stability (free bars formation) by means of an two-parameters analytical perturbation model.

Chapter 6

A theoretical analysis of river bars stability under changing channel width

The biomorphodynamic model developed in Chapter 6 is based on a rather simplified morphodynamic modelling approach and has deliberately kept at the lowest level of complexity especially being it a first modelling approach to investigate the interplay among flow, sediment transport and riparian vegetation dynamics able to explicitly account for such dynamic interaction within the advancing bank. Flow unsteadiness has been shown to play a key role in the overall process, but its effect on the channel bed morphodynamics, modelled through the sub-model described in Section 5.2.5, has been neglected so far. Actually most analytical models in river morphodynamics suffer from this limitation, apart from few exception (e.g. Tubino, 1991; Hall, 2004). A step forward in this direction is needed as one of the most relevant improvements of the biomorphodynamic model presented in Chapter 5, which clearly showed the tendency of a meander bend to develop temporal oscillations of the active channel width during its evolution. Such improvements also bears broader implications for a variety of problems in theoretical morphodynamics, because of the paucity of contributions in this direction so far more generally in relation to river bars

The present Chapter aims to make a first attempt in this direction by developing a novel theoretical model to investigate the influence of temporal changes in channel width on river morphodynamics. The emphasis here is placed on the classical problem of free bar stability, but the presented approach can be easily extended to investigate the effect of temporal width oscillations to the temporal dynamics of a point bar in a meander bend.

6.1 Introduction

River bars have been extensively studied, analytically, as an instability phenomenon of an incompressible flow over a flat mobile bed in a single-thread river channels. Practical reasons of this interest lays in the need to predict bars formation in channelized rivers and the related scour and deposition processes that can affect navigation or damage engineering structures (e.g. bank protection).

Most of these *bar theories* have been developed under simplifying assumptions of steady discharge and fully sediment transporting cross section, therefore their application is strictly suitable mostly for single-thread channels and alternate bar patterns. Despite many simplifying assumptions, bar theories have been effective in supporting quantitative understanding of bar processes (e.g. conditions of occurrence; lenght scales) and have received quantitative support from laboratory experiments. Despite their simplifying assumptions, their application has been extended to be used as physically-based predictors of alluvial channel pattern (e.g. Parker, 1976; Crosato and Mosselman, 2009) with some degree of success.

Moreover evidence has been reported that rather simple and regular bar dynamics can take place also in complex channel morphologies, as wandering (Church and Rice, 2009) or braiding (Zolezzi et al., 2012a). In this latter study the formation and downstream migration of alternate and central bar patterns has been observed in a main individual branch of a braided river during a bar-forming flood event below bankfull stage. In such case, the channel transporting sediments expands its width during the rising stage of the flood, and is afterwards contracted during the falling limb. Application of the classical bar theory using constant discharge and channel width values, averaged over the flood duration, yields several discrepancies in bar wavelength and dominant transverse modes.

In principle, however, bar theory can be applied to laterally unconfined channels, provided temporal variations of discharge and actively transporting channel width are properly accounted for.

The aim of the present work is therefore to investigate, on a modelling basis, the stability of river bars in channels where the active width changes with time, thus possibly affecting bar morphodynamics. Because the channel width-to-depth ratio plays a key role on bar development, its temporal variations associated with the widening process can be expected to affect the dynamics of contemporarily developing bars. Existing theoretical analyses (e.g. Repetto et al., 2002) have investigated the influence of spatial planform variability on bars formation showing how spatial changes in channel width, influencing river bars, may produce planform instability and a related tendency to braid. The role of width unsteadi-

ness may become relevant especially in laterally unconfined channels with non-cohesive banks, as it has been observed in laboratory experiments on the initiation of braided and of 'pseudo-meandering' streams (Ashmore, 1982, 1991; Bertoldi and Tubino, 2005; Visconti et al., 2010). Evidence of this dynamics has been provided, also, by field observation on an artificially re-shaped natural river consequentially to a series of flood events (Lewin, 1976); this highlights the mutual influence between planform and bar instability in streams where the evolution of bed and banks occur at comparable time scales. Despite the fact that unsteadiness is ubiquitous in natural river systems, only very few theoretical analyses have addressed the role of flow unsteadiness on bars formation (Tubino, 1991; Hall, 2004) while an analysis of the role of width unsteadiness is even lacking. Overall, the present work is therefore expected to contribute a novel theoretical understanding about the applicability of analytical bar theories to real river systems.

6.2 Methods

6.2.1 Conceptual approach

In order to understand the impact of width unsteadiness on bar stability in a straight channel, we first need to characterize the processes that lead to temporal changes in the active channel width. Their mathematical description will then be included in existing approaches for classical bar stability analyses, allowing to build the desired model. Four main hydromorphological configurations, based on different combinations of channel width and discharge variability, are examined (figure 6.1): a) ideal channels with both constant width and discharge, like in most common laboratory flume experiments on river bars; b) channelized rivers with constant width subject to streamflow variability and often developing alternate bars; c) constant discharge flowing in an initially overnarrow channel with non cohesive banks, as typical of the initial experimental condition of physical models of braided rivers; and d) laterally unconfined channels subject to floods, as it can be the case of the main active branches of braided rivers. Configuration a) is representative of most of the conditions to which classical bar theories strictly apply. Bar dynamics in configuration b) has been investigated only by the theories of Tubino (1991), Hall (2004) and by the field investigations by Welford (1994). The present contribution specifically aims to investigate free bar stability referring to configurations c) and d).

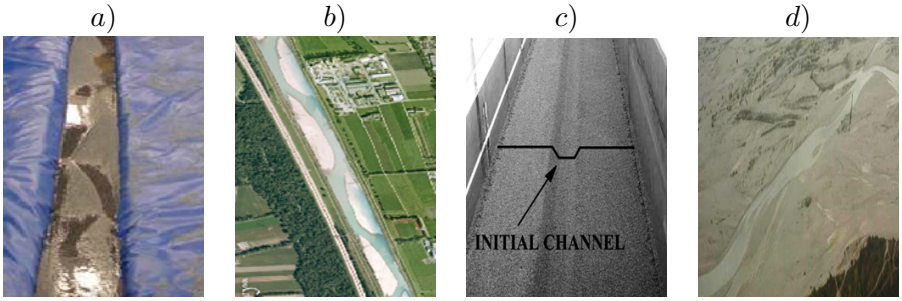

Figure 6.1: Examples of channels belonging to the four reference configurations considered in the stability analysis. Each class presents different combinations of discharge and width unsteadiness. More in detail: a) constant discharge and width (courtesy of Grecia Garcia Lugo), b) variable discharge and fixed width, c) erodible channel with unsteady width and constant discharge; d) natural, laterally unconfined channel with unsteady width and discharge.

6.2.2 Quantification of width unsteadiness

In order to keep the mathematical problem suitable for analytical solutions, simple relationships to express channel width variability are needed. A first, simple attempt has been made by using classical regime formulaes to relate bankfull discharge with channel width in single-thread channels. Such relationships are strictly valid under long-term, equilibrium conditions: therefore the present approach is based on the assumption of an 'instantaneous' validity of regime equations. Note that this assumption should be less crude than it may appear, because we are interested here more in a simple mathematical law describing the trends and order of magnitude of width unsteadiness rather than in a predictive formnula quantitatively valid for a specific case. To this aim we use the empirical formula proposed by Ashmore (1982) to predict the width at river equilibrium stage for anabranch channels in braided rivers:

$$W^* = \alpha_W Q^{*n_W} \qquad \alpha_W = 8.1019,\ n_B = 0.4738 \tag{6.1}$$

In equation (6.1) W^* represent the dimensional channel width and Q^* the related flow discharge in equilibrium conditions. According with the notation used in the previous Chapters, hereinafter a star (*) indicate dimensional quantities. According to our purposes relation (6.1) can be read as the equilibrium width to which a laterally unconfined channel tends asimptotically for a given discharge. A suitable dimensionless expression for equation (6.1) has been derived to fit a dimensionless mathematical approach. Such expression is obtained by following the procedure proposed by Parker et al. (2007). In the following relation the dimensionless channel

half-width B is also introduced for formal consistency with existing bar theories:

$$W = 2B = 2\alpha_n Q^{n_W} \tag{6.2}$$

$$\alpha_n = 0.5\alpha_W F_0^{n_W} \bar{\beta}^{n_W - 1} \bar{d_s}^{-5/2n_W + 1} \tag{6.3}$$

where the dimensionless parameters are defined as follows:

$$F_0 = \frac{U_0^*}{\sqrt{gD_0^*}} \qquad \bar{\beta} = \frac{B_0^*}{D_0^*} \qquad \bar{d_s} = \frac{d_s^*}{D_0^*} \tag{6.4}$$

with d_s^* the median sediment grain size, B_0^* the reference half-channel width value and U_0^*, D_0^* the components of the uniform flow chosen as reference scales.

Two different time variables are considered when examining both cases. The variable τ will vary on the externally imposed time scale of width and discharge unsteadiness, while the variable t will be used to denote the relevant 'intrinsic' time variable for the temporal morphodynamics of bars. These two variables will be considered as mutually independent within the present theoretical analysis, while for applications of the theory to specific real cases the related time scales shall be quantified and possible interactions assessed. In general, the externally imposed time scale is quite 'fast', i.e. much shorter than that associated with temporal width adjustments that occur in regulated rivers because of land-use changes, gravel mining, dam construction (Surian and Rinaldi, 2003).

Constant discharge This is the case of an initially overnarrow channel fed by constant discharge, for which the minimum width for bars formation predicted by the bar theories is larger than the imposed initial width (figure 6.1c; Bertoldi and Tubino, 2005). To describe the widening process, we simply assume that the erosion occurs homogeneously at the banks and that the channel tends, asimptotically, to achieve the equilibrium width at a widening rate that linearly decreases with the distance from the equilibrium conditions. This simplified law is based on the consideration that the erosion process, increases the channel width and decreases the sediment transport of the flow, reducing, in turn, its ability of entering sediments from the banks and thus slowing down the widening process. This process occurs faster while the initial geometry of the channel is far from equilibrium and reduces its effect progressively approaching the final conditions. Therefore, under this assumption, the relaxation relation (6.5) is proposed whereby the value of channel width ($2B_E^*$) at equilibrium with

the specified discharge is evaluated through equation (6.2):

$$\begin{cases} B^*(\tau^*)_{,\tau^*} = \left(\frac{U^*}{B^*}\right)_E \left(B_E^* - B^*(\tau^*)\right) \\ \\ B^*(\tau^* = 0) = B_0^* \\ B^*(\tau^* \to \infty) = B_E^*. \end{cases} \tag{6.5}$$

The complete solution for this case reads:

$$B^*(\tau^*) = B_E^* + (B_E^* - B_0^*)\left(-e^{-\alpha\tau^*}\right), \tag{6.6}$$

which, scaled by the unperturbed half channel width B_E^*, can be written in its dimensionless form as:

$$B(\tau) = \frac{B_E^*}{B_E^*} + \frac{(B_E^* - B_0^*)}{B_E^*}\left(-e^{-\alpha\tau}\right). \tag{6.7}$$

In equation (6.7) τ is a dimensionless time variable defined as

$$\tau = k\frac{U_E^*}{(B_E^* - B_0^*)}\tau^*, \tag{6.8}$$

where the parameter k accounts for the erodibility of both banks, assumed to be uniform in space.

Unsteady discharge This configuration can be representative of a main active branch of a braided river that laterally expands during a flood event (Zolezzi et al., 2012a). To predict the temporal variability of the active (i.e. sediment-transporting) channel width, we extend the validity of equilibrium regime formulae to instantaneous discharge values during a flood event. Despite being rather crude, this assumption can be justified by the need to use a simple, physics-based relationship in a first theoretical attempt of this type. In addition, better alternatives don't seem to be available at present, despite recent approaches to investigate planform evolution of river channel with self evolving banks (Parker et al., 2011). We therefore assume the channel width being instantaneously at equilibrium with the imposed flow hydrograph and according to (6.2) we write this relationship as:

$$B(\tau) = \alpha_n Q(\tau)^{n_W} \qquad \tau = \sigma_T^* \tau^* \tag{6.9}$$

where τ denotes dimensionless time, τ^* dimensional time and σ_T reciprocal of the flood event duration. In this configuration, equation (6.9) has been assumed to describe both channel narrowing and widening.

6.2.3 Mathematical formulation

The analysis refers to a straight channel with erodible bed and banks made of homogeneous non-cohesive sediment. The governing equations are the 2-D shallow water equation and the sediment continuity equation, which can be written in the following dimensionless form:

$$\frac{\partial U}{\partial t} + U\frac{\partial U}{\partial s} + V\frac{\partial U}{\partial n} + \frac{\partial H}{\partial s} + \bar{\beta}\frac{\tau_s}{D} = 0; \tag{6.10}$$

$$\frac{\partial V}{\partial t} + U\frac{\partial V}{\partial s} + V\frac{\partial V}{\partial n} + \frac{\partial H}{\partial n} + \bar{\beta}\frac{\tau_n}{D} = 0; \tag{6.11}$$

$$\frac{\partial D}{\partial t} + \frac{\partial UD}{\partial s} + \frac{\partial VD}{\partial n} = 0; \tag{6.12}$$

$$\frac{\partial}{\partial t}(F_0^2 H - D) + Q_0(\frac{\partial Q_s}{\partial s} + \frac{\partial Q_n}{\partial n}) = 0. \tag{6.13}$$

In equations (6.10)-(6.13) classical scalings for theoretical river morphodynamics are employed: the longitudinal and transversal variables s and n are scaled by the half-channel width $\bar{B}_0^*$, chosen as reference, the averaged velocity components (U, V), the water depth D, the free surface elevation H and the shear stress are scaled using the reference state quantities $(\bar{U_0}*, \bar{D_0^*})$. The reference, basic state is defined through three dimensionless parameters: the mean width ratio $\bar{\beta}$, the mean relative roughness $\bar{d}_s$ and the mean Shields parameter $\bar{\theta}$, which read:

$$\bar{\beta} = \frac{\bar{B}_0^*}{\bar{D_0}^*} \qquad \bar{d}_s = \frac{d_s^*}{\bar{D_0}^*} \qquad \bar{\theta} = \frac{S}{\Delta \bar{d}_s} \tag{6.14}$$

where S is the longitudinal slope of the channel, $\Delta = (\rho_s/\rho - 1)$ the submerged sediment gravity and d_s^* the sediment diameter.

Boundary conditions in the lateral direction impose vanishing water and sediment flux orthogonal to the banks. When the active channel width changes in time, either because of bank erosion (constant discharge, Figure 6.1c) or because of a combination of lateral inundation with erosional dynamics (variable discharge, Figure 6.1d), the banklines are laterally moving at the timescale imposed by the process of temporal width variation (described through equation 6.20). Under those conditions, the vanishing lateral flux condition is assumed to apply at the instantaneous (moving) bank line position. Overall, the adopted approach results in neglecting the effect of sediment supply to the channel associated with lateral erosion on the process of bar stability. This seems reasonable given this first theoretical attempt although investigation of the actual role played by that effect will deserve attention in the future.

6.2.4 Perturbation solution

We solve the governing differential problem through a nonlinear, two-parameters perturbation approach. We then investigate under which conditions the reference uniform basic flow is unstable with respect to infinitesimal and sinusoidal perturbations of the bed elevation and of the other relevant flow quantities. The following two-parameters perturbation expansion, say for the water depth D, is adopted:

$$D = 1 + \epsilon[A(t)S_m d_{10}E_1(s) + c.c.] + \delta d_{01}(\tau) + \epsilon\delta[A(t)S_m d_{11}E_1(s)d_{01}(\tau) + c.c.] + O(\epsilon^2, \delta^2) \tag{6.15}$$

where *c.c.* denotes the complex conjugate, ϵ and δ are small parameters related to the amplitude of free bars and to the rate of width unsteadiness respectively. Moreover:

$$S_m = sin\left(\frac{\pi}{2}mn\right) \qquad C_m = cos\left(\frac{\pi}{2}mn\right) \qquad m = 1, 2, ... \tag{6.16}$$

$$E_1 = exp(i\lambda s) \tag{6.17}$$

where λ is the dimensionless bar wavenumber.

By substituting the structure of (6.15) into (6.10)-(6.13), the original differential system is transformed into a series of linear homogeneous algebraic systems, at each order of approximation comparing in (6.15). The key property of this two-parameters perturbation expansion is that the $O(\epsilon\delta)$ is the lowest at which the spatial pattern of free bars is reproduced, because the solution at the order $O(\delta)$ is a perturbation of the reference basic flow and thus it is spatially uniform. The details of the solution procedure at the different orders of approximations are reported below.

O(ϵ): classical bar stability under conditions of constant width and discharge By substituting equation (6.15) into (6.10)-(6.13) and collecting all terms at the leading order ϵ, the classical linear free bar stability is recovered. This requires solving the following linear system:

$$\mathbf{L}_{10}\begin{pmatrix} u_{10} \\ v_{10} \\ h_{10} \\ d_{10} \end{pmatrix} = \begin{pmatrix} 0 \\ 0 \\ 0 \\ 0 \end{pmatrix} \tag{6.18}$$

where the linear differential operator $\mathbf{L_{10}}$ is reported, in its extended form, in appendix B. Solution of (6.18) reveals that the amplitude of bars behaves exponentially in time:

$$A(t) = exp(\Omega_{10}t) \tag{6.19}$$

with $\Omega_{10} = \Omega_{10,R} + i\Omega_{10,I}$, $\Omega_{10,R}$ bars growth rate and $\Omega_{10,I}$ bars angular frequency. Solution of (6.18) for the unknowns u_{10},v_{10},h_{10} and d_{10} with the parameters Ω, λ, $\bar{\beta}$, $\bar{\theta}$ and $\bar{d}_s$ requires a solvability condition, which allows calculation of the growth rate of bars and their angular frequency, for a given combination of bar wavenumber λ, the unperturbed width ratio $\bar{\beta}$, Shields parameter $\bar{\theta}$ and relative roughness $\bar{d}_s$.

O(δ): linear correction to the basic flow related to width unsteadiness
If the length of the channel is much shorter than the typical length of a flood wave, the temporal variability of channel width can be modelled as a temporal sequence of instantaneously uniform flows. To fit within the perturbation scheme, the adopted empirical relations for width unsteadiness are expanded in power of the small parameter δ, which takes slightly different meanings depending on the considered hydromorphological configuration. In both the examined configurations c) and d) in figure 6.1 the perturbed channel width is then written in the form:

$$B(\tau) = 1 + \delta b_{01}(\tau) \quad \delta << 1 \tag{6.20}$$

where b_{01} is described through different functional expressions in the two cases, as it occurs for δ. More specifically, for initially overnarrow channels subject to constant discharge and erodible banks:

$$b_{01}(\tau) = -e^{-\tau} \quad \delta = \frac{B_E^* - B_0^*}{B_E^*}, \tag{6.21}$$

while for the flood event over a laterally unconfined channels it holds:

$$b_{01}(\tau) = \alpha_n n_B q_{01}(\tau) \quad Q_0(\tau) = 1 + \delta q_{01}(\tau) \quad \delta = \frac{Q_{max}^* - Q_0^*}{Q_0^*}. \tag{6.22}$$

Here the unsteady discharge term q_{01} is assigned as input data and it represents the functional shape of the given flow hydrograph.

According to the adopted perturbation approach, an analytical solution expressing the correction to the reference uniform flow due to width unsteadiness is obtained for the two configurations, c) and d). Therefore the unsteadiness-corrected basic flow reads:

$$U_0 = 1 + \delta u_{01}(\tau) + O(\delta^2), \tag{6.23}$$

$$D_0 = 1 + \delta d_{01}(\tau) + O(\delta^2). \tag{6.24}$$

By feeding the expansion (6.23) into the governing equations (6.10)-(6.13) we find for the unsteady discharge configuration (d):

$$d_{01}(\tau) = p(1-\alpha)q_{01}(\tau), \tag{6.25a}$$
$$u_{01}(\tau) = (1-p)(1-\alpha)q_{01}(\tau); \tag{6.25b}$$

and, for steady discharge configuration (c):

$$d_{01}(\tau) = -pb_{01}(\tau), \tag{6.26a}$$
$$u_{01}(\tau) = -(1-p)b_{01}(\tau). \tag{6.26b}$$

In the above expressions the parameters p and α take the value:

$$p = \frac{2}{3 - C_D} \qquad \alpha = \alpha_n n_B. \tag{6.27}$$

$\mathbf{O}(\epsilon\delta)$: effect of width variations on free bar stability By considering that the solution at the order δ is not dependent on the longitudinal variable s, the smallest order at which the spatial dependence of the fundamental is reproduced is the order $\epsilon\delta$ (equation 6.15). At this order, therefore, the solution accounts for the effect of the temporal width variation on free bar instability. Using the mathematical operator $\mathbf{L_{10}}$ introduced in equation (6.18), at the order $\epsilon\delta$ the governing differential system reads:

$$\mathbf{L}_{10}\begin{pmatrix} u_{11} \\ v_{11} \\ h_{11} \\ d_{11} \end{pmatrix} = \begin{pmatrix} -a^1_{11}u_{10} - a^1_{14}d_{10} \\ -a^1_{22}v_{10} \\ -a^1_{31}u_{10} - a^1_{32}v_{10} - a^1_{34}d_{10} \\ i\Omega_{11}K_1 + (-i\Omega_{10})K_2 - Q_0\Phi_0 K_3 \end{pmatrix}; \tag{6.28}$$

$$K_1 = (F_0^2 h_{10} - d_{10}),\ K_2 = K_1\Phi_T[2u_{01}(\tau) + c_D d_{01}(\tau)],$$

$$K_3 = a^1_{41}u_{10} + a^1_{42}v_{10} + a^1_{43}h_{10} + a^1_{44}d_{10};$$

where $\mathbf{L}_{10}$ is the same linear algebraic operator found at the leading $\mathbf{O}(\epsilon)$ and the coefficients $a^1_{i,j}$, K_i are related to the nonlinear, unsteady effect arising from the interaction between the fundamental perturbation (ϵ) and the unsteady correction to the basic flow due to width variability (δ). The expression of $a^1_{i,j}$, K_i are reported in appendix B for the sake of brevity.

As for the leading order, since the determinant of $\mathbf{L}_{10}$ vanishes, a solvability (eigenrelation) analogous to that occurring at the leading order holds:

$$f(\Omega_{11}, \lambda; \Omega_{10}, \bar{\beta}, \bar{\theta}, \bar{d}_s) = 0, \tag{6.29}$$

which allows to compute the correction $\Omega_{11} = \Omega_{11,R} + i\Omega_{11,I}$ to bar growth rate and angular frequency at the order $\epsilon\delta$. As it can be easily seen from (6.28) and (6.29), the solution of the system (6.28) depends on the solution found at the previous order $O(\epsilon)$, so the problem is solved in cascade. The solvability condition (6.29) leads to an amplitude relation of the type (6.19) that includes a new term accounting for width unsteadiness. The new relation therefore reads

$$A(t) = exp\left[(\Omega_{10} + \delta\Omega_{11}(\Omega_{10})b_{01}(\tau))\, t\right] \tag{6.30}$$

where Ω_{10} and Ω_{11} account respectively for the growth rate associated to the fundamental perturbation and for the component related to the unsteadiness due to channel width variability.

6.3 Results

Results obtained by performing the analysis described above are here reported for the two analyzed morphological configurations: a laterally unconfined channel during a flood event (unsteady discharge and width) and widening of an initially overnarrow channel under constant discharge.

6.3.1 Unsteady discharge and variable width

Figure 6.2 refers to the case of a flood event that occurs in a laterally unconfined channel. Figure 6.2a shows the dimensionless hydrograph of the flood event $Q_0(\tau)$ together with the linearized temporal variation of channel width, expressed by equation (6.20). The reference flow (basic state) has been assumed as the uniform flow with constant width occurring for the value $Q_0 = 1$. As already pointed out by Tubino (1991) free bars under unsteady flow conditions are more stable during the rising and peak stage of the hydrograph, because the aspect ratio β is decreasing and the critical value for bar formation β_c is increasing. In a channel with constant width the decrease of β during the rising stage of the flood is related to decrease in water depth, while the increase of β_c is mainly associated with the increase in the Shields stress. On the contrary, bars are more likely to form during the decreasing phase where the value of β increases against a decreasing β_c value.

Figure 6.2b shows that accounting for temporal width variability results in damping the stabilizing effect associated with flow unsteadiness in a channel where the width does not change in time. Namely, when discharge exceeds the reference flow value ($Q_0(\tau) > 1$) the reduction in the bar growth rate is less pronounced than in the case with constant width.

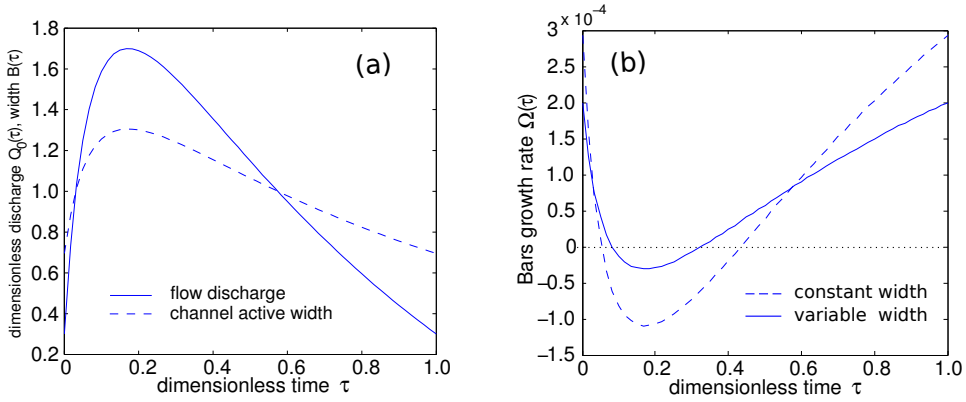

Figure 6.2: Values of the total growth rate coefficient $\Omega(\tau)$ for the flow event on the left. The graph on the right shows how unsteady discharge affects bars growth rate in laterally confined (dashed line) and unconfined (solid line) channels.s

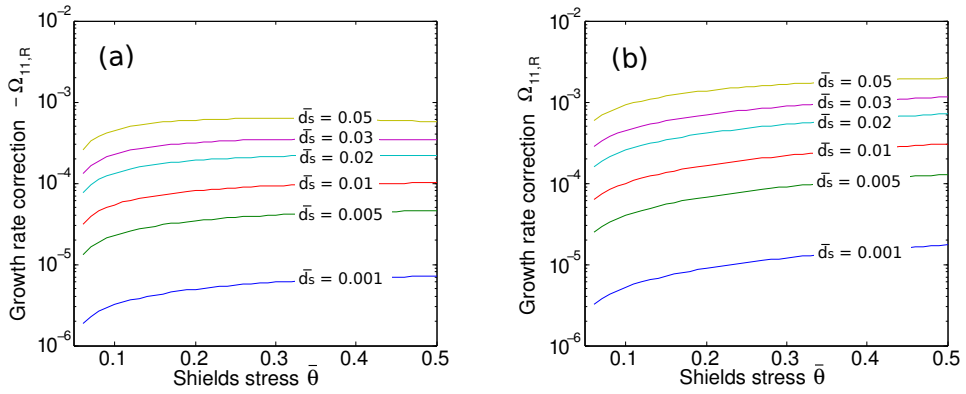

Figure 6.3: The linear growth rate of alternate bars (real part of Ω_{11}) is plotted versus the Shields stress $\bar{\theta}$ for different values of the roughness parameter $\bar{d}_s$ for the cases of variable (a), constant (b) discharge and variable width.

As the temporal behavior of the complete solution is fundamentally controlled by the structure assigned to the temporal variable q_{01} or b_{01}, it is informative to focus on the contribution given by the unsteady term $\Omega_{11,R}$, which is invariably negative, as reported in figure 6.3a.

6.3.2 Constant discharge and variable width

Application of the bar theory with reference flow parameters that instantaneously adapt to the evolving width value indicate that free bars tend to form during the widening process because the value of the aspect ratio β increases, while the critical value β_c is decreasing, being β_c a growing function of the Shields stress, which decreases with widening. Moreover, results obtained by applying the present theoretical analysis to an initially overnarrow channel, characterized by erodible banks and constant discharge, reveals a net positive contribution of the width unsteadiness to bar growth rate, $\Omega_{11,R} > 0$ (figure 6.3b). Channel widening is therefore predicted to enhance bar instability compared to the configuration with constant width. Moreover, as it can be recognized from equation (6.21), this effect is stronger when the difference between the initially imposed channel width and the equilibrium width is higher (figure 6.4a). Width unsteadiness may therefore determine a complete reversal of bar stability conditions compared to the constant width case. This behaviour is related to the continuity equation for the fluid phase: in channels with constant discharge, the widening process is associated with a decrease of the cross-sectional averaged velocity and depth (equation 6.26), while in channels with variable discharge the temporal width variability is driven by the flood hydrograph: therefore widening during the rising stage is related to a contemporary increase in both cross-sectional averaged velocity and depth (equation 6.25). Such continuity effect mathematically determines opposite signs of the term b_{01} in the two configurations, which are then reflected in the opposite signs of $\Omega_{11,R}$ (figures 6.3b and 6.3a).

More general results can be presented by examining the dependence of the most unstable wavelength at the initial time on the Shields stress θ and on the relative roughness d_s (figure 6.4b). This was achieved by assigning as reference state (equilibrium) a wide enough channel to guarantee bar-forming condition at the initial stage of the erosion process, where, the width is smaller. Shorter bars are therefore promoted, as the most unstable wavenumber is larger. Theoretical predictions of instability enhancement of shorter bars are in qualitative agreement with the experimental observations of Bertoldi and Tubino (2005).

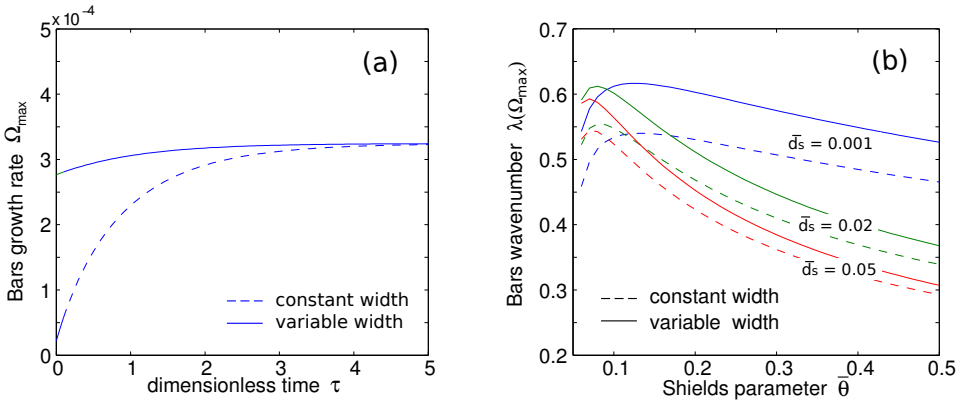

Figure 6.4: Comparison between values predicted by applying the theory here presented (solid line) and using the steady approach (dashed line); for the latter case we are assuming the flow steady at each temporal step. a) shows difference in bars maximum growth rate and b) the values of the most unstable bar wavenumber plotted against the Shields parameter θ for different value of the roughness parameter d_s at the initial time of the process.

6.4 Discussion

A novel stability analysis for free bars in channels with temporally variable channel width has been developed. Simple relationships describing the variability of the active channel in time allow us to develop a two-parameters perturbation expansion able to quantify the role of width unsteadiness by the interaction of the fundamental bar perturbation with the correction of the basic flow associated with the widening / narrowing processes. Despite the adopted simplifying hypothesis to describe the widening process in rivers channel, the method developed allows a first quantitative investigation of bars dynamics in laterally unconfined channels. Considering that little has been done in literature to investigate the effect of temporal width adjustments (see Parker et al., 2011), another novel point of the work consists in the derivation of a physically-based relationship for width variability under both steady and unsteady discharge conditions. The suitability of the adopted approach finds qualitative support in the experiments of Bertoldi and Tubino (2005) and of Visconti et al. (2010), who specifically mentioned that in the initial stage of a run, bank erosion increases the channel width keeping the channel straight. The assumption of width variation to be small (say initial stage of laboratory experiment) seems to be reasonable in the light of this. Moreover, data provided from laboratory experiments can be used to validate the relaxation relation here proposed as well as the related time scale adopted.

Results obtained show, curiously, two formally opposite behaviours for the unsteady term $\Omega_{11,R}$ when considering channel width variability. The sign of $\Omega_{11,R}$ is controlled in a rather complex way by the variables defining the basic flow: β, θ, ds and the growth rate computed for the fundamental perturbation $\Omega_{10,R}$ as reported in equation (6.29). Namely, in the case of unsteady discharge this term is found to be negative, while in the other case it gives a positive contribution to bars growth rate. Moreover, during the rising and peak stage of a flood in a laterally unconfined channel, bar stability is increased, thus suggesting a non-trivial effect of width unsteadiness. In association to this destabilizing action, the most unstable bars present a shorter length compared to that predicted by the same theory developed for steady channel width.

Overall, theoretical predictions are in qualitative agreement with both the field observations of Zolezzi et al. (2012a) and the experimental observation of (Bertoldi and Tubino, 2005). Further research is needed to apply the present theory to real cases, both in the field and in the laboratory, to assess to which extent the present theory can actually provide a relevant step towards an increased applicability of bar theories to complex channel geometries. Further research shall also concentrate to derive physically-based relationships for channel width variability.

6.5 Conclusions

A theoretical morphodynamic model has been developed and solved through a nonlinear perturbation technique to investigate the effect of temporal width variation on river bed morphodynamics. The analysis is referred to the classical problem of free bars in an indefinitely long straight channel, but the same approach can be easily adapted to different morphodynamic problems, such as the response of a point bar in a meander bend to temporal oscillations of channel width, like those suggested in Chapter 5.

The model is solved by performing a nonlinear stability analysis, which includes temporal width variations as a small-amplitude perturbation of the basic flow. In order to quantify width variability, channel width is related with the instantaneous discharge using existing empirical formulae proposed for channels with cohesionless banks. Therefore, width can vary (increase and/or decrease) either because it adapts to the temporally varying discharge or, if discharge is constant, through a relaxation relation describing widening of an initially overnarrow channel towards the equilibrium width. Unsteadiness related with changes in channel width is found to directly affect the instantaneous bar growth rate, depending on the conditions under which the widening process occurs. The govern-

ing mathematical system is solved by means of a two-parameters (ϵ, δ) perturbation expansion, where ϵ is related to bar amplitude and δ to the temporal width variability. In general width unsteadiness is predicted to play a destabilizing role on free bar stability, namely during the peak stage of a flood event in a laterally unconfined channel and invariably for overnarrow channels fed with steady discharge. In this latter case, width unsteadiness tends to shorten the most unstable bar wavelength compared to the case with constant width, in qualitative agreement with existing experimental observations.

Chapter 7

Conclusions

Interactions between fluvial processes and vegetation along river channel margins have been shown to be fundamental in determining meandering rivers development. Several bio-morphological dynamics have been observed to direct control accretion and degradation rates of meander bends.

Despite recent advances in field and laboratory techniques and modelling development of the last decades, little is known about the quantitative relation between these floodplain patterns and their controlling bio-morphological interactions that determine the bank accretion process. This knowledge gap has so far limited the development of physically-based models for the evolution of meandering rivers able to describe the lateral migration of banklines separately. Most existing meander migration models are indeed based on the hypothesis of constant channel width.

The present doctoral research has aimed to provide more insight in the mutual interactions among flow, sediment transport and riparian vegetation dynamics, with a special focus on the patterns that such relationships generate within the advancing banks of meandering rivers. The research has been designed as an integration of remote sensing and in-situ field observations with a mathematical modelling approach to elucidate the fundamental physical controls of the accretion processes that characterised meanders convex bank.

In meandering rivers vegetation encroachments within the point bar (i.e. colonizing species and stranded large wood), initiate pioneer landforms that, when evolving, determine the lateral shifting of the margin that separates the active channel from the mature river floodplain and thus inner bank aggradation (*bar push*). This diminishes the portion of the morphologically active channel cross-section, influencing the erosion of the cutting bank and promoting channel widening (*bank pull*). Moreover, difference in migration rate between the two banks have been observed to

induce local temporal variations in channel width that affect river channel morphodynamics and its overall planform through their influence on the local flow field and channel bed morphology. The *bar push* phenomenon can be put in relation with the erosion processes at the outer bank (*bank pull*). The cyclic occurrence of this process determines meander bend migration with the subsequent formation of typical patterns of meandering rivers floodplain, such as benches, scrolls and chutes (see Chapter 2).

Because of the gaps related with quantitative, process-based knowledge about these patterns and the interaction between flow, sediment transport and riparian vegetation driving them during bank accretion processes, the present research work has investigated such dynamics to i) provide a quantitative description of vegetation and floodplain topography patterns in advancing meander bends and ii) to explore the key control factors and their role in generating the observed patterns.

To this aim the work has been structured as follows. Information on the temporal evolution of the meander bend and of vegetation cover extent, and on their influence on the present channel topography and riparian vegetation structure has been obtained from the combined analysis of historical aerial photographs and Lidar data for two meander bends of the lower reach of the Tagliamento River, NE Italy (see Chapter 3). The outcome of this analysis, together with the results of field investigations (see Chapter 4), suggested the modelling approach to adopt, the physical process to account for and the most appropriate physical-based relationships to describe them (see Chapter 5). Moreover, flow regime and riparian vegetation characteristics estimated from the field have been used, in association with the measured topography, to provide preliminarily validation of the model.

Furthermore, results obtained from the application of the bio-morphodynamic model proposed have revealed a tendency of the meander bend to develop temporal oscillations of the active channel width during its evolution, which role on the in-channel morphological processes has been investigated, in a first attempt, in Chapter 6.

Main achievements of the present work

A strong correspondence between riparian canopy structure and geomorphological patterns within the floodplain area has been revealed from the analysis of the two airborne historical data (air photographs and Lidar). In particular riparian vegetation has been found to be organized according to a ridge and swale pattern, which is typically associated to the development of benches and scroll bars formation within the convex bank during the meander evolution. Moreover, the performed analysis have shown that

the influence of river hydromorphological processes diminishes while the effect due to the presence of trees increases with the lateral distance from the contemporary channel edge and this behaviour encompasses a buffer zone where the accretion processes take place.

Similar conclusions have been obtained by investigating collected field data on river bend cross section topography, historical water stage and riparian vegetation properties. Results obtained from this analysis have shown that inner bank morphology organizes in macro oscillations associated with different time periods that in turn influence the vegetation spatial distribution, changing from dense woody to sparse vegetation reaching the channel edge. Moreover, the analysis reveals a further complex structure for the inner bank morphology characterized by two levels of organization: one (macroscale variation) dependent on the water stage, the other determined by the presence or absence of vegetation and its interaction with the water flow (micro variation).

Understanding form the field and remote sensing analysis have suggested to focus the modelling investigation on meander migration accounting for a vegetated river corridor at the cross-section scale.

The model developed in Chapter 5 is a first, biophysically based attempt to overcome the simplifying hypothesis of constant channel width on which meander migration models have been traditionally based. Differently from the closure for bank erosion and deposition proposed by Eke et al. (2014), which is based on the framework for self evolving bank of Parker et al. (2011), in this approach inner bank advancing is related with vegetation dynamic on the point bar accounted for through physically-based relationships for vegetation biomass dynamics. Despite the simplified closure used to describe vegetation-induced deposition and the continuous transversal distribution of the vegetation biomass, the results obtained are encouraging of the model adequacy to reproduce observed processes. Discharge unsteadiness coupled with the active role of vegetation has been found as crucial ingredients for the development of characteristic ridge-swales patterns in ground topography and riparian vegetation most often observed in advancing meandering floodplains.

A theoretical morphodynamic model has been developed and solved through a nonlinear perturbation technique to investigate the effect of temporal width variation on river bed morphodynamics, such as the response of a point bar in a meander bend to temporal oscillations of channel width, like those suggested in Chapter 5. In order to study the effect of channel width variation on river bed instability, two case were investigated: width can vary adapting to the temporally varying discharge or, if discharge is constant, through a relaxation relation describing widening of an initially overnarrow channel towards the equilibrium width. Unsteadi-

ness related with changes in channel width was found to directly affect the instantaneous bar growth rate, depending on the conditions under which the widening process occurs.

Overall, results obtained are satisfactory and give evidence of the fact that a cooperation between different scientific disciplines that involved different investigations techniques is a fundamental conditions to develop a comprehensive framework for investigating meandering rivers evolution in vegetated floodplain.

General discussion and future developments

The analysis conduced highlights the potential of remotely sensed data, such as Lidar and and air photographs, in providing important information on the accretion process at the inner bank and lateral banks dynamics (erosion and deposition) when applied to the scale of individual meander bends.

It has been also demonstrated that analysis focused on the morphological and vegetation patterns can be extended by including the relevant hydrological processes and associate them with the geometry of the structures observed within the inner bank to quantitatively investigate the scales of the physical phenomena that are involved. Interestingly, the existence of three zones within the inner bank was detected independently from three different analysis: from the analysis of the historical hydrological data as difference water persistence time- length above the ground and, more qualitatively, from the observation of the cross section topography, as well as from the combination of Lidar data and historical aerial photographs.

Moreover, the conducted analyses show how the information collected in the field to characterize the riparian canopy structure are complementary to the remote sensed analysis. For instance the growth curve of the analysis on vegetation properties can be used, for known riparian species, to convert maps showing the tree height distribution with tree age and, conversely, to interpret the values in the persistence map in order to estimate the height of the riparian canopy; thus completely characterizing riparian woody structure. On the other hand, remote sensing techniques further support field investigations: Lidar data allows to investigate canopy and terrain structure at the reach length, while analysis of historical photographs provide information on the dynamics of the bend.

The attempt to estimate meander bend migration rate from the aerial images and related it with the historical water stage, could be improved, when information are available, by using digital elevation model of the active river corridor. In particular, the DEM of difference associated with

relevant flood events, could provide information on the amount of sediments eroded or deposited (i.e negative or positive values, respectively).

In general width unsteadiness was predicted to play a destabilizing role on free bar stability, namely during the peak stage of a flood event in a laterally unconfined channel and invariably for overnarrow channels fed with steady discharge. In this latter case, width unsteadiness tends to shorten the most unstable bar wavelength compared to the case with constant width, in qualitative agreement with existing experimental observations. The analysis conduced can be extended to the case of width oscillation induced by meandering migration as predicted from the application of the bio-morphodynamic model proposed in Chapter 5.

The developed bio-morphodynamic model could be used to derive physically-based relationships for describing channel widening (narrowing) in a overnarrow (wide) channel, which represent one of the major issue in introducing unsteadiness in the analytical theory of bend/bar stability, as already pointed out in Chapter 6.

The present work also constitutes a further step in understanding the still unsettled biophysical controls of the accretion processes in meander evolution and provides information to support future research in developing bio-morpho-dynamic models for meandering rivers able to investigate processes related to the analysed floodplain patterns, such as chute cutoffs. Time-scale dependence of vegetation dynamics in relation with that of the fluvial processes (i.e. high/low rapidity of vegetation colonization) are associated with the formation of the observed riparian patterns. Understanding the controls of these patterns can provide and added value in the long-lasting debate on river channel pattern selection, because increased/reduced prevalence of chutes implies more or less pronounced tendency from a single-thread to a multi-thread channel pattern.

Results obtained from the modelling analysis are encouraging and constitute a first attempt towards the development of coupled channel-floodplain biomorphodynamic models. Improvements are required to reach this aim and in particular future research needs to:

- comprehensively incorporate include the unsteadiness effects induced by channel width oscillation, here studied separately, in the bio-morphodynamic model for meandering river evolution;
- extend this model to the more general case of a channel with longitudinally variable channel centerline curvature;
- account for net sediment exchange between the main channel and the lateral bank regions and for the possible unbalance between erosion and accretion processes;

- be based on targeted field investigations in order to provide insight into the role of several vegetation characteristics that are described through a simplified parameterization and include effects that are not present so far, such as plant roots that can improve the extremely simplified closure relationships used in this analysis.

Despite not being exhaustive, the above research developments will generate a more comprehensive bio-morphodynamic model, providing a useful tool to support river management and river restoration projects, where the co-evolution of channel curvature, width and riparian vegetation and topography patterns have specific ecological relevance.

Notation

List of the most used symbols

$A(t)$	bars amplitude;
B	half channel width;
b, b_{eq}	overall and maximum biomass;
$\mathcal{C}$	curvature of channel axis;
C_0	friction coefficient;
D, D_0	local and uniform depth;
d_s	sediment grain size;
F_0	Froude number;
$\mathcal{F}$	logarithmic profile function;
$\mathcal{G}$	vertical structure of the secondary flow;
g	gravity acceleration;
H	water free surface elevation;
k	biomass decay rate;
k_{sg},k_{sv},k_s	Strickler coeff. for bare sediments, vegetated area and mixed terrain;
M	lateral migration coefficient;
N	longitudinal metric coefficient;
P	pressure;
Q	water discharge;
q	sediment rate vector;
$\bar{Q}, Q_f$	maximum, formative discharge;
R	radius of curvature;
r	empirical constant in q_n;
s, n, z	longitudinal, transverse, vertical direction, respectively;
t	time;
U, V, W	longitudinal, transverse,vertical velocity component;
U_0, V_0, W_0	longitudinal, transverse,vertical uniform flow velocity component;
W_c	channel width;
z_{b0}	ideal distance from water table ;
α_t	coeff. root properties;
α_Q	coeff. formative discharge;
β	hal-width to depth ratio;

δ	perturbation parameter for the width;
Δ	submerged sediment gravity;
ϵ	perturbation parameter for bars;
ζ	lateral erosion ;
η	channel bed elevation;
θ	Shields parameter;
$\theta_c, \theta_c v$	critical value of Shields parameter for sediments, vegetation;
λ	dimensionless bar wavenumber;
$\lambda_{1,2}$	rate biomass decrease;
λ_{sed}	deposition rate;
ν	perturbation parameter for the curvature;
ν_T	eddy viscosity;
ξ	normalized vertical variable;
ρ_s, ρ	sediment and water density;
σ_1	biomass growth rate;
σ_T	reciprocal of flood event duration;
τ,τ_c	shear stress value and its critical value;
τ_s,τ_n	longitudinal and transverse shear stress component;
Ω	bars growth rate ;

Appendices

Appendix A

Image classification analysis

In this section we present the outcomes of the classification process described in chapter 3. For each of the panchromatic and colour air photographs (RGB) of the historical dataset we reported: the original image, the main statistics of the colour intensity distribution of the training area used for the supervised classification, the final thematic map produce (used for the further analysis), the confusion matrix and the related statistics used to assess the accuracy of the classification process. Information on the distribution of the training samples, help in understanding the eventuality of overlapping between two distributions (this occurred often between water-covered area and vegetation category) that might lead to misclassification in the final result. Moreover, we coupled the error matrix related to the final map with that obtained by classifying the whole image (no masking operation) in order to provide evidence of the accuracy improvement achieved by classifying separately the river channel from the river floodplain.

Furthermore, a short explanation of the statistics associated with the confusion matrix is here reported. According with the generic confusion matrix reported in Figure A.1, the most common measures for assessing accuracy are:

$$overall\,accuracy = \frac{\sum n_{ii}}{n} 100; \tag{A.1}$$

$$kappa\,coefficient = \frac{n\sum n_{ii} - \sum n_{+i}n_{i+}}{n^2 \sum n_{+i}n_{i+}}; \tag{A.2}$$

$$commission = \frac{n_{ij}}{n_{i+}}; \tag{A.3}$$

$$omission = \frac{n_{ij}}{n_{+i}}; \tag{A.4}$$

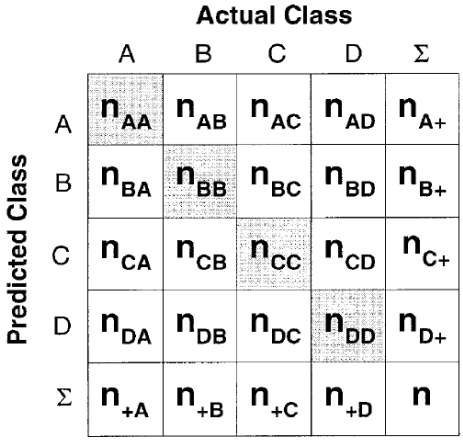

Figure A.1: The confusion matrix use for assessing classification accuracy (Foody, 2002).

$$procedure's\, accuracy = \frac{n_{ii}}{n_{+i}}; \tag{A.5}$$

$$user's\, accuracy = \frac{n_{ii}}{n_{i+}}; \tag{A.6}$$

where i, j represent the category used for the discretization of the image, while n is the total number of points used for the validation procedure (in this case 90).

Lists of the panchromatic historical images:

1966

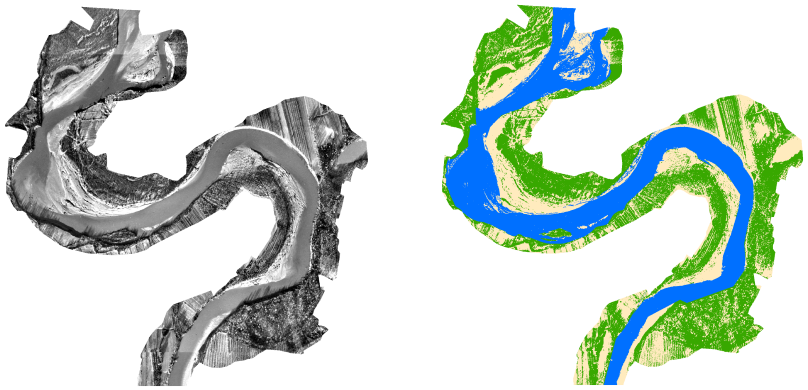

1966	Min	Max	Mean	Std. dev	Covar
Vegetation	35.00	139.00	65.53	12.94	167.44
Ground	89.00	208.00	129.22	17.52	306.97
Water	64.00	182.00	100.99	10.26	105.37

Table A.1: Main statistics computed for the frequency distribution of the training sample extracted from the 1966 panchromatic aerial photograph. Min = minimum, Max = maximum, Std. dev = standard deviation, Covar = covariance.

(A)	Veg(R)	Sed(R)	Water(R)	Row total
Veg(CL)	29	2	0	31
Sed(CL)	1	27	0	28
Water (CL)	0	1	30	31
Column total	30	30	30	90

(B)	Veg(R)	Sed(R)	Water(R)	Row total
Veg(CL)	25	0	3	28
Sed(CL)	0	16	0	16
Water (CL)	5	14	27	46
Column total	30	30	30	90

Table A.2: Confusion matrixes computed for the thematic map obtained by A) masking the river area B) classifying the whole image.

(A)	Commission	Omission	Producers	Users
Veg	6.45	3.33	96.67	93.54
Sed	3.57	10.0	90.00	96.43
Water	3.23	0.00	100.0	96.77
Overall				95.5
Kappa				0.93

(B)	Commission	Omission	Producers	Users
Veg	0.96	0.76	1	0.63
Sed	1.00	0.97	1.00	0.95
Water	0.98	0.72	0.97	0.58
Overall				0.42
Kappa				0.34

Table A.3: Statistics parameters computed from the value of the confusion matrix to assess the accuracy of the classification method applied.

1970

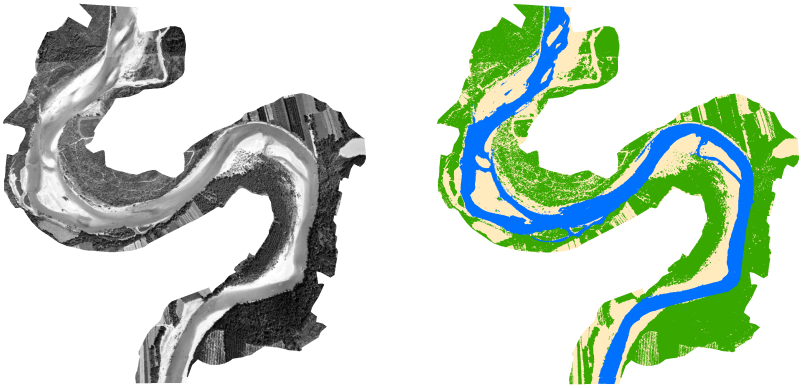

1970	Min	Max	Mean	Std. dev	Covar
Vegetation	17.00	162.00	59.31	22.99	528.39
Ground	144.00	227.00	214.91	7.56	57.18
Water	96.00	177.00	140.94	10.76	115.70

Table A.4: Main statistics computed for the frequency distribution of the training sample extracted from the 1970 panchromatic aerial photograph. Min = minimum, Max = maximum, Std. dev = standard deviation, Covar = covariance.

(A)	Veg(R)	Sed(R)	Water(R)	Row total
Veg(CL)	30	0	0	30
Sed(CL)	0	30	0	30
Water (CL)	0	0	30	30
Column total	30	30	30	90

(B)	Veg(R)	Sed(R)	Water(R)	Row total
Veg(CL)	30	0	0	30
Sed(CL)	0	27	0	27
Water (CL)	0	3	30	33
Column total	30	30	30	90

Table A.5: Confusion matrixes computed for the thematic map obtained by A) masking the river area B) classifying the whole image.

(A)	Commission	Omission	Producers	Users
Veg	0.00	0.00	100.00	100.00
Sed	0.00	0.00	100.00	100.00
Water	0.00	0.00	100.00	100.00
Overall				100.00
Kappa				1

(B)	Commission	Omission	Producers	Users
Veg	0.00	0.00	100.00	100.00
Sed	0.00	10.0	90.00	100.00
Water	9.09	0.00	100.00	90.91
Overall				96.7
Kappa				0.95

Table A.6: Statistics parameters computed from the value of the confusion matrix to assess the accuracy of the classification method applied.

1983

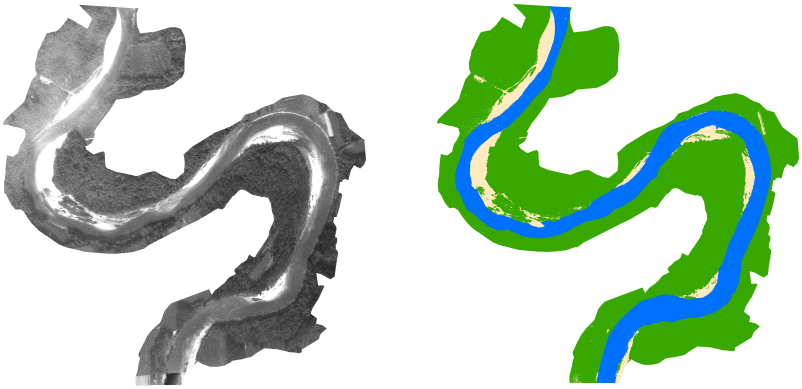

1983	Min	Max	Mean	Std. dev	Covar
Vegetation	42.00	183.00	77.52	9.56	91.35
Ground	85.00	204.00	95.03	8.95	80.05
Water	59.00	176.00	95.03	15.92	253.60

Table A.7: Main statistics computed for the frequency distribution of the training sample extracted from the 1983 panchromatic aerial photograph. Min = minimum, Max = maximum, Std. dev = standard deviation, Covar = covariance.

(A)	Veg(R)	Sed(R)	Water(R)	Row total
Veg(CL)	29	1	0	30
Sed(CL)	0	29	0	29
Water (CL)	1	0	30	31
Column total	30	30	30	90

(B)	Veg(R)	Sed(R)	Water(R)	Row total
Veg(CL)	15	0	9	24
Sed(CL)	0	29	0	29
Water (CL)	15	1	21	37
Column total	30	30	30	90

Table A.8: Confusion matrixes computed for the thematic map obtained by A) masking the river area B) classifying the whole image.

(A)	Commission	Omission	Producers	Users
Veg	3.33	3.33	96.67	96.67
Sed	0.00	3.33	96.67	100.00
Water	3.23	0.00	100.00	96.77
Overall				97.7
Kappa				0.97

(B)	Commission	Omission	Producers	Users
Veg	37.5	50.00	50.00	62.50
Sed	0.00	3.33	96.67	100.00
Water	43.24	30.00	70.00	56.76
Overall				72.2
Kappa				0.58

Table A.9: Statistics parameters computed from the value of the confusion matrix to assess the accuracy of the classification method applied.

1993

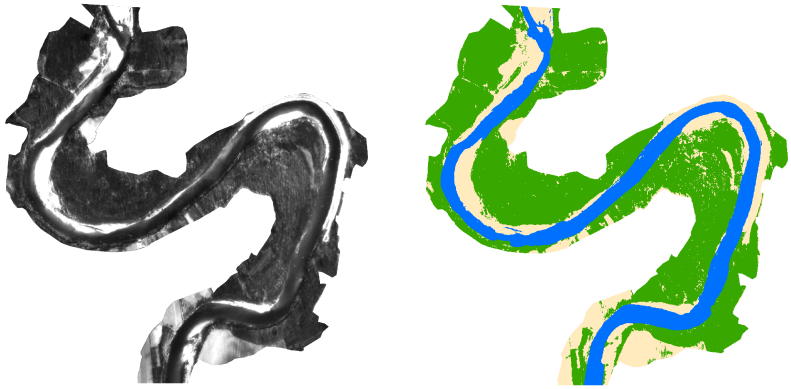

1993	Min	Max	Mean	Std. dev	Covar
Vegetation	38.00	232.00	61.46	17.76	315.29
Ground	67.00	255.00	147.89	45.03	2027.84
Water	45.00	155.00	64.89	11.60	134.51

Table A.10: Main statistics computed for the frequency distribution of the training sample extracted from the 1993 panchromatic aerial photograph. Min = minimum, Max = maximum, Std. dev = standard deviation, Covar = covariance.

(A)	Veg(R)	Sed(R)	Water(R)	Row total
Veg (CL)	29	0	1	30
Sed (CL)	1	30	0	31
Water (CL)	1	0	29	29
Column total	30	30	30	90

(B)	Veg(R)	Sed(R)	Water(R)	Row total
Veg(CL)	25	0	26	51
Sed(CL)	5	30	4	39
Water (CL)	0	0	0	0
Column total	30	30	30	90

Table A.11: Confusion matrixes computed for the thematic map obtained by A) masking the river area B) classifying the whole image.

(A)	Commission	Omission	Producers	Users
Veg	3.33	3.33	96.67	96.67
Sed	3.23	0.00	100.00	96.77
Water	0.00	3.33	96.67	100.00
Overall				97.7
Kappa				0.97

(B)	Commission	Omission	Producers	Users
Veg	50.98	16.67	83.33	49.02
Sed	23.08	0.00	100.00	76.92
Water	–	100.00	0.00	–
Overall				61.1
Kappa				0.42

Table A.12: Statistics parameters computed from the value of the confusion matrix to assess the accuracy of the classification method applied.

1997

Vegetation	Band1	Band2	Band3
Min	19.00	70.00	84.00
Max	199.00	173.00	189.00
Mean	78.04	110.06	115.17
St dev	18.98	14.34	8.13
Covariance			
Band1	360.28	261.67	137.63
Band2	261.67	205.59	105.75
Band3	137.63	105.75	66.06

Ground	Band1	Band2	Band3
Min	0.00	0.00	0.00
Max	254.00	241.00	213.00
Mean	240.10	220.82	183.49
St dev	44.36	40.90	34.19
Covariance			
Band1	1968.18	1812.42	1507.80
Band2	1812.41	1672.83	1349.19
Band3	1507.80	1349.19	1168.88

Water	Band1	Band2	Band3
Min	25.00	91.00	97.00
Max	170.00	163.00	162.00
Mean	86.53	122.43	124.11
St dev	30.03	16.86	7.47
Covariance			
Band1	901.82	491.87	191.47
Band2	491.87	284.15	115.17
Band3	191.47	115.17	55.80

Table A.13: Main statistics computed for the frequency distribution of the training sample extracted from the 1997 colour (RGB) aerial photograph. Min = minimum, Max = maximum, Std. dev = standard deviation, Covar = covariance.

(A)	Veg(R)	Sed(R)	Water(R)	Row total
Veg (CL)	27	1	0	28
Sed (CL)	3	24	0	27
Water (CL)	0	5	30	35
Column total	30	30	30	90

(B)	Veg(R)	Sed(R)	Water(R)	Row total
Veg(CL)	11	1	3	15
Sed(CL)	0	13	0	13
Water (CL)	13	16	21	50
Column total	24	30	30	78

Table A.14: Confusion matrixes computed for the thematic map obtained by A) masking the river area B) classifying the whole image.

(A)	Commission	Omission	Producers	Users
Veg	3.57	10.00	90.00	96.43
Sed	11.11	20.00	80.00	88.88
Water	14.29	0.00	100.00	85.71
Overall				90.0
Kappa				0.85

(B)	Commission	Omission	Producers	Users
Veg	26.07	54.17	45.83	73.33
Sed	0.00	56.67	43.33	100.00
Water	58.00	12.50	87.50	42.00
Overall				57.7
Kappa				0.34

Table A.15: Statistics parameters computed from the value of the confusion matrix to assess the accuracy of the classification method applied.

2001

Vegetation	Band1	Band2	Band3
Min	48.00	35.00	48.00
Max	178.00	157.00	153.00
Mean	99.28	87.95	100.25
St dev	12.43	14.12	10.15
Covariance			
Band1	154.58	152.62	71.50
Band2	152.62	199.51	86.94
Band3	71.50	86.94	102.98

Ground	Band1	Band2	Band3
Min	122.00	71.00	102.00
Max	233.00	212.00	208.00
Mean	174.35	137.48	147.85
St dev	16.04	14.50	13.71
Covariance			
Band1	257.13	220.86	177.76
Band2	220.86	210.36	159.58
Band3	177.76	159.58	187.91

Water	Band1	Band2	Band3
Min	120.00	134.00	133.00
Max	216.00	194.00	202.00
Mean	195.88	169.82	173.88
St dev	13.84	6.58	8.44
Covariance			
Band1	191.44	67.58	55.52
Band2	67.58	43.27	20.35
Band3	55.52	20.35	71.28

Table A.16: Main statistics computed for the frequency distribution of the training sample extracted from the 2001 colour (RGB) aerial photograph. Min = minimum, Max = maximum, Std. dev = standard deviation, Covar = covariance.

(A)	Veg(R)	Sed(R)	Water(R)	Row total
Veg (CL)	30	1	0	31
Sed (CL)	0	23	0	23
Water (CL)	0	6	30	36
Column total	30	30	30	90

(B)	Veg(R)	Sed(R)	Water(R)	Row total
Veg(CL)	30	1	0	31
Sed(CL)	0	22	0	22
Water (CL)	0	6	30	36
Column total	30	29	30	89

Table A.17: Confusion matrixes computed for the thematic map obtained by A) masking the river area B) classifying the whole image.

(A)	Commission	Omission	Producers	Users
Veg	3.23	0.00	100.00	96.77
Sed	0.00	23.33	76.67	100.00
Water	16.67	0.00	100.00	83.33
Overall				92.2
Kappa				0.88

(B)	Commission	Omission	Producers	Users
Veg	3.23	0.00	100.00	96.77
Sed	0.00	24.14	75.86	100.00
Water	16.67	0.00	100.00	83.33
Overall				92.1
Kappa				0.86

Table A.18: Statistics parameters computed from the value of the confusion matrix to assess the accuracy of the classification method applied.

Appendix B

Coefficients of the linear system at the order $\mathbf{O}(\epsilon)$ and $\mathbf{O}(\epsilon\delta)$

Collecting the terms at the order (ϵ) and $(\epsilon\delta)$ in the system

$$a_{i1}(t)u_1 + a_{i2}(t)v_1 + a_{i3}(t)h_1 + a_{i4}(t)d_1 = 0, \qquad i = 1,2,3,4 \quad \text{(B.1)}$$

the coefficients $a_{i,j}(t)$ can be expaned as

$$a_{i,j}(t) = a^0_{i,j} + a^1_{i,j}(t) \qquad i,j = 1,2,3,4 \qquad \text{(B.2)}$$

and for the specific case they read as follow:

$$
\begin{aligned}
a^0_{11} &= i\lambda + 2\beta_0 C_0 \\
&\quad a^1_{11}(t) = a^0_{11} u_{01}(t) + [2\beta_0 C_0 (C_D - 1)] d_{01}(t); \\
a^0_{13} &= i\lambda \\
&\quad a^1_{13}(t) = 0; \\
a^0_{14} &= \beta_0 C_0 (C_D - 1) \\
&\quad a^1_{14}(t) = [2\beta_0 C_0 (C_D - 1)] u_{01}(t) + [\beta_0 C_0 (P_{11} + C_D (C_D - 1) + 2] d_{01}(t); \\
a^0_{22} &= i\lambda + \beta_0 C_0 \\
&\quad a^1_{22}(t) = [i\lambda + \beta_0 C_0] u_{01}(t) + \beta_0 C_0 (C_D - 1) d_{01}(t); \\
a^0_{23} &= \tfrac{\pi}{2} \\
&\quad a^1_{23}(t) = 0; \\
a^0_{31} &= i\lambda \\
&\quad a^1_{31}(t) = a^0_{31} d_{01}(t); \\
a^0_{32} &= -\tfrac{\pi}{2} \\
&\quad a^1_{32}(t) = a^0_{32} d_{01}(t); \\
a^0_{34} &= i\lambda \\
&\quad a^1_{34}(t) = a^0_{34} u_{01}(t); \\
a^0_{41} &= 2i\lambda \Phi_T \\
&\quad a^1_{41}(t) = \left[2i\lambda (P_{21F} - \Phi_T)\right] u_{01}(t) + 2i\lambda P_{21D} d_{01}(t); \\
a^0_{42} &= -\tfrac{\pi}{2} \\
&\quad a^1_{42}(t) = -a^0_{42} u_{01}(t); \\
a^0_{43} &= \tfrac{\pi^2 r F_0^2}{4\beta_0 \sqrt{\theta_0}} \\
&\quad a^1_{43}(t) = -a^0_{43} u_{01}(t) + \left[-\tfrac{C_D}{2} a^0_{43}\right] d_{01}(t); \\
a^0_{44} &= -\tfrac{\pi^2 r F_0^2}{4\beta_0 \sqrt{\theta_0}} + i\lambda \Phi_T C_D \\
&\quad a^1_{44}(t) = \left[\tfrac{a^0_{43}}{F_0^2} + i\lambda C_D P_{21F}\right] u_{01}(t) + \left[\tfrac{C_D a^0_{43}}{2F_0^2} + i\lambda \left(\Phi_T C_D P_{11} + C_D P_{21D}\right)\right] d_{01}(t),
\end{aligned}
\tag{B.3}
$$

having defined

$$
P_{11} = C_D \left(\frac{C_D}{2} - 1\right), \quad P_{21F} = -2\theta_c \Phi_T, \quad P_{21D} = -C_D \theta_c \Phi_T \tag{B.4a-c}
$$

and

$$
C_D = \frac{C_{f,D}|_0}{C_{f0}}, \quad \Phi_T = \frac{\theta_{*0}}{\Phi_0} \Phi_{,\theta_*}|_0, \tag{B.5a-b}
$$

where C_f denotes the friction coefficient, Φ the intensity of bedload transport and the subscript 0 refers to the reference state.

The system (6.18) for the order $O(\epsilon)$ is therefore written in the form

$$\begin{pmatrix} a_{11}^0 & 0 & a_{13}^0 & a_{14}^0 \\ 0 & a_{22}^0 & a_{23}^0 & 0 \\ a_{31}^0 & a_{32}^0 & 0 & a_{34}^0 \\ a_{41}^0 Q_o \Phi_o & a_{42}^0 Q_o \Phi_0 & a_{43}^0 Q_0 \Phi_o F_0^2(-i\Omega_{10}) & a_{44}^0 Q_0 \Phi_o F_0^2(i\Omega_{10}) \end{pmatrix} \begin{pmatrix} u_{10} \\ v_{10} \\ h_{10} \\ d_{10} \end{pmatrix} = \begin{pmatrix} 0 \\ 0 \\ 0 \\ 0 \end{pmatrix}. \tag{B.6}$$

The matrix of the system (B.6) has been represented in the text through the linear differential operator $\mathbf{L_{10}}$.

Bibliography

Abad, J. and Garcia, M. (2006). Vr meander: A toolbox for re-meandering of channelized streams. *Computers and Geosciences*, 32:92–101.

Allmendinger, N. E., Pizzuto, J. E., Jr, N. P., Johnson, T. E., and Hession, W. C. (2005). The influence of riparian vegetation on stream width, eastern pensylvania, usa. *Geological Society of America Bulletin*, 117:229–243.

Armanini, A., Righetti, M., and Grisenti, P. (2005). Direct measurement of vegetation resistance in prototype scale. *Journal of Hydraulic Research*, 43(5):481–487. DOI: 10.1080/00221680509500146.

Ashmore, P. (1982). Laboratory modelling of gravel braided stream morphology. *Earth Surface Processes and Landforms*, 7:201–225.

Ashmore, P. (1991). How do gravel-bed rivers braid? *Can. J . Earth Sci.*, 28:326–341.

Atonarakis, A., Richards, K., and Brasington, J. (2008). Object-based land cover classification using airborne lidar. *Remote Sensing of Environment*, 112:2988–2998.

Beechie, T. J., Liemann, M., Pollock, M. M., Baker, S., and Davies, J. (2006). Channel pattern and riverfloodplain dynamics in forested mountain river systems. *Geomorphology*, 78:124–141.

Bendix, J. and Hupp, C. (2000). Hydrological and geomorphological impacts on riparian plant communities. *Hydrol. Process.*, 14:2977–2990.

Bertoldi, W., Drake, N. A., and Gurnell, A. M. (2011a). Interactions between river flows and colonizing vegetation on a braided river: exploring spatial and temporal dynamics in riparian vegetation cover using satellite data. *Earth Surface Processes and Landforms*, 36(11):1474–1486.

Bertoldi, W., Gurnell, A. M., and Drake, N. A. (2011b). The topographic signature of vegetation development along a braided river: Results of a combined analysis of airborne lidar, color air photographs, and ground measurements. *Water Resources Research*, 47(6):W06525. doi:10.1029/2010WR010319.

Bertoldi, W., Gurnell, A. M., and Welber, M. (2013). Wood recruitment and retention: The fate of eroded trees on a braided river explored using a combination of field and remotely-sensed data sources. *Geomorphology*, 180-181:146–155.

Bertoldi, W., Siviglia, A., Tettamanti, S., Toffolon, M., Vetsch, D., and Francalanci, S. (2014). Modeling vegetation controls on fluvial morphological trajectories. *Geophysical Research Letters*, 41(20):7167–7175.

Bertoldi, W. and Tubino, M. (2005). Bed and bank evolution of bifurcating channels. *Water Resour. Res.*, 41:W07001, doi:10.1029/2004WR003333.

Bertoldi, W., Zanoni, L., and Tubino, M. (2010). Assessment of morphological changes induced by flow and flood pulses in a gravel bed braided river: The tagliamento river (italy). *Geomorphology*, 114:348–360.

Blondeaux, P. and Seminara, G. (1985). A unified bar-bend theory of river meanders. *J. Fluid Mech.*, 157:449–470.

Braudrick, C. A., Dietrich, W. E., Leverich, G. T., and Sklar, L. S. (2009). Experimental evidence for the conditions necessary to sustain meandering in coarse-bedded rivers. *Proceedings of the National Academy of Sciences*, 106(40):16936–16941. 10.1073/pnas.0909417106.

Bridge, J. S., Alexander, J., Collier, R. E. L., Gawthorpes, R. L., and Jarvis, J. (1995). Ground-penetrating radar and coring used to study the large-scale structure of point-bar deposits in three dimensions. *Sedimentology*, 42:839–852.

Camporeale, C., Perucca, E., Ridolfi, L., and Gurnell, A. (2013). Modeling th einteractions between river morphodynamics and riparian vegetation. *Rev. Geophys.*, 51:379–414. doi:10.1002/rog.20014.

Camporeale, C. and Ridolfi, L. (2006). Riparian vegetation distribution induced by river flow variability: A stochastic approach. *Water Resour. Res.*, 42. doi: 10.1029/2006WR004933.

Camporeale, C. and Ridolfi, L. (2010). Interplay among river meandering, discharge stochasticity and riparian vegetation. *Journal Of Hydrology*, 382:138–144.

Chen, D. and Stow, D. (2002). The effect of training strategies on supervised classification at different spatial resolutions. *Photogrammetric Engineering Remote Sensing*, 68:1155–1161.

Church, M. (1992). *Channel morphology and typology*, pages 129–158. In: The Rivers Handbook, Calow P., Petts G. E. (eds). Oxford: Blackwell.

Church, M. and Rice, S. (2009). Form and growth of bars in a wandering gravel-bed river. *Earth Surf. Process. Landforms*, 34:1422–1432.

Cingolani, A. M., Renison, D., Zak, M. R., and Cabido, M. R. (2004). Mapping vegetation in a heterogeneous mountain rangeland using landsat data: an alternative method to define and classify land-cover units. *Remote Sensing of Environment*, 92:84–97.

Colombini, M., Seminara, G., and Tubino, M. (1987). Finite-amplitude alternate bars. *Journal of Fluid Mechanics*, 181:213–232.

Congalton, R. G. (1991). A review of assessing the accuracy of classifications of remotely sensed data. *Remote Sens. Environ.*, 37:35–46.

Congalton, R. G. (1994). Accuracy assessment of remotely sensed data: future needs and directions. In *Proceedings of Pecora 12 land information from space-based systems*, page 383–388. Bethesda: ASPRS.

Constantine, C. R., Dunne, T., and Hanson, G. J. (2009). Examining the physical meaning of the bank erosion coefficient used in meander migration modeling. *Geomorphology*, 106(3–4):242 – 252.

Corenblit, D., Steiger, J., Gurnell, A. M., Tabacchi, E., and Roques, L. (2009). Control of sediment dynamics by vegetation as a key function driving biogeomorphic succession within fluvial corridors. *Earth Surface Processes and Landforms*, 34:1790–1810.

Corenblit, D., Tabacchi, E., Steiger, J., and Gurnell, A. M. (2007). Reciprocal interactions and adjustments between fluvial landforms and vegetation dynamics in river corridors: A review of complementary approaches. *Earth-Science Reviews*, 84:56–86.

Crosato, A. and Mosselman, E. (2009). Simple physics-based predictor for the number of river bars and the transition between meandering and braiding. *Water Resources Researcg*, 44:W03424.

Crosato, A. and Saleh, S. M. (2011). Numerical study on the effects of floodplain vegetation on river planform style. *Earth Surf. Process. Landforms.*, 36:711–720.

Crouzy, B. and Perona, P. (2012). Biomass selection by floods and related timescales. part 2: Stochastic modeling. *Advances in Water Resources*, 39:97–105.

Dach, R., Hugentobler, U., Fridez, P., and Meindl, M. (2007). *Bernese GPS Software Version 5.0*. User manual, Astronomical Institute, University of Bern.

Darby, S. E., Rinaldi, M., and Dapporto, S. (2007). Coupled simulations of fluvial erosion and mass wasting for cohesive river banks. *J. Geophys. Res.*, 112.

Dean, R. B. (1974). *Aero. Rep.*, pages 74–11. Imperial College, London.

Décamps, H., Tabacchi, E., Giller, P., Hildrew, A., Raffaelli, D., et al. (1994). Species richness in vegetation along river margins. In *Aquatic ecology: scale, pattern and process. The 34th Symposium of the British Ecological Society with the American Society of Limnology and Oceanography, University College, Cork, 1992.*, pages 1–20. Blackwell Scientific Publications Ltd.

Edwards, B. and Smith, D. (2002). Critical wavelength for river meandering. *Physical Review E*, 63(4). DOI: 10.1103/PhysRevE.63.045304.

Einstein, A. (1926). The cause of the formation of meanders in the courses of rivers and of the so-called baer's law. *Die Naturwissenschaften*, 14.

Eke, E., Gary, P., and Yasuyuki, S. (2014). Numerical modeling of erosional and depositional bank processes in migrating river bends with self-formed width: morphodynamics of bar push and bank pull. *American Geophysical Union*. doi: 10.1002/2013JF003020.

Eke, E. and Parker, G. (2011). Comparison of linear and nonlinear models of steady morphodynamics in channels of constant curvature and meandering channels. Abstract EP32A-0692 presented at 2011 Fall Meeting, AGU, San Francisco, Calif.

Eke, E., Shimizu, Y., and Parker, G. (2011). Numerical modeling of meander migration incorporating erosional and depositional bank processes. Proceedings, RCEM Conference, Beijing, China.

Engelund, F. (1964). Flow resistance and hydraulic radius. *Basic Research Progress Rep.*, (6):3–4. ISVA, Technical Univ. of Denmarck.

Foody, G. M. (2002). Status of land cover classification accuracy assessment. *Remote Sensing of Environment*, 80:185–201.

Francis, R. A. (2007). Size and position matter: riparian plant establishment from fluvially deposited trees. *Earth Surface Processes and Landforms*, 32(8):1239–1243.

Francis, R. A. and Gurnell (2006). Sinitial establishment of vegetative fragments within the active zone of a braided gravel-bed river (river tagliamento, ne italy). *Wetlands*, 26(3):641–648.

Frascati, A. and Lanzoni, S. (2009). Morphodynamic regime and long-term evolution of meandering rivers. *J. Geophys. Res.*, 114(F02002). doi: 10.1029/2008JF001101.

Frascati, A. and Lanzoni, S. (2010). Long-term meandering evolution as part of chaotic dynamics? a contribution from mathematical modelling. *Earth Surf. Proc and Land.*, (Special Issue on River Meander Dynamics, Eds. J.M. Hooke, E. Gautier and G. Zolezzi). in press.

Frascati, A. and Lanzoni, S. (2013). A mathematical model for meandering rivers with varying width. *J. Geophys. Res.Earth Surf.*, 118:1641–1657. doi:10.1002/jgrf.20084.

Friedkin, J. (1945). A laboratory study of the meandering of alluvial rivers. *U.S. Waterways Experiment Station*.

Garófano-Gómez, V., Martínez-Capel, F., Bertoldi, W., Gurnell, A., Estornell, J., and Seguran-Beltrán, F. (2013). Six decades of changes in the riparian corridor of a mediterranean river: a synthetic analysis based on historical data sources. *Ecohydrol.*, 6:536–553.

Geerling, G. W., Vreeken-Buijs, M. J., Jesse, P., Ragas, A. M. J., and Smits, A. J. M. (2009). Mapping river floodplain ecotopes by segmentation of spectral (casi) and structural (lidar) remote sensing data. *River Res. Appl.*, 25:795–813.

Grabowski, R., Surian, N., and Gurnell, A. (2014). Characterizing geomorphological change to support sustainable river restoration and management. *WIREs Water 2014*.

Gran, K. and Paola, C. (2001). Riparian vegetation controls on braided stream dynamics. *Water Resource Research*, 37(12):3275–3283.

Grenfell, M., Aalto, R., and Nicholas, A. (2011). Chute channel dynamics in large, sand-bed meandering rivers. *Earth Surf. Process. Landforms*. DOI:10.1002/esp.2257.

Güneralp, I. and Rhoads, B. (2011). Influence of floodplain erosional heterogeneity on planform complexity of meandering rivers. *Geophys. Res. Lett.*, 38(L14401). doi:10.1029/2011GL048134.

Gurnell, A. (2014). Plant as riversystem engineers. *Earth Surf. Process. Landforms*, 39:4–25.

Gurnell, A., Bertoldi, W., and Corenblit, D. (2012). Changing river channels: The roles of hydrological processes, plants and pioneer fluvial landforms in humid temperate, mixed load, gravel bed rivers. *Earth-Science Reviews*, 111:129–141.

Gurnell, A. M., Downward, S. R., and Jones, R. (1994). Channel planform change on the river dee meanders, 1876–1992. *Regul. Rivers: Res. Mgmt.* 9: 187–204. doi: 10.1002/rrr.3450090402.

Gurnell, A. M. and Petts, G. (2006). Trees as riparian engineers: The tagliamento river, italy. *Earth Surf. Process. Landforms*, 31:1558–1574.

Gurnell, A. M., Petts, G., Hannah, D., Smith, B., Edwards, P., Kollmann, J., Ward, J., and Tockner, K. (2001). Riparian vegetation and island formation along the gravel-bed fiume tagliamento, italy. *Earth Surf. Process. Landforms*, 26:31–62.

Gurnell, A. M., Tockner, K., Edwards, P., and Petts, G. (2005). Effect of deposited wood on biocomplexity of river corridors. *Front. Ecol. Environ*, 3(7):377–382.

Hall, P. (2004). Alternating bar instabilities in unsteady channel flows over erodible beds. *J. Fluid Mech.*, 499:49–73. doi: 10.1017/S0022112003006219.

Hasegawa, K. (1977). Computer simulation of the gradual migration of meandering channels. In *Proceedings of the Hokkaido Branch, Japan Society of Civil Engineering*, pages 197–202. in Japanese.

Henshaw, A. J., Gurnell, A. M., Bertoldi, W., and Drake, N. A. (2013). An assessment of the degree to which landsat tm data can support the assessment of fluvial dynamics, as revealed by changes in vegetation extent and channel position, along a large river. *Geomorphology*, 202:74–85.

Hickin, E. and Nanson, G. (1975). The character of channel migration on the beatton river, northeast british columbia, canada. *Geological Society of America Bulletin*, 86(4):487–494.

Hickin, E. J. (1974). The development of meanders in natural river-channels. *American Journal of Science*, 274:414–442.

Hickin, E. J. (1984). Vegetation and river channel dynamics. *Journal of Hydraulic Engineering, ASCE*, XXVIII(2):111–126.

Hooke, J. (2007). Spatial variability, mechanisms and propagation of change in an active meandering river. *Geomorphology*, 84:277–296.

Hooke, J. (2008). Temporal variations in fluvial processes on an active meandering river over a 20-year period. *Geomorphology*, 100:3–13.

Howard, A. (1992). *Modelling channel migration and floodplain development in meandering streams*, pages 1 – 41. in: Lowland Flood-Plain Rivers: Geomorphological Perspectives. M.G Anderson, D.E. Walling, P.D. Bates (Eds.) John Wiley, Hoboken, N. J.

Hubert-Moy, L., Cotonnec, A., and Le Du, L. (2001). A comparison of parametric classification procedures of remotely sensed data applied on different landscape units. *Remote Sens. Environ.*, 75:174–187.

Hupp, C. and Osterkamp, W. (1985). Bottomland vegetation distribution along passage creek, virginia, in relation to fluvial landforms. *Ecology*, 66(3):670–681.

Hupp, C. and Rinaldi, M. (2007). Riparian vegetation patterns in relation to fluvial landforms and channel evolution along selected rivers of tuscany (central italy). *Annals of the Association of American Geographers*, 97(1):12–30.

Ikeda, S., Parker, G., and Sawai, K. (1981). Bend theory of river meanders. Part 1 - Linear development. *J. Fluid Mech.*, 112:363–377.

Johnson, W. C. (1994). Woodland expansion in the platte river, nebraska:patterns and causes. *Ecological Monographs*, 64:45–84.

Karrenberg, S., Kollmann, J., Edwards, P., Gurnell, A., and Petts, G. (2003). Patterns in woody vegetation along the active zone of a near-natural alpine river. *Basic Appl. Ecol.*, 4:157–166.

Kraus, K. and Pfeifer, N. (1998). Determination of terrain models in wooded areas with airborne laser scanner data. *ISPRS J. Photogramm. Remote Sens.*, 53:193–203.

Landgrebe, D. A. (2003). *Signal Theory Methods in Multispectral Remote Sensing*. John Wiley Sons, Inc.

Lanzoni, S. and Seminara, G. (2006). On the nature of meander instability. *Journal of Geophysical Research*, 111(F04006). doi:10.1029/2005JF000416.

Lauer, J. and Parker, G. (2008). Net local removal of floodplain sediment by river meander migration. *Geomorphology*, 96:123–149. doi: 10.1016/j.geomorph.2007.08.003.

Leclerc, R. F. and Hickin, E. J. (1997). The internal structure of scrolled floodplain deposits based on ground-penetrating radar, north thompson river, british columbia. *Geomorphology*, 21:17–38.

Leopold, L. and Wolman, G. (1957). River channel patterns: braiding, meandering and straight. *U.S. Geological Survey Professional Paper 282-B*, page 51 pp.

Leopold, L. B. and Wolman, G. M. (1960). River meanders. *Bulletin of the Geological Society of America*, 71.

Lewin, J. (1976). Initiation of bed forms and meanders in coarse grained sediment. *Geolog. Soc. America Bull.*, 87(2):281–285.

Li, S. S. and Millar, R. G. (2011). A two-dimensional morphodynamic model of gravel-bed river with floodplain vegetation. *Earth Surf. Process. Landforms*, 36:190–202.

Lotter, G. K. (1933). Considerations on hydraulic design of channels with different roughness of walls. *Izvestiia Vsesoiuznago Nuchno-Issledovatel'skogo Instituta Gildrotekhniki Leningrad*, 9:238–241 (in Russian).

Luchi, R., Bertoldi, W., Zolezzi, G., and Tubino, M. (2007). Monitoring and predicting channel change in a free-evolving, small Alpine river: Ridanna Creek (North East Italy). *Earth Surface Processes and Landforms*, 32(14):2104–2119.

Luchi, R., Zolezzi, G., and Tubino, M. (2011). Bend theory of river meanders with spatial width variations. *J. Fluid Mech*, 681:311–339. doi:10.1017/jfm.2011.200.

Mackin, J. (1956). Causes of braiding by a graded river. *Geol. Soc. Am. Bull.*, 37:1717–1718.

Mahoney, J. M. and Rood, S. B. (1998). Streamflow requirements for cottonwood seedling recruitment - an integrative model. *WETLANDS*, 18(4):634–645.

Mao, L. and Surian, N. (2010). Observations on sediment mobility in a large gravel-bed river. *Geomorphology*, 114(3):326 – 337.

Marani, M., Lio, C. D., and D'Alpaos, A. (2013). Vegetation engineers marsh morphology through multiple competing stable states. *PNAS*, 110(9):3259–3263.

Marcus, W. A. and Fonstad, M. A. (2008). Optical remote mapping of rivers at submeter resolutions and watershed extents. *Earth Surface Processes and Landforms*, 33:4–24.

Marcus, W. A., Legleiter, C. J., Aspinall, R. J., Boardman, J. W., and Crabtree, R. L. (2003). Candidate high spectral resolution infrared indices for crop cover. *Remote Sensing of Environment*, 46:204–212.

Mather, P. M. and Koch, M. (2011). *Classification, in Computer Processing of Remotely-Sensed Images: An Introduction*. John Wiley Sons, Ltd, Chichester, UK, fourth edition. doi: 10.1002/9780470666517.ch8.

McKenney, R., Jacobson, R. B., and Wertheimer, R. C. (1995). Woody vegetation and channel morphogenesis in low-gradient, gravel-bed streams in the ozark plateaus, missouri and arkansas. *Geomorphology*, 13:175–198.

Meyer-Peter, E. and Müller, R. (1948). Formulas for bed load transport. In *Proceedings of 2nd Meeting IAHSR, Stockholm, Sweden*, pages 1–26.

Micheli, E. and Kirchner, J. (2002a). Effects of wet meadow riparian vegetation on streambank erosion. 1. remote sensing measurements of streambank migration and erodibility. *Earth Surf. Process. Landforms*, 27:627–639.

Micheli, E. and Kirchner, J. (2002b). Effects of wet meadow riparian vegetation on streambank erosion. 2. measurements of vegetated bank strength and consenquences for failure mechanics. *Earth Surf. Process. Landforms*, 27:687–697.

Micheli, E., Kirchner, J., and E.W., L. (2004). Quantifying the effect of riparian forest versus agricultural vegetation on river meander migration rates, central sacramento river, california, usa. *River Research and Applications*, 20:537–548.

Millar, R. G. (2000). Influence of bank vegetation on alluvial channel patterns. *Water Resources Res*, 36(4):1109–1118.

Moggridge, H. and Gurnell, A. (2009). Controls on the sexual and asexual regeneration of salicaceae along a highly dynamic, braided river system. *Aquatic Sciences*, 71:305–317.

Montserud, R. A. and Leamans, R. (1992). Comparing global vegetation maps with the kappa statistic. *Ecological Modelling*, 62:275–293.

Motta, D., Abad, J. D. A., Langendoen, E. J., and Garcia, M. H. (2012a). The effects of floodplain soil heterogeneity on meander planform shape. *Water Resour. Res.*, 48. W09518, doi:10.1029/2011WR011601.

Motta, D., Abad, J. D. A., Langendoen, E. J., and Garcia, M. H. (2012b). A simplified 2d model for meander migration with physically-based bank evolution. *Geomorphology*, 163-164:10–25. doi:10.1016/j.geomorph.2011.06.036.

Nakayama, K., Fielding, C. R., and Alexander, J. (2002). Variations in character and preservation potential of vegetation-induced obstacle marks in the variable discharge burdekin river of north queensland, australia. *Sedimentary Geology*, 149:199–218.

Nanson, G. and Croke, J. (1992). A genetic classification of floodplains. *Geomorphology*, 4(6):459–486.

Nanson, G. and Hickin, E. (1983). Channel migration and incision on the Beatton River. *Journal of Hydraulic Engineering*, 109:327–337.

Nanson, G. C. (1980). Point bar and floodplain formation of the meandering beatton river, northeastern british columbia, canada. *Sedimentology*, 27:3–29.

Nanson, G. C. (1981). New evidence of scroll-bar formation on the beatton river. *Sedimentology*, 28:889–891.

Nanson, G. C. (1986). Episodes of vertical accretion and catastrophic stripping: A model of disequilibrium flood-plain development. *Geological Society of America Bulletin*, 97:1467–1475.

Nicholas, A. P. (2013). Modelling the continuum of river channel patterns. *Earth Surf. Process. Landforms*, 38:1187–1196.

O'Neal, M. A. and Pizzuto, J. E. (2011). The rates and spatial patterns of annual riverbank erosion revealed through terrestrial laser-scanner surveys of the south river, virginia. *Earth Surf. Process. Landforms*, 36:695–701.

O'Connor, J. E., Jones, M. A., and Haluska, T. L. (2003). Flood plain and channel dynamics of the quinault and queets rivers, washington, usa. *Geomorphology*, 51:31–59.

Parker, G. (1976). On the cause and characteristic scales of meandering and braiding in rivers. *Journal of Fluid Mechanics*, 76:457–480. doi:10.1017/S0022112076000748.

Parker, G., Diplas, P., and Akiyama, J. (1983). Meanders bends of high amplitude. *Journal of Hydraulic Engineering ASCE*, 109:1323–1337.

Parker, G., Shimizu, Y., Eke, G. W. E., Abad, J., Lauer, J., Paola, C., Dietrich, W., and Voller, V. (2011). A new framework for modeling the migration of meandering rivers. *Earth Surface Processes and Landforms*, 36:70–86. doi:10.1002/esp.2113.

Parker, G., Wilcock, P. R., Paola, C., Dietrich, W. E., and Pitlick, J. (2007). Physical basis for quasi-universal relations describing bankfull hydraulic geometry of single-thread gravel bed rivers. *J. Geophys. Res.*, 112. F04005,doi:10.1029/2006JF000549.

Pasquale, N., Perona, P., Francis, R., and Burlando, P. (2012). Effects of streamflow variability on the vertical root density distribution of willow cutting experiments. *Ecological Engineering*, 40:167–172.

Perona, P., Molnar, P., Crouzy, B., Perucca, E., Jiang, Z., McLelland, S., Wüthrich, D., Edmaier, K., Francis, R., Camporeale, C., and Gurnell, A. (2012). Biomass selection by floods and related timescales: Part 1. experimental observations. *Advances in Water Resources*, 39:85–96.

Perucca, E., Camporeale, C., and Ridolfi, L. (2006). Influence of river meandering dynamics on riparian vegetation pattern formation. *J. Geophys. Res.*, 111(G01001). doi:10.1029/2005JG000073.

Perucca, E., Camporeale, C., and Ridolfi, L. (2007). Significance of the riparian vegetation dynamics on meandering river morphodynamics. *Water Resour. Res.*, 43(W03430). doi:10.1029/2006WR005234.

Pizzuto, J., O'Neal, M., and Stotts, S. (2010). On the retreat of forested, cohesive riverbanks. *Geomorphology*, 116:341–352.

Pizzuto, J. E. (1994). Channel adjustments to changing discharges, powder river, montana. *Geological Society of America Bulletin*, 106:1494–1501.

Pollen-Bankhead, N., Simon, A., Jaeger, K., and Wohl, E. (2009). Destabilization of streambanks by removal of invasive species in canyon de chelly national monument, arizona. *Geomorphology*, 103:363–374.

Posner, A. J. and Duan, J. G. (2012). Simulating river meandering processes using stochastic bank erosion coefficient. *Geomorphology*, 163-164:26–36.

Repetto, R., Tubino, M., and Paola, C. (2002). Planimetric instability of channels with variable width. *J. Fluid Mech.*, 457:79–109.

Righetti, M. (2008). Flow analysis in a channel with flexible vegetation using double-averaging method. *Acta Geophysica*, 5(3):801–823. DOI: 10.2478/s11600-008-0032-z.

Rinaldi, M., Mengoni, B., Luppi, L., Darby, S. E., and Mosselman, E. (2008). Numerical simulation of hydrodynamics and bank erosion in a river bend. *Water Resour. Res.*, 44. W09428, doi:10.1029/2008WR007008.

Robertson, K. M. (2006). Distributions of tree species along point bars of 10 rivers in the south-eastern us coastal plain. *ournal of Biogeography*, 33:121–132.

Robertson, K. M. and Augspurger, C. (1999). Geomorphic processes and spatial patterns of primary forest succession on the bogue chitto river, usa. *Journal of Ecology*, 87:1052–1063.

Rodnight, H., Duller, G., Tooth, S., and Wintle, A. (2005). Optical dating of a scroll-bar sequence on the klip river, south africa, to derive the lateral migration rate of a meander bend. *he Holocene*, 15:802–811.

Rozo, M. G., Nogueira, A. C., and Truckenbrodt, W. (2012). The anastomosing pattern and the extensively distributed scroll bars in the middle amazon river. *Earth Surf. Process. Landforms*, 37:1471–1488. DOI: 10.1002/esp.3249.

Rozovskij, I. L. (1957). Flow of water in bends of open channels. *Acad. Sci.* Ukrainian SSR, Kiev.

Seminara, G. (2006). Meanders. *Paper invited for the 50th Anniversary issue of the J. Fluid. Mech.*, 554:271–297. DOI: 10.1017/S0022112006008925.

Seminara, G. and Bolla Pittaluga, M. (2012). Reductionist versus holistic approaches to the study of river meandering:an ideal dialogue. *Geomorphology*, 163-164:110–117.

Seminara, G. and Solari, L. (1998). Finite amplitude bed deformations in totally and partially transporting wide channel bends. *Water Resources Research*, 34 (6):1585–1594.

Seminara, G., Zolezzi, G., Tubino, M., and Zardi, D. (2001). Downstream and upstream influence in river meandering. Part 2. Planimetric development. *Journal of Fluid Mechanics*, 438:213–230. doi:10.1017/S0022112001004281.

Shafroth, P. B., Stromberg, J. C., and Patten, D. T. (2002). Riparian vegetation response to altered disturbance and stress regimes. *Ecological Applications*, 12:107–123.

Shankman, D. (1993). Channel migration and vegetation patterns in the southeastern coastal plain. *Conservation Biology*, 7(1):176–183.

Sun, T., Meaking, P., Jossang, T., and Schwarz, K. (1996). A simulation model for meandering rivers. *Water Resources Research*, 32(9):2937–2954. doi: 10.1029/96WR00998.

Surian, N., Mao, L., Giacomin, M., and Ziliani, L. (2009). Morphological effects of different channelforming discharges in a gravel-bed river. *Earth Surf. Process. Landforms*, 34:1093–1107.

Surian, N. and Rinaldi, M. (2003). Morphological response to river engineering and management in alluvial channels in italy. *Geomorphology*, 50:307–326.

Tal, M. and Paola, C. (2010). Effects of vegetation on channel morphodynamics: results and insights from laboratory experiments. *arth Surf. Process. Landforms*, 35:1014–1028.

Talmon, A. M., Struiksma, N., and van Mierlo, M. C. L. M. (1995). Laboratory measurements of the direction of sediment transport on transverse alluvial-bed slopes. *J. Hydraul. Res.*, 33:519–534.

Tockner, K., Ward, J. V., Arscott, D. B., Edwards, P. J., Kollmann, J., Gurnell, A. M., Petts, G. E., and Maiolini, B. (2003). The tagliamento river: A model ecosystem of european importance. *Aquat. Sci.*, 65:239–253.

Toledo, Z. and Kauffman, J. (2001). Root biomass in relation to channel morphology of headwater streams. *Journal of the American Water Resources Association*, 37:1653–1663.

Tubino, M. (1991). Growth of alternate bars in unsteady flow. *Water Resources Research*, 27(1):37–52.

van Dijk, W. M., van de Lageweg, W. I., and Kleinhans, M. G. (2012). Experimental meandering river with chute cutoffs. *J. Geophys. Res.*, 117. F03023, doi:10.1029/2011JF002314.

van Dijk, W. M., van de Lageweg, W. I., and Kleinhans, M. G. (2013). Formation of a cohesive floodplain in a dynamic experimental meandering river. *Earth Surf. Process. Landforms*, 38:1550–1565.

Vargas-Luna, A., Crosato, A., and Uijttewaal, W. S. J. (2014). Effects of vegetation on flow and sediment transport: comparative analyses and validation of predicting models. *Earth Surf. Process. Landforms*. DOI: 10.1002/esp.3633.

Visconti, F., Camporeale, C., and Ridolfi, L. (2010). Role of discharge variability on pseudomeandering channel morphodynamics: Results from laboratory experiments. *J. Geophys. Res.*, 115(F04042). doi:10.1029/2010JF001742.

Wasser, L., Day, R., Chasmer, L., and Taylor, A. (2013). Influence of vegetation structure on lidar-derived canopy height and fractional cover in forested riparian buffers during leaf-off and leaf-on conditions. *PLoS ONE*, 8(1). :e54776. doi:10.1371/journal.pone.0054776.

Welford, M. R. (1994). A field test of tubino's (1991) model of alternate bar formation. *Earth Surface Processes and Landforms*, 19(4):287–297.

Welling, D. and He, Q. (1998). The spatial variability of overbank sedimentation on river floodplains. *Geomorphology*, 24:209–223.

White, B. and Nepf, H. M. (2008). vortex-based model of velocity and shear stress in a partially vegetated shallow channel. *Water Resour. Res.*, 44. W01412, doi:10.1029/2006WR005651.

Whited, D. C., Lorang, M. S., Harner, M. J., Hauer, F. R., Kimball, J. S., and Stanford, J. A. (2007). Climate, hydrologic disturbance, and succession: drivers of floodplain pattern. *Ecology*, 88:940–953.

Zanoni, L., Gurnell, A. M., Drake, N., and Surian, N. (2008). Island dynamics in a braided river from analysis of historical maps and air photographs. *River. Res. Applic.*, 24:1141–1159.

Ziliani, L. and Surian, N. (2012). Evolutionary trajectory of channel morphology and controlling factors in a large gravel-bed river. *Geomorphology*, 173–174(0):104 – 117.

Zolezzi, G., Bertoldi, W., and Tubino, M. (2012a). *Morphodynamics of Bars in Gravel-Bed Rivers: Bridging Analytical Models and Field Observations*, pages 69–89. John Wiley Sons, Ltd.

Zolezzi, G., Guala, M., Termini, D., and Seminara, G. (2005). Experimental observation of upstream overdeepening. *Journal of Fluid Mechanics*, 531:191–219.

Zolezzi, G., Luchi, R., and Tubino, M. (2009). Morphodynamic regime of gravel bed, single-thread meandering rivers. *Journal of Geophysical Research - Earth Surface*, 114. F01005, doi:10.1029/2007JF000968.

Zolezzi, G., Luchi, R., and Tubino, M. (2012b). Modeling morphodynamic processes in meandering rivers with spatial width variations. *Reviews of Geophysics*, 50(4). RG4005, doi:10.1029/2012RG000392.

Zolezzi, G. and Seminara, G. (2001). Downstream and upstream influence in river meandering. Part 1. General theory and application of overdeepening. *J. Fluid Mech.*, 438:183–211.